HHS Public Access

Author manuscript

Prog Retin Eye Res. Author manuscript; available in PMC 2022 July 01.

Published in final edited form as:

Prog Retin Eye Res. 2021 July ; 83: 100920. doi:10.1016/j.preteyeres.2020.100920.

Promises and pitfalls of evaluating photoreceptor-based retinal disease with adaptive optics scanning light ophthalmoscopy (AOSLO)

Niamh Wynne[a,1], **Joseph Carroll**[a,b,c,1], **Jacque L. Duncan**[d,1,*]

[a]Department of Ophthalmology and Visual Sciences, Medical College of Wisconsin, Milwaukee, Wisconsin, USA

[b]Department of Cell Biology, Neurobiology & Anatomy, Medical College of Wisconsin, Milwaukee, Wisconsin, USA

[c]Department of Biomedical Engineering, Medical College of Wisconsin, Milwaukee, Wisconsin, USA

[d]Department of Ophthalmology, University of California, San Francisco, San Francisco California, USA

Abstract

Adaptive optics scanning light ophthalmoscopy (AOSLO) allows visualization of the living human retina with exquisite single-cell resolution. This technology has improved our understanding of normal retinal structure and revealed pathophysiological details of a number of retinal diseases. Despite the remarkable capabilities of AOSLO, it has not seen the widespread commercial adoption and mainstream clinical success of other modalities developed in a similar time frame. Nevertheless, continued advancements in AOSLO hardware and software have expanded use to a broader range of patients. Current devices enable imaging of a number of different retinal

[1]Percentage of work contributed by each author in the production of the manuscript is as follows: Niamh Wynne: 50%, Joseph Carroll: 25%, Jacque Duncan: 25%

[*]Corresponding author: Dr. Jacque L. Duncan, Jacque.Duncan@ucsf.edu.

Author Statement:
Niamh Wynne: Conceptualization, Investigation, Writing-Original draft, Writing-reviewing and editing revisions, Visualization.
Joseph Carroll: Conceptualization, Investigation, Writing-Original draft, Writing-reviewing and editing revisions, Visualization and Supervision.
Jacque Duncan: Conceptualization, Investigation, Writing-Original draft, Writing-eviewing and editing revisions, Visualization and Supervision.

Declaration of interest
N.W.: none
J. C.: receives research support from AGTC, MeiraGTx, and OptoVue, is a consultant for MeiraGTx, andhas personal financial interest in Translational Imaging Innovations.
J.L.D.: receives financial support as a member of the data safety monitoring committee or scientific advisory board for AGTC Therapeutics, the California Institute for Regenerative Medicine, ProQR Therapeutics, SparingVision, Spark Therapeutics and Vedere Bio. She has consulted for Biogen/Nightstarx, DTx Pharma, Editas, Eloxx, Gyroscope and Horama. She receives research funding to support clinical trials from Abbvie, Acucela, Biogen/Nightstarx, Neurotech USA, Second Sight, the National Eye Institute, Research to Prevent Blindness and the Foundation Fighting Blindness.

cell types, with recent improvements in stimulus and detection schemes enabling monitoring of retinal function, microscopic structural changes, and even subcellular activity. This has positioned AOSLO for use in clinical trials, primarily as exploratory outcome measures or biomarkers that can be used to monitor disease progression or therapeutic response. AOSLO metrics could facilitate patient selection for such trials, to refine inclusion criteria or to guide the choice of therapy, depending on the presence, absence, or functional viability of specific cell types. Here we explore the potential of AOSLO retinal imaging by reviewing clinical applications as well as some of the pitfalls and barriers to more widespread clinical adoption.

1. Introduction

Inherited retinal degenerations are a heterogeneous group of diseases that all share in common the progressive death of photoreceptors, resulting in blindness. Inherited retinal degenerations are orphan diseases, affecting less than 100,000 people in the United States, so developments that can identify treatment effects on smaller numbers of patients would facilitate trials of new therapies. Treatments for these conditions have been challenging to develop because they are genetically and mechanistically diverse, progress slowly over decades and the most common clinical outcome, visual acuity, is often preserved until the disease is very advanced. The photoreceptors, which are the primary site of disease, have traditionally been challenging to assess on a cellular level in living eyes. Improved methods of evaluating photoreceptor structure and function could expedite the development of treatments to slow or reverse vision loss. High resolution retinal images could make it possible to identify patients who retain sufficient photoreceptor structure to benefit from treatments. This could reduce the number of patients and length of time required to demonstrate safety and efficacy compared with traditional, less sensitive outcome measures (Duncan et al., 2018; Thompson et al., 2020).

While vision loss is the defining *functional* manifestation of retinal diseases, clinical diagnosis and management of these conditions has long relied on non-invasive imaging tools to assess retinal *structure*. Over the last few decades, there has been an impressive co-evolution of the treatments for use in a wide range of retinal diseases along with the retinal imaging modalities available to clinicians and researchers for studying and managing these conditions. We find ourselves in truly unprecedented times with respect to the capabilities of retinal imaging technologies.

For example, in over 29 years since its initial development (Huang et al., 1991), the speed of clinical optical coherence tomography (OCT) has improved from 500 to 400,000 Hz and there has been a 7-fold improvement in axial resolution from 15 micrometers to the 2 micrometers now achievable with visible light OCT (Shu et al., 2017). Similarly, fundus autofluorescence (AF) had its origins in a fundus spectrophotometry technique and was developed to detect patterns of endogenous retinal fluorophores (such as lipofuscin and melanin) using short wavelength light (Delori, 1994) or near infrared wavelengths (Keilhauer and Delori, 2006). Now, when the principle is employed with confocal scanning laser ophthalmoscopy it provides a tool capable of conveying more than qualitative information and allows for reliable quantitative assessment of these reflexes, enhancing

its utility in tracking disease progression and response to treatment (Delori et al., 2011). The closely related fluorescence lifetime imaging ophthalmoscopy (FLIO) does not elucidate concentrations of fluorophores but can provide information on molecular micro-environmental changes based on the time taken for fluorescence of an ocular structure to return to normal following excitation (Bernstein et al., 2019; Dysliet al., 2017). These imaging tools have unquestionable value for the management of retinal diseases, though they remain limited by the monochromatic aberrations of the human eye and thus offer limited transverse (or lateral) resolution.

Perhaps the biggest advance in retinal imaging came from efforts to compensate for the eye's aberrations and improve transverse resolution (Dreher et al., 1989; Liang and Williams, 1997; Liang et al., 1997). The concept of using a wavefront sensor and deformable mirror to measure and compensate aberrations was introduced in astronomy and was termed adaptive optics (AO). In 1997, David Williams and colleagues at the University of Rochester employed a Hartmann-Shack wavefront sensor to measure the optical aberrations introduced by the cornea and lens, a piezo electric deformable mirror to correct those aberrations and a flash-illuminated fundus camera to acquire an image of the photoreceptor mosaic (Liang et al., 1997). While the imaging of photoreceptors in the living eye had previously been demonstrated in eyes with superior optical quality without the use of AO (Miller et al., 1996; Wade and Fitzke, 1998), the ability to correct for the eye's aberrations expanded the population of eyes in which cellular resolution imaging could be achieved. Despite the significant growth in AO-based imaging tools in the last 20 years, there are currently no FDA-approved AO devices (though the AO flood-illuminated retinal camera, rtx1 from Imagine Eyes is currently approved for marketing within the European Union, Japan and China). Nevertheless, AO technology continues to evolve. For example, wavefront "sensorless" strategies are being developed (Hagan et al., 2020; Hofer et al., 2011), which have potential application in expanding the clinical population in which AO imaging can be applied successfully. There have also been significant advances in detection strategies for the retinal image, including optimizing illumination wavelength, detection apertures, illumination pupil apodization and polarized detection (Chui et al., 2012; Guevara-Torres et al., 2015; Rossi et al., 2017; Scoles et al., 2014a; Sulai et al., 2014; Wang et al., 2016). A detailed description of the technical trajectory of AO retinal imaging can be found in a recent review (Burns et al., 2019).

The application of AO to a range of imaging modalities (e.g., scanning light ophthalmoscopy and OCT) improves both the lateral and axial resolution of the retinal image, albeit to varying degrees (Figure 1). This has facilitated imaging of many cell types including photoreceptors, retinal pigment epithelium (RPE) cells, ganglion cells, pericytes, and even individual blood cells (Burns et al., 2019; Williams, 2011). In retinal imaging research, AOSLO is currently the most widespread modality – numerous AOSLO-based studies have made major contributions to our knowledge of disease pathophysiology, revealing substantial promise for use in clinical trials for inherited retinal diseases. The reader is referred to recent outstanding reviews on AO-OCT (Jonnal et al., 2016; Miller and Kurokawa, 2020), which has a number of important features that complement AOSLO. Despite the superior transverse resolution afforded by imaging the retina with AO systems, their use remains largely limited to academic and research facilities. The difference in

widespread adoption of OCT and the more limited dissemination of AO imaging systems can be explained by the lack of commercial imaging systems, challenges posed by transpupillary imaging in patients with media opacity, tear film abnormalities and small pupils, and time-consuming, labor-intensive image acquisition and analysis. However, AO imaging offers opportunities to study photoreceptor structure and function non-invasively and holds great promise to provide outcome measures for emerging clinical trials of retinal disease.

Here we review current and emerging clinical applications of AOSLO (with an emphasis on photoreceptor-based diseases), examine how AOSLO imaging compares to other clinical imaging modalities, and discuss future areas of development in AOSLO imaging. We will primarily use examples from relatively rare retinal conditions to review the application of AOSLO and discuss the challenges associated with using AOSLO to assess the photoreceptor mosaic. However, it is important to note that AOSLO has been used in more common conditions like diabetic retinopathy and AMD (Nesper et al., 2017; Sun et al., 2012; Zayit-Soudry et al., 2013; Zhang et al., 2014), and that the general utility and limitations presented here also apply to these and other conditions.

2. Imaging the normal retina

The retina is comprised of an assortment of specialized cell types that work synergistically to convert light captured by photoreceptors into a neural signal for visual processing in the brain. Structural or functional defects at any point in this network can disrupt visual processing and result in severe visual impairment. A vital step toward deploying AOSLO to study these conditions is establishing a robust characterization of these cells in the normal retina. The various retinal cell types have unique anatomical and physiological characteristics that pose different imaging challenges, though correction of the eye's monochromatic aberrations is common to all AO techniques regardless of the intended cell type to be imaged. The specific physical attributes of each cell type dictate how light interacts with them and the different optimization strategies for imaging. We review these approaches below, but also refer the reader to additional reviews on imaging various cell types in the living human retina with AO-based imaging tools (Burns et al., 2019; Jonnal et al., 2016; Williams, 2011).

2.1 Photoreceptors

2.1.1 Imaging the cone photoreceptor mosaic—Healthy cone photoreceptors are the most easily visualized structures in confocal AOSLO images, appearing as bright spots. Although the consensus is that the bright spots are a composite signal resulting from light waveguided by multiple interfaces that originate from organized photoreceptor structures, the remainder of the manuscript will refer to this signal as representing organized photoreceptor structures with waveguiding inner and outer segments. Cone structure causes unabsorbed imaging light to be reflected back along their axis toward the pupil, a property called waveguiding. The spatial topography of the cone mosaic varies significantly and consistently with retinal eccentricity, a feature of the photoreceptor mosaic first characterized by *ex vivo*, histological examination (Curcio et al., 1990; Osterberg,

1935). Numerous groups have used AOSLO to characterize the normal cone mosaic, (Chui et al., 2008; Cooper et al., 2016; Dubra et al., 2011; Sredar et al., 2018; Wang et al., 2019; Wells-Gray et al., 2016) with data on density and topography generally matching previous reports from histology (Curcio et al., 1990). Cone density peaks in the fovea, where individual cones have small Gaussian profiles when imaged with confocal AOSLO and are tightly packed in a contiguous triangular array (Figure 2). With increasing eccentricity from the fovea, cone density decreases precipitously with a concomitant increase in cone spacing and diameter. Due to the relationship between cone size and the number of waveguide modes that can propagate effectively, this change in diameter is accompanied by more variable cone reflectance profiles. Some cones appear as several smaller clustered regions of intensity rather than one discrete area, an appearance termed ‘multimodal’ which makes them difficult to disambiguate from the surrounding rod photoreceptors. Using non-confocal split detection AOSLO, cone inner segments (IS) can be visualized outside the fovea (Scoles et al., 2014b) (Figure 3). Cross referencing of these ambiguous cones on confocal AOSLO with the cone IS structures on split detection images can aid in accurate classification of these cones and therefore facilitate calculation of more accurate cone (and rod) metrics. The structures on the split detection images agree with IS dimensions obtained from *ex vivo* histological measurements (Scoles et al., 2014b). *In vivo* imaging has the distinct advantage of being available in real time, informing clinicians on the evolution of pathology longitudinally and providing input to decisions on active clinical care, rather than the static postmortem histological assessments. AOSLO measurements are considered by some as more accurate than histology, given they are not subject to histological artifacts such as tissue shrinkage. However, as we review later, AOSLO images have other potential sources of inaccuracy including residual image distortion and uncertainties around the absolute scale of AOSLO retinal images. Nevertheless, AOSLO has been widely used to assess various properties of the normal cone mosaic.

The normal human cone mosaic contains three types of cone, termed long- (L-), middle- (M-), and short-wavelength (S-) sensitive based on the region of the visible spectrum in which they have their peak sensitivity. There is over an 80-year history of studying the relative numerosity of these cone types in the human retina using *in vivo* (psychophysics, electroretinography) (Cicerone and Nerger, 1989; DeVries, 1948) and *ex vivo* (mRNA analysis, microspectrophotometry) (Dartnall et al., 1983; Hagstrom et al., 1998) approaches. However, the first direct visualization of the trichromatic cone mosaic was made possible through the use of flood-illuminated AO retinal imaging coupled with retinal densitometry (Hofer et al., 2005a; Roorda and Williams, 1999). The L:M cone ratio was highly variable between subjects, and their relative arrangement within the mosaic was disordered; however, not all subjects had random organization, with some showing local clumping of cones of like type. Each cone in the retinal image is false-colored red, green, or blue according to its spectral subtype, and while this may convey some technical inaccuracies (Hofer et al., 2005b; Sabesan et al., 2016) about how the individual cone types subserve color perception, they are nonetheless aesthetically useful (Figure 4).

Though a wealth of information is available in these images, it takes multiple imaging sessions over multiple days to infer the spectral identity of individual cones within a small patch of parafoveal retina. Using AOSLO to measure bleaching kinetics, (Sabesan et al.,

2015) reduced the process of labeling the spectral identity of individual cones from days to hours. Offering further efficiency, stimulus-induced optical phase changes were monitored with AO-OCT, allowing cones to be spectrally identified based on their differential responses to a long-wavelength (637 nm) bleach (Zhang et al., 2019b). Regardless of the method used, the ability to visualize the trichromatic cone mosaic has ushered in a number of psychophysical studies aimed at correlating the spatial and spectral topography of the three cone types with various perceptual tasks (Hofer et al., 2005b; Sabesan et al., 2016; Schmidt et al., 2018a; Schmidt et al., 2018b). While this is interesting from a basic science perspective, there may be clinical applications as well, as discussed in Section 3.

2.1.2 Imaging the rod photoreceptor mosaic—Even though rods outnumber cones nearly 20-to-1 in the normal human retina, rods are difficult to visualize with AOSLO due to their smaller diameter compared to cones. Rods were first captured with an AO flood-illuminated system in achromatopsia (ACHM), which was possible due to a significant reduction in cone density that resulted in an apparent increase in rod diameter (Carroll et al., 2008). Using the same device, (Doble et al., 2011) used post-processing (deconvolution and filtering) to resolve smaller structures between the cones that matched the expected spacing of rods from histological studies. Around the same time, improvements in AOSLO optical design were used to decrease overall system aberrations, resulting in more accurate wavefront correction and reduced beam-wandering in the pupil plane (Burns et al., 2007; Dubra and Sulai, 2011; Merino et al., 2011). Further improvements in resolution came from using a smaller confocal pinhole and a shorter imaging wavelength. Albeit with somewhat variable success across patients and devices, these strategies allowed direct visualization of the rod photoreceptor mosaic in the normal retina within the central 12 degrees of the retina.

The greatest barrier to producing accurate rod metrics in more eccentric retinal locations is disambiguation of rods and the cones with variable reflectance profiles described above. Two factors exacerbate this – the increasing prevalence of these complex profiles with increasing diameter and eccentricity, where rods are more numerous, and the difference in the depth of focus of at which rods and cones are best visualized (10 – 20 μm), meaning that when rods are nicely resolved, these complex cone reflectance profiles are most prominent (Dubra et al., 2011). Split detection images can be used to aid with this specific difficulty (Figure 3), but accurate identification remains challenging even for experienced AOSLO image graders (Morgan et al., 2018). Another strategy for improving rod visualization relates to their variable reflectance. Irrespective of the AO imaging modality, the reflectivity of individual rod (and cone) photoreceptors is inherently variable, over space and time (Cooper et al., 2011; Pallikaris et al., 2003; Zhang et al., 2006). By averaging images of the same retinal location acquired at different times, the contrast of individual cells improves (Cooper et al., 2011). This not only improves the ability to resolve neighboring rods, but can also result in a more uniform appearance of the larger cones (Cooper et al., 2011; Dubra et al., 2011).

A number of factors make rod photoreceptors more challenging to visualize with AOSLO than cone photoreceptors, especially in the periphery; their smaller diameter, different refractive index, and the potential for greater interference of RPE with their light reflex, as well as an increased Stiles Crawford effect. These factors are presumed to have

contributed to the incomplete visualization of rod photoreceptors at wider eccentricities with a multimodal AO system reported by Liu et al. (2018) Nevertheless, key AOSLO studies have successfully imaged rod photoreceptors centrally in diseased subjects and more eccentrically in normal retinas out to 30 degrees nasal and temporal (Wells-Gray et al., 2016), and density measurements taken from these images are in line with histological measurements (Curcio et al., 1990), showing rod density increasing up to 25 degrees temporally and 20 degrees nasally, and decreasing with eccentricity from there.

2.2 Retinal pigment epithelium (RPE)

The RPE plays a vital role in the maintenance and support of the overlying photoreceptors, and RPE dysfunction is directly linked to several disease states (Lakkaraju et al., 2020; Sparrow et al., 2010). Owing in large part to the presence of melanin, RPE cells are highly light scattering structures which creates both opportunities and challenges to imaging them *in vivo* (Pollreisz et al., 2020). Here we review the evolving AO-based imaging approaches used to resolve the RPE mosaic over the last 15 years.

2.2.1 Imaging RPE reflectance—Given the strong light scattering properties of RPE cells and their diameter of approximately 10 micrometers (many multiples of the cone photoreceptors), these structures should be easily resolvable with AOSLO. However, low internal contrast and proximity to the overlying high-contrast photoreceptors obscures the RPE, exceeding the axial optical sectioning capabilities of AOSLO and making them an elusive cell to image. The first *in vivo* AOSLO images of the human RPE mosaic were obtained by capitalizing on the absence of light-scattering photoreceptors in subjects with cone-rod dystrophy and photoreceptor atrophy (Roorda et al., 2007) (Figure 5). Interest in reflectance-based imaging stems from light safety concerns with AF techniques, discussed below. One such technique successfully used to image RPE cells, ‘dark field’ AOSLO imaging, is achieved by directing confocal light to one detector while non-confocal light is split between two other detectors. The image of the RPE is constructed from the average of the two non-confocal images. Dark field imaging is considerably more comfortable for subjects than combining AO with short-wavelength autofluorescence (SW-AF) imaging (see below, section 2.2.2.1). However, lower contrast on dark-field imaging compromises image quality and creates difficulty identifying RPE cells in rod-dominated areas of the retina due to ‘point-like structures’, thought to represent residual photoreceptor signals (Scoles et al., 2013). Additional techniques aimed at reducing non-confocal light back-scattered by the photoreceptors did not improve the contrast of the RPE mosaic (Scoles et al., 2013).

High speed (120,000 depth scans/second), ultrahigh resolution OCT in combination with AO and an achromatizing lens, for compensation of monochromatic and longitudinal chromatic ocular aberrations, respectively, produces superior axial and lateral resolution and three dimensional cellular level images of many structures that had traditionally been difficult to image, including the RPE (Torti et al., 2009). AO-OCT can reveal subcellular RPE details and even organelle motility – a feature that has the potential to become a biomarker of RPE health (Liu et al., 2016; Liu et al., 2019). Multimodal AO imaging confirms cell densities and cone-to-RPE ratios equivalent to previous studies (Liu et al., 2018). Transscleral optical phase images (TOPI) of the retina provide high-resolution images of

all retinal layers and RPE cells. TOPI uses near infrared light to illuminate the retina through the sclera and reveals RPE cell structure with high contrast because signals from cone photoreceptors imaged with transpupillary illumination are highly reflective due to the optical Stiles-Crawford effect (Gao et al., 2008). By bypassing transpupillary illumination, TOPI offers a quantitative, non-mydriatic method of imaging RPE cells without extrinsic dye or exposure to short-wavelength light (Caetano Dos Santos et al., 2020; Laforest et al., 2020).

2.2.2 Fluorescence-based RPE imaging

2.2.2.1 Autofluorescence (AF): Autofluorescence fundus imaging has become an important component of any diagnostician's toolkit, and is particularly well poised to inform on the status of the RPE, given its inherent fluorophores. Its full capabilities and their applications are discussed in a recent review (Schmitz-Valckenberg et al., 2020). Imaging the RPE through intact photoreceptors with AO was first achieved in non-human primates (Morgan et al., 2009a) (Figure 5). Reflectance and SW-AF imaging were simultaneously captured – reflectance images were used to determine image registration parameters, and AF images of the RPE were subsequently averaged to reveal a honeycomb mosaic – a hypoautofluorescent center with hyperautofluorescent surround caused by the distribution of lipofuscin within the cytoplasm, outside of the nucleus (Morgan et al., 2009a).

Application of this AF technique in humans reveals RPE cell densities largely in agreement with histological data (Ach et al., 2014; Snodderly et al., 2002; Watzke et al., 1993), and decreasing density with increasing eccentricity (Morgan et al., 2009a). Higher exposure levels to short wavelength light are required for this AO AF method, raising safety concerns. Following use of this technique in macaques, progressive changes in AF were seen in areas exposed to 560 nm light while the same phenomenon was not seen in areas exposed to 830 nm light (Morgan et al., 2008). This was particularly concerning given the potential clinical application of these techniques to imaging compromised retinae with established disease and provided impetus to investigate alternative approaches. AO combined with two-photon imaging showed some promise for visualizing the RPE in non-human primates, but at light exposures beyond the maximum permissible in humans (Sharma et al., 2016).

The RPE mosaic has been successfully imaged with AO assisted SW-AF (Morgan et al., 2009a) and NIR-AF (Liu et al., 2017b) in healthy subjects and those with pathology including radiation retinopathy, age-related macular degeneration, drusen and geographic atrophy (Grieve et al., 2018). The images from each modality rely on the different fluorophores within the RPE cells: lipofuscin for SW and likely melanin for NIR, and thus the characteristics of the RPE mosaic with each modality are slightly distinct (Granger et al., 2018). Cell size and location are similar in both SW-AF and NIR-AF images. They conclude that while SW light is not required to resolve RPE cells, it does provide higher contrast images relative to NIR-AF images. The group reported that the one subject in which images were not obtained was the first subject imaged, and difficulties were suspected to have been due to optimization of the imaging protocol. Differences in cell fluorescent structure and visibility beneath vasculature were observed between modalities (Granger et al., 2018).

One cause for concern was subsequent reports of an 8–13% reduction in NIR-AF in subjects of studies employing NIR light sources to minimize light damage. Though these changes were temporary, with resolution seen between 1 and 21 months the fact that they occurred at light exposures <4% of the maximum permissible and only 10–15% of retinal radiant exposures previously observed to cause reduction in NIR-AF is concerning (Masella et al., 2014b). Work is ongoing to elucidate the mechanism responsible for changes to RPE cells in response to imaging and determine whether these changes are indicative of true cellular damage (Dhakal et al., 2020; Masella et al., 2014a; Morgan et al., 2008; Morgan et al., 2009b; Schwarz et al., 2018; Schwarz et al., 2016; Strazzeri et al., 2014). Irrespective of the outcome of these studies AO may be used to inform safety standards for other, more commonly used clinical ophthalmic imaging given the exquisite sensitivity of imaging with the improved resolution capable with AO.

2.2.2.2 Fluorescence lifetime imaging ophthalmoscopy (FLIO): The retina has intrinsic fluorescent properties first measured in 1994 (Delori, 1994). Initial interest was primarily in lipofuscin as the major retinal fluorophore, and its link to pathology with its accumulation in the RPE cells with age and AMD. Initial studies examining fundus autofluorescence linked changes in RPE AF to AMD, and greater interest was piqued in understanding the full fluorescent constituents of the retina and their potential link to disease. One way to examine this was to infer the presence of different fluorophores within the retina based on known *in vitro* emission spectra and timing of their decay. This was first described by (Schweitzer et al., 2004) in 2004, with an expansion of the characterised fluorophores ‘toward metabolic mapping of the human retina’ described in 2007 (Kayatz et al., 2001; Schweitzer et al., 2007). In normal human retinae, shortest fluorescence times are at the fovea and increase towards the periphery of the macula (Dysli et al., 2017; Kwon et al., 2019). Although the fundus AF emission spectra and timings are only validated by *in vitro* calibrations, e*x vivo* investigations in porcine eyes show lipofuscin in the RPE fluoresces to SW light, supporting the *in vitro* findings (Schweitzer et al., 2007). Significant differences in these measurements can be detected with age (Bernstein et al., 2019; Kwon et al., 2019), in patients with diabetic retinopathy (Schmidt et al., 2017) and may even be used as markers for disease progression in choroideremia (Dysli et al., 2016b) and Stargardt disease (Dysli et al., 2016a). Although the reported findings to date are empirical, disambiguation of the signatures is still necessary (Schmitz-Valckenberg et al., 2020), and a thorough pathophysiological explanation for these differences requires larger prospective studies, combination of AO with FLIO holds great promise in this regard. Feeks and Hunter (2017) have demonstrated two-photon based AO-FLIO in the mouse retina – this technique adapted for humans may prove useful in this pursuit.

2.2.2.3 Indocyanine green (ICG) assisted fluorescence imaging: While the endogenous fluorescence of RPE cells is imaged using NIR and SW-AF, ICG dye is an exogenous source of fluorescence used in clinical imaging of the choroid (Destro and Puliafito, 1989). Following intravenous injection for imaging purposes it results in late staining of RPE cells for up to 24 hours. The localization of this staining to the RPE layer was confirmed in histological samples from mice (Tam et al., 2016). Although ICG can be used clinically to identify choroidal neovascularization (Destro and Puliafito, 1989; Dobi et al., 1989;

Schneider et al., 1997), late staining observed with ICG was not associated with neovascular complexes in histological studies from mice (Tam et al., 2016) and though early reports describe late staining of CNV by ICG, this finding is not uniform (Schneider et al., 1997). AOSLO-ICG ophthalmoscopy revealed heterogenous fluorescence signals across the RPE mosaic (Tam et al., 2016) (Figure 5). A subsequent study by the same group showed the heterogeneous pattern was robustly reproduced longitudinally in human subjects (Jung et al., 2019). Thus, ICG AOSLO imaging represents a promising modality for imaging the RPE. Identification of the sources of the heterogeneous signal between cells could facilitate detection of subclinical changes within the RPE in disease. Although as with all fluorescence imaging techniques light safety concerns remain to be fully investigated, ICG AOSLO employs near-infrared (NIR) light, which may have less potential for retinal damage than SW-AF, but the risk of intravenous injection using ICG may cause bruising and poses a small risk of allergic reaction (Tam et al., 2016), thus the potential benefit to the subject must be clearly elucidated.

2.3 Inner retinal layers

The majority of AOSLO (and other AO-based imaging modality) applications discussed to this point are focused on the outer retina. This is primarily due to three factors – the ease of imaging photoreceptors (discussed above), the involvement of the outer retina in a wide variety of inherited and age-related diseases, and the position of the photoreceptors as “the initiator of vision”. In addition, AOSLO has also been employed to image the inner retina, though with minimal success. Although AOSLO provides superior contrast and lateral resolution of nerve fiber bundles in the retinal nerve fiber layer (Huang et al., 2014; Swanson et al., 2019; Takayama et al., 2012), the relative transparency of the inner retinal layers required for normal vision results in reduced image contrast of most layers. Secondly, the organization of inner retinal layers, multiple cells thick, by contrast to the monolayers of the RPE and the photoreceptors, represents a challenge to the limited axial resolution of AOSLO. The greatest success in imaging inner retinal cells in animals has been with transgenic models (Geng et al., 2012; Schallek et al., 2013), by inducing the expression of fluorescent proteins (McGregor et al., 2018) or via invasive methods using delivery of exogenous contrast agents directly into the lateral geniculate nucleus (Gray et al., 2006). These invasive methods most certainly will not be translatable to humans. However, approaches that involve delivery of exogenous contrast in less invasive ways – such as intravenously – are already accepted clinically, as in fluorescein and ICG angiography. Recent studies have used intravenous annexin-V in humans to detect ganglion cells undergoing apoptosis (Cordeiro et al., 2017) in a technique called detection of apoptosing retinal cells (DARC), evidence that requirement for exogenous contrast alone does not necessarily contraindicate exploring a technique in human research subjects.

Owing to novel AOSLO detection schemes aimed at revealing low-contrast structures, there has been some recent success in resolving individual ganglion cells in the human retina (Rossi et al., 2017). The close agreement between measures of cell soma diameter from the AOSLO images and previous estimates from histology provide confidence that these structures are indeed ganglion cells, though the study included only a small number of subjects. Additionally, multi-volume averaging techniques using AO-OCT have also

recently revealed exquisite images of the retinal ganglion cell mosaic (Liu et al., 2017c). The AO-OCT approach not only delivers higher contrast images of the ganglion cells, but also provides volumetric images with superior axial sectioning capabilities compared to AOSLO. While also only applied to a small number of subjects and requiring extensive image processing, the quality of these images is so striking that their clinical potential is undeniable. In addition, the underlying contrast generating mechanisms for these translucent cells have recently begun to be modeled (Guevara-Torres et al., 2020), which should aid in the application these techniques to more widespread study of human disease.

Aside from cell bodies, other microscopic structures at the level of the inner retina can be resolved with AO imaging, such as Gunn's dots (hyperreflective foci found in the inner retina). Their constituents, structure and significance are yet unproven, despite their first description in the literature in 1883 (Gunn, 1883). They are hypothesized to be Müller cell end feet or hyalocytes. Although Gunn's dots can be identified on regular fundus photography, AO imaging is contributing to elucidation of their anatomy. Initial imaging with NIR AO flood-illumination revealed directional variability in line with an internal limiting membrane (ILM) locus (Paques et al., 2015). More recent AOSLO and AO-OCT combined images confirm an axial location at the ILM, without extension into the vitreous or the retinal nerve fiber layer (Hammer et al., 2020). Cross-sectional images through the Gunn's dots were possible with this approach, and comparisons between healthy subjects and glaucoma suspects prompted suspicion of microglia as the origin of Gunn's dots. Features similar to Gunn's dots have been reported in other neurological diseases such as Parkinson disease, multiple sclerosis (Scoles et al., 2014a) and LaFora disease (Heitkotter et al., 2020). As they have also been identified in a high proportion (82%) of normal young subjects (Boberg-Ans et al., 2017), it remains unknown what their clinical significance may be.

2.4 Vascular structure

Clinical monitoring of the retinal vascular system is not only important for retinal vascular diseases, but also a number of systemic diseases. It has the potential to provide a strategic, non-invasive window into the health of the systemic microvasculature. This has potential clinical utility for early identification of vascular remodeling that can accompany underlying multisystem microangiopathy found in common systemic disorders including diabetes and hypertension. Optical coherence tomography angiography (OCT-A) is the most commonly used clinical imaging modality to image the retinal vasculature, with fluorescein angiography and ICG angiography forming other components of the retinal vascular imaging armamentarium. Multiple different AO techniques have been used to successfully image the retinal vasculature, recent reviews of which are available elsewhere (Bedggood and Metha, 2020; Paques et al., 2018). Each has its own limitations and specific advantages which we will discuss here.

The dependence of traditional, non-AO imaging techniques on vessel contents to delineate vessels (motion contrast in OCT-A (Hagag et al., 2017) and optical contrast of blood constituents in color fundus photography) causes a systematic underestimation of vessel size (Mo et al., 2016). Estimation of clinically relevant measures of vessel morphology such

as the wall-to-lumen ratio, an indicator of vessel hypertrophy in response to hypertension (Heagerty et al., 1993), are not possible with these imaging modalities given the relatively static nature and optical translucency of the cells of the vessel walls. AO flood-illumination imaging has been used to calculate these ratios and showed the expected correlation between increased blood pressure and wall-to-lumen ratio (Koch et al., 2014). These methods could be used to calculate cross-sectional area of the vascular wall and distinguish between eutrophic and hypertrophic vascular remodeling (Meixner and Michelson, 2015).

The AO flood system described by Koch et al. (2014) revealed vascular wall details down to the level of the smallest precapillary retinal arterioles; however, AOSLO with video processing techniques that enhance motion contrast have allowed imaging down to the smallest parafoveal capillaries (Tam et al., 2010). Multiple approaches to enhance the resolution of the vasculature with AOSLO reflectance have been employed including use of forward scatter (Chui et al., 2012), offset pinhole (Chui et al., 2013) and split detection (Sulai et al., 2014). Vascular wall cells, called pericytes, were first imaged using offset pinhole (Chui et al., 2013; Pinhas et al., 2013), a technique employed to successfully image pathological microaneurysms in diseased retinae (Chui et al., 2014). Dark-field AOSLO using multiply scattered light demonstrated the morphological features of vessel walls and their dependence on vessel diameter (Chui et al., 2013).

Though in mice, recently published work characterizing intravital behavior of immune cells in response to endotoxin induced uveitis is very exciting. Overcoming previous confounders like the use of surgical techniques, exogenous substances or transgenic strategies to induce inflammation or enhance visualization of cells, Joseph et al. (2020) use AOSLO with phase contrast and time lapse videography to dynamically document the behavior of myeloid cells within the retina. Use of AOSLO in correlative human studies will allow direct examination of the behavior of immune cells at the root of myriad inflammatory disorders. This is sure to be illuminating not only for troubling ocular inflammatory conditions but would also have implications for our understanding of the function and dysfunction of the immune cells in systemic inflammatory disorders.

2.5 Blood flow

AO imaging is useful not only in characterizing vascular structures, but also in imaging the blood flow within these structures – both binary assessments such as presence or absence (as in retinal vascular occlusions) or perfusion mapping and the characteristics of the flow, such as velocimetry. AOSLO has been combined with fluorescein angiography to produce ultra-high-resolution vascular maps that have slightly higher lateral resolution than motion contrast based OCT-A images; however, superior axial sectioning capabilities of OCT-A allows the visualization of superficial, middle and deep capillary plexuses (Park et al., 2016), which is not possible with SLO based technology. Both OCT-A and AO scanning based modalities are vulnerable to eye motion artifacts. These artifacts can interfere with the ability to assess blood flow velocity because the physiological motion within the vessels can be of similar velocity to the eye motion artifacts, making them difficult to distinguish from one another.

Flood imaging captured over shorter time periods is less vulnerable to these difficulties. AO NIR flood imaging was coupled with a new computational method relying on spatiotemporal filtering of the sequence to isolate blood flow from noise in low-contrast sequences. This provided a wide field of view, minimized distortion and addressed issues of low contrast, allowing calculation of blood flow velocity (Gofas-Salas et al., 2019). AOSLO fluorescein angiography can also capture simultaneous structure and flow information, and though the resolution of the images acquired with this method is exquisite, the minimal additional benefit over OCT-A images does not outweigh the small but present risks attendant to exogenous fluorescein administration. One advantage to retinal vascular imaging with fluorescein or ICG with or without AO is the ability to detect leakage from capillaries and vessels, which is not possible with OCT-A and may indicate microscopic damage to capillary endothelial cells in eyes with retinal vascular disease before these are visible on standard dye-assisted fundus angiography techniques.

Another effective strategy for imaging blood flow with AOSLO systems involves tracking leukocyte motion within vessels. Leukocytes appear as bright spots on AOSLO images, which may occur by direct visualization of the leukocytes or ‘indirect’ visualization due to reflection of light from underlying photoreceptors (Martin and Roorda, 2005). The smallest capillaries in the retinal vasculature are narrower in diameter than erythrocytes and therefore cause their “squeezing” and aggregation as they pass through. These are seen as darker shadows or tails that follow the leukocytes and their velocity has been examined as a marker of retinal hemodynamics (Arichika et al., 2013). Methods for taking into account the speed of three moving entities in relation to one another – blood flow movement relative to background tissue, background tissue in relation to eye movement and the motion of the AOSLO as it performs raster scanning – to accurately determine blood flow velocity were described by Tam and Roorda (2011).

Leukocytes make up only 1% of blood cells, therefore imaging based on their movement suffers from temporal sparsity and is limited to smaller vessels in which the blood flow forms a single column. The velocity of erythrocytes, which make up 40–50% of blood volume, can be imaged in medium-sized vessels using confocal AOSLO. Despite traditionally lower frame rates due to the time required to form the image, a technique to ‘freeze’ scanning on the cross-section of a single vessel facilitates accurate reconstruction and measurement of flow (Zhong et al., 2008). This method has been employed to examine the variation of blood flow throughout the cardiac cycle (Zhong et al., 2011) and has been adapted to image a range of vessel sizes in animal models non-invasively with safe light levels (Joseph et al., 2019). Line scanning can facilitate a faster scan rate up to 800 Hz but with sacrifices in field of view (Flower et al., 2008; Gu et al., 2018).

3. Understanding physiology and pathology in disease

As reviewed in the previous section, AOSLO enables non-invasive imaging of many different cell types with single-cell resolution. Accordingly, there are a host of fundamental neuroscience and basic biological questions that have been explored with AOSLO (Burns et al., 2019; Roorda and Duncan, 2015; Williams, 2011), but we will focus on clinical applications here. We have chosen a subset of the hundreds of clinical studies using AOSLO

to review here as they provide clear examples of both the promises and pitfalls of AOSLO in the clinical realm – specifically with respect to photoreceptor imaging.

3.1 Inherited color vision defects

While there were earlier reports of applying AOSLO to image the retina in patients with cone-rod dystrophy, (Duncan et al., 2007; Wolfing et al., 2006) the first examples where AO imaging enabled a significant discovery relating to disease mechanism came from studies in individuals with inherited red-green color vision deficiency (Carroll et al., 2004). Clinical applications have expanded to other less common forms of color vision deficiency and we review these below.

3.1.1 Red-green color vision deficiency—Congenital red-green color vision defects are due to mutations within the *OPN1LW* and *OPN1MW* photopigment gene array on the X chromosome and affect approximately 8% of men (Neitz and Neitz, 2011). Normal trichromatic color vision requires expression of functional *OPN1LW* and *OPN1MW* genes in the retina, which results in the existence of L- and M-cone classes, respectively. The relationship between genotype and the severity of color vision deficiency is fairly well understood (Neitz and Neitz, 2011). Anomalous trichromacy is the most common variant of red-green color vision deficiency and arises when the first two genes in the array encode spectrally-distinct photopigments belonging to the same spectral class (L- or M-), resulting in a retina that contains either two types of L cone (deuteranomalous trichromacy) or two types of M cone (protanomalous trichromacy). The more severe dichromatic phenotypes arise when patients have only a single functional gene in their array (a single functional *OPN1LW* gene results in deuteranopia, while a single functional *OPN1MW* gene results in protanopia). This can be due to a deletion of all but one of the genes in the array or a mutation within the other gene(s) in the array.

Given that mutations within the rhodopsin gene, which encodes the photopigment in rods, cause degeneration of rod photoreceptors, it seemed plausible that similar mutations in the *OPN1LW* and *OPN1MW* photopigment genes could not only result in a loss of function but may also cause changes in photoreceptor structure. This was first explored using a flood-illuminated AO fundus camera – patients with a single *OPN1LW* or *OPN1MW* gene had a contiguous cone mosaic (Carroll et al., 2009; Carroll et al., 2004; Wagner-Schuman et al., 2010). This was not unexpected given the stochastic nature of gene expression within the *OPN1LW* and *OPN1MW* photopigment gene array – when only a single gene is present, the non-S cones simply express the remaining gene in the array. In contrast, a sparse array of gaps (Figure 6) in the mosaic was visible in a patient harboring a unique *OPN1MW* variant that results in exon skipping, and thus no functional photopigment (Carroll et al., 2004). Subsequent work with split-detector AOSLO showed that these gaps contained remnant IS of non-functional cones (Patterson et al., 2018), so we now believe that the presence of this gene variant disrupts normal OS structure and thus normal waveguiding is impaired. Other work in patients with missense mutations revealed contiguous but disordered cone mosaics, suggesting early degeneration of the cones expressing the mutant photopigment (Carroll et al., 2012).

3.1.2 Blue cone monochromacy (BCM)—Blue cone monochromacy (BCM) is an X-linked condition characterized by absence of both L- and M-cone function. Like the red-green defects, there are multiple genetic pathways that lead to BCM – often referred to as 'one-step' or 'two-step' pathways (Ayyagari et al., 2000; Nathans et al., 1989; Nathans et al., 1993), though it is more useful in the modern era to disclose the specific mutations. One mutational pathway involves a deletion in the cis-regulatory DNA elements (locus control region; LCR) necessary for transcription of the L- and M-opsin genes. The other genetic pathway involves the presence of a mutation in all of the expressed *OPN1LW* and *OPN1MW* genes in the array, with the most common mutation being the C203R substitution. In most cases, the presence of this mutation is accompanied by gene rearrangements that result in only *OPN1LW* or *OPN1MW* genes being present (thus the 'two-step' nomenclature). Regardless of the underlying genetic mechanism, affected individuals have poor acuity (20/80 to 20/120), impaired color discrimination, myopia, nystagmus, and minimally detectable photopic electroretinogram (ERG) responses with normal amplitudes and delayed timing of scotopic responses (Nathans et al., 1989). There is accumulating evidence for macular atrophy and progressive loss of visual function in BCM (Ayyagari et al., 1999; Fleischman and O'Donnell, 1981; Kellner et al., 2004; Michaelides et al., 2005; Mizrahi-Meissonnier et al., 2010) though it is not currently understood why some individuals show progression and others do not.

There has been successful restoration of cone function in a mouse model of BCM (Deng et al., 2018; Zhang et al., 2017b). As such, understanding cone structure in BCM has taken on increased clinical importance in recent years. Given how rare BCM is, the ability to obtain cellular-resolution assessment of retained photoreceptor structure is of tremendous value in identifying which patients may be most likely to benefit from therapies that emerge for human trials. Initial imaging with confocal AOSLO revealed an absence of normal cone structure at the central fovea (Carroll et al., 2012), with the pattern of visible cells (presumably S-cones) revealing what appears to be the S-cone-free zone known to exist at the foveal center (Curcio et al., 1991) (Figure 7). Presence of remnant L- and M-cones in the retina of individuals with BCM caused by an LCR deletion was confirmed using OCT and AOSLO (Cideciyan et al., 2013). This is somewhat controversial though, as the absence of any opsin in a photoreceptor is not thought to be compatible with cell viability (Carroll et al., 2010). More recently, work with split-detection AOSLO has revealed cone IS structures in the retina of individuals with BCM caused by multiple C203R mutations (Patterson et al., 2017). These cells were at a density higher than that expected for the S-cone mosaic and in many cases they co-localized with hyporeflective cells in the confocal image – offering support for an interpretation that they are indeed remnant non-functional L/M cones. However, an alternate explanation is that post-natal migration of S cones in the absence of L/M cones results in an altered topography of the S-cone mosaic. It may be that some of the evolving advanced AO-OCT methods could be leveraged in these patients to assess both the IS and outer segment (OS) structure with greater axial precision and to conclusively identify the location of the S-cones (Zhang et al., 2019a).

3.1.3 Achromatopsia (ACHM)—Patients with congenital ACHM have severely diminished or absent cone function, with about 70–80% of cases due to mutations in the

genes encoding the alpha and beta subunits of the cone cyclic-nucleotide gated ion channel (*CNGA3* and *CNGB3*, respectively) (Michaelides et al., 2004). Symptoms include reduced visual acuity, increased light sensitivity, nystagmus, and a lack of color discrimination. ACHM is thought to be a stationary condition – the reduced visual acuity, photoaversion, and impaired color discrimination are largely stable throughout life, though nystagmus tends to decrease with age (Michaelides et al., 2004; Simunovic and Moore, 1998). However, there are conflicting reports regarding the stability of retinal structure over the lifespan of individual subjects. Several cross-sectional studies report increasingly abnormal cone structure imaged with OCT at older ages (Langlo et al., 2016; Thomas et al., 2012; Yang et al., 2014). Longitudinal OCT studies (mean follow-up duration of 62 months) revealed minimal change in outer retinal structure, although 6 of the 50 patients (12%) showed qualitative progression of foveal structure between baseline and follow-up, and a small (average < 2 um) but significant increase in outer nuclear layer thickness, which the authors attributed to intervisit variation in scan placement in eyes with nystagmus (Hirji et al., 2018). Most clinical trials in inherited retinal degenerations are expected to last between 12–48 months since clinically significant changes in current standard outcomes such as ellipsoid zone band and quantitative perimetry have been reported over that time frame (Birch et al., 2015; Csaky et al., 2017). Comprehensive natural history data over periods of time comparable to the length of a clinical trial are invaluable, as they provide an expected rate of change against which to assess any therapeutic response in treated patients.

In fact, as with BCM, recent years have seen renewed clinical interest in ACHM, as gene replacement therapies have proven effective at restoring cone function in multiple animal models of ACHM (Zobor et al., 2015). AOSLO has played a critical supporting role in translating these successes to human trials, providing direct evidence of remnant cone structure in patients with ACHM. An early case report in a patient with *CNGB3*-associated ACHM revealed absence of normal cone structure using flood-illuminated AO, with dark gaps throughout the retinal images (interleaved amongst presumed rod photoreceptors) (Carroll et al., 2008; Genead et al., 2011). However, the presence of remnant cone IS structure was confirmed in these patients by aligning the structures visible in split detector AOSLO images with the dark gaps in the confocal AOSLO photoreceptor mosaic (Figure 8) (Scoles et al., 2014b). A larger subsequent natural history study of *CNGB3*-associated ACHM revealed that while all patients had remnant cone structure, peak foveal cone density was significantly reduced compared to normal values (Langlo et al., 2016). This direct evidence that the necessary cellular target for gene replacement therapy exists in nearly all patients with ACHM provides the basis for the potential success of phase I/II studies underway at multiple sites around the world (ClinicalTrials.gov Identifiers NCT02599922, NCT02935517, NCT03758404). However, the degree of remnant cone structure was highly variable between patients (Figure 9) (Langlo et al., 2016). Such variability suggests that not all patients with ACHM may have the same therapeutic potential – all other things being equal, patients with more remnant cones may have greater potential for functional recovery. As is the case with BCM, the ability to identify patients with the greatest potential of success for gene replacement therapy could be enormously valuable to early phase trials where patient cohorts are typically smaller in number. The emerging importance of such data

requires tools that can provide accurate measures of the extent of residual cone structure (see Section 4).

Continued AOSLO studies in patients with ACHM have revealed a number of new insights related to the disease. First, longitudinal studies lasting up to 26 months have not shown significant changes in cone structure assessed with AOSLO (Langlo et al., 2017), in agreement with some of the OCT studies mentioned above. In addition, a recent study has observed a high degree of inter-ocular symmetry of remnant cone structure within individual subjects (Litts et al., 2020), which suggest the contralateral eye could be used as a control for the treated eye in longitudinal clinical trials. Finally, detailed studies have so far failed to identify any differences in cone structure in patients with *CNGA3*- vs *CNGB3*-associated ACHM (Georgiou et al., 2019a). In contrast, AOSLO has shown that patients with *GNAT2*-associated ACHM have relatively well-preserved cone structure (Georgiou et al., 2020), while a near absence of cone structure was reported in all patients with *ATF6*-associated ACHM (Mastey et al., 2019). Patients with *PDE6C* mutations present with typical symptoms of ACHM but show a slowly progressive maculopathy and little residual macular cone structure in adulthood (Georgiou et al., 2019b). Taken together, these various studies suggest there is a range of therapeutic opportunity in patients with ACHM, both between and within genotypes.

3.2 Retinitis pigmentosa (RP)

Rods are the primary site of disease in retinitis pigmentosa (RP), causing difficulty with night vision and mid-peripheral visual field loss. Eventually cone function is also affected, either secondary to rod degeneration or directly in forms of RP caused by genes expressed in both rods and cones. AO imaging enables characterization of cones in eyes with RP, both in combination with flood-illuminated (Gale et al., 2019) and AOSLO systems (Duncan et al., 2007; Makiyama et al., 2013; Sun et al., 2016a). The ability to isolate the IS and OS structure of the photoreceptor is important, as photoreceptors are thought to degenerate in a stepwise fashion – first with changes to the OS, then the IS, and finally the nucleus (Milam et al., 1998). As different modalities depend on different aspects of retinal structure to create images, their use can be complementary and provide synergistic information regarding disease pathophysiology and progression. Shortening of the OS can be adequately estimated by bulk OS band thickness measurements on standard OCT but the potential for segmentation error is high (Stepien et al., 2014). AO flood imaging can be used to assess change of OS length (Jonnal et al., 2010) but definitive OS length measurements require ultra-high resolution AO-OCT to measure optical path length (Liu et al., 2016). AOSLO can also be used to estimate cone IS diameter (Scoles et al., 2014b), with enlarged remnant cones being demonstrated in RP (Sun et al., 2016a) and choroideremia (Sun et al., 2016b).

Using multiple imaging modalities (AOSLO in combination with OCT) to image the same patch of retina in RP patients could provide a means to stage the relative state of degeneration on a more focal basis, potentially even allowing the staging of the health of individual cells (Foote et al., 2019b; Foote et al., 2020; Sun et al., 2016a; Sun et al., 2016b).

AOSLO images of the cone mosaic have been correlated with images from other modalities, including OCT, SW-AF, NIR-AF and OCT-A, to characterize the retinal phenotype of

many different genetic forms of RP. The relationship between AOSLO and OCT differs in different conditions, and the features provide insight into how different genetic mutations affect cone and rod photoreceptors. For example, eyes with choroideremia show early loss of choriocapillaris flow, whereas eyes with achromatopsia and *RPE65*-related retinal degeneration often show retained cone structure in regions with severely reduced function. Subjects with RP may have lower macular photoreceptor density, even in the presence of preserved acuity. OS length and outer nuclear layer (ONL) thickness measured on OCT are considered indirect markers of photoreceptor density, as the ellipsoid zone (EZ) or inner segment/outer segment junction band represents intact photoreceptor OS segments, and the ONL represents photoreceptor nuclei. AOSLO images showed reduced cone density correlates with ONL thinning at the fovea (Makiyama et al., 2013), although eccentricity is a better predictor of cone density than ONL thickness. Though there is an association between density and ONL thickness across all eccentricities in both normal subjects and RP patients, ONL cannot be used to predict cone density measurements (Menghini et al., 2014).

Patients with RP due to mutations in rod-specific genes like rhodopsin (*RHO*) may show similar cone losses in the macula as patients with mutations in genes expressed both in rods and cones, such as *RPGR,* but cone function and OS length is better preserved in patients with *RHO* mutations (Foote et al., 2020). When macular function was tested using AO, sensitivity per cone was normal in eyes with *RHO* mutations, but reduced in eyes with *RPGR* mutations (Foote et al., 2020) (Figure 10). Several genes that cause retinal degeneration result in dissociation between visual function and measures of retinal structure, including *RPGR* (Foote et al., 2020), *RPE65* (Jacobson et al., 2005), *RPGRIP1, TULP1, NPHP5,* and *CEP290* (Garafalo et al., 2019). When genes cause retinal degeneration where retinal structure does not predict function, the likelihood of visual improvement after therapeutic intervention is greater. In support of this principle, gene augmentation for patients with *RPE65*-related retinal degeneration received approval from the U.S. Food and Drug Administration (Russell et al., 2017) and patients with *CEP290*-related RP demonstrated visual improvement in response to treatment with an antisense oligonucleotide treatment (Cideciyan et al., 2019). As described above, *CNGA3*- and *CNGB3*-associated ACHM also demonstrate structure-function dissociation and therefore may be good candidates for gene augmentation. Even in retinal degenerations featuring structure-function dissociation, candidates for therapeutic improvement must be selected based on preserved retinal structure to predict improvement in visual function after treatment.

Syndromic forms of RP such as Usher syndrome types 1, 2 and 3 (Ratnam et al., 2013b; Sun et al., 2016a), in which rod-cone degeneration is associated with hearing loss, have shown lower cone density than RP (Sun et al., 2016a). Cone structure measured within 0.2 degrees of the foveal center correlates with visual acuity in eyes with RP (Bensinger et al., 2019; Foote et al., 2018; Ratnam et al., 2013a). Cone density decreases by up to 62% in eyes that retain visual acuity of 20/25 or better (Ratnam et al., 2013a; Sun et al., 2016a), suggesting AOSLO images may be a more sensitive measure of photoreceptor degeneration than measures from other modalities (Sun et al., 2016a). Cone spacing increases during longitudinal evaluation of RP patients while visual acuity does not change significantly (Bensinger et al., 2019). Longitudinal measures of cone density at selected regions of interest (ROIs) showed significant declines of about 20% over 2–3 years (Talcott et al.,

2011) (Figure 11), suggesting AOSLO cone metrics could also be a useful measure of disease progression or outcome measure for clinical treatment trials. Larger longitudinal studies of disease progression in eyes with RP are necessary to demonstrate intervisit, interocular and intergrader variability and rate of progressive cone loss over time (see Section 4).

As discussed, rods can be visualized with AOSLO systems (Dubra et al., 2011; Merino et al., 2011; Wells-Gray et al., 2016). Split detection images are necessary to reliably disambiguate cone and rod profiles on confocal AOSLO images (Morgan et al., 2018). As the lateral resolution of split detection images is lower, rods are not always clearly visualized on split detection. In patients with ACHM, the reduction in cone density results in the surrounding rods expanding to fill in the vacant space in the photoreceptor mosaic, allowing them to occasionally be resolved on split detection. There is one report of AOSLO imaging of rods in RP (Sun et al., 2016a), though they are not easily resolved (see Figure 12 for an example). Another contributing factor to the lack of routine imaging of rods in RP is that cone degeneration is secondary to rod degeneration in RP – by the time changes in the cone mosaic are seen in AOSLO, there has been significant rod loss. Developing improved techniques to resolve rod and cone structures in RP is essential for advancing our understanding of the early pathophysiological changes in RP.

3.3 Choroideremia

Choroideremia is an X-linked form of retinal degeneration, affecting about 1 in 50,000–100,000 males who carry hemizygous mutations in the *CHM* gene, which encodes Rab escort protein 1 (REP1) (Pennesi et al., 2019). Women with heterozygous *CHM* mutations may also develop retinal degeneration due to Lyonization (Coussa and Traboulsi, 2012; Renner et al., 2009; Syed et al., 2001; Syed et al., 2013). The *CHM* gene is expressed in all cells but doesn't have any extraocular manifestations. Although disease severity does not correlate with the extent or type of *CHM* mutation, levels of messenger RNA (mRNA) transcript produced by the mutant gene correlate with disease severity (Di Iorio et al., 2019). Because *CHM* is expressed in photoreceptors, RPE cells and choroidal cells (Bernstein and Wong, 1998), degeneration affects all cell types. The earliest manifestations of disease are rod-mediated, including nyctalopia, and rod function is reduced early in disease prior to visible RPE atrophy (Aleman et al., 2017). Choriocapillaris perfusion measured with OCT-A is also affected in regions of preserved outer retinal structure (Foote et al., 2019c; Jain et al., 2016). AOSLO images have demonstrated preservation of cone structure in the macula of patients with choroideremia (Morgan et al., 2014; Syed et al., 2013; Tuten et al., 2019) and extending beyond the margins of preserved RPE imaged using SW-AF (Foote et al., 2019b) (Figure 13). Split detector AOSLO has been used to visualize remnant cone IS in outer retinal tubulations, regions of RPE loss where photoreceptors remodel that are common in patients with choroideremia (Sun et al., 2016b; Tuten et al., 2019). AOSLO has also been used to deliver visual stimuli precisely to retinal regions with outer retinal tubulations, where visual function was recordable but severely reduced, suggesting photoreceptors in regions with RPE loss may not be amenable to gene augmentation therapies (Tuten et al., 2019) (Figure 13). However, the persistence of cone IS and cone profiles in confocal AOSLO images that extend beyond RPE visualized with SW-AF suggests the use of SW-AF as

an outcome measure to identify regions for treatment may underestimate retinal cells with potential to respond to therapy (Foote et al., 2019b). Combined with OCT and OCT-A, AOSLO may play an important role in identifying candidates likely to benefit from gene augmentation and may provide a more sensitive outcome measure of treatment response than SW-AF.

3.4 Albinism

Albinism is a multi-system inherited disorder that disrupts melanin biosynthesis and/or trafficking and presents with hypopigmentation of the skin, hair and eyes. Subtypes are classified depending on amount of residual melanin, presence or absence of cutaneous involvement, and presence or absence of other systemic associations such as platelet dysfunction in Hermansky Pudlak syndrome and immunodeficiency in Chediak Higashi syndrome. The most common inheritance pattern is autosomal recessive, followed by X-linked and rare dominant inheritance reported. The most common subtypes are oculocutaneous albinism (OCA) 1–7 and ocular albinism 1. Mutations in *TYR*, *OCA2*, *TYRP1*, *SLC45A2 SLC24A5*, *C10ORF11*, and *GPR143* account for most cases, however not all mutations have been identified and work is ongoing to identify all causative mutations (Montoliu et al., 2014; Simeonov et al., 2013). Regardless of gene implicated all forms of albinism are associated with abnormal development of the visual system; reduced visual acuity, foveal hypoplasia and aberrant decussation at the optic chiasm. Visual function is highly variable among subjects with albinism and there has long been an interest in understanding the anatomical basis of visual dysfunction in an effort to provide an accurate visual prognosis to families (since albinism can often be diagnosed at birth or shortly thereafter) and to guide therapeutic development.

The fovea is critical for high acuity vision and has a number of anatomical specializations relative to the rest of the retina. As such, the reduced visual acuity in albinism was initially attributed to the absence of a foveal pit (Seo et al., 2007). However, recent OCT studies have revealed enormous variability in the degree of foveal hypoplasia in albinism, with categorical clinical grading schemes developed to assess the severity of hypoplasia (Thomas et al., 2011). Grade 1 foveal hypoplasia is described as having a shallow foveal pit – further subdivided into 1a and b depending on whether this pit has normal pit characteristics or is a tiny dip by Wilk et al., 2014. Grade 2 does not have an identifiable foveal pit but has demonstrable OS lengthening. Grade 3 has no OS lengthening but ONL widening and Grade 4 demonstrates none of these features. Many individuals with poorly defined foveal pits according to these categorizations have relatively preserved visual acuity (Harvey et al., 2006; Summers et al., 1996), and there is significant overlap in visual acuity between these categorical foveal hypoplasia grades. (Curcio, 2001)This lack of concordance has motivated additional anatomical studies of the retina in albinism.

A comprehensive AOSLO study by (Wilk et al., 2014) revealed variable foveal cone density in albinism, with some patients having values within normal limits. This was in conflict with existing models of foveal development that suggested cone packing did not occur in the absence of a pit. Further work with OCT has advanced quantitative measures of other anatomical specializations of the foveal region, including ONL thickening and the

displacement of inner retinal layers (Lee et al., 2018; Woertz et al., 2020a). Rather than remarking on the presence or absence of a given specialization, high resolution imaging, including AOSLO, allows precise quantitative measurement of the structure of interest. This allows placement of any given retina on a developmental spectrum of foveal maturity relative to another retina, which may aid in future structure-function correlations in albinism. A similar approach is being taken in aniridia, another condition associated with foveal hypoplasia (Pedersen et al., 2019). An example of the anatomical manifestations of foveal hypoplasia in albinism is shown in Figure 14.

It is worth noting that, Wilk et al. (2014) did not observe a correlation between visual acuity and foveal cone density. This observation, together with the lack of a relationship between cone density and cortical magnification in albinism (Woertz et al., 2020b), suggests that altered post-receptoral connectivity of the foveal cones may underlie the visual acuity deficits in albinism. Larger studies seeking to incorporate estimates of foveal cone packing into their structure-function models are hindered by the inability to obtain high quality AOSLO images in a subset of those with albinism due to the presence of nystagmus. (Wilk et al., 2017) found that OS length measured using OCT correlates with peak foveal cone density in subjects with albinism. This relationship is consistent with histological data showing that cones have a nearly constant volume (Hoang et al., 2002), meaning that as cone packing density increases, the length of the OS would also increase. In this way, OS length can be used as a surrogate marker for foveal cone density. This is important as AOSLO is not widely available and is only successful in about 60% of patients with albinism, whereas OCT is widely available and high-quality OCT images can be obtained in upwards of 90–95% of these patients. Thus, even as the direct clinical applications of AOSLO imaging continue to be debated by some, the value of AOSLO in validating other clinical imaging approaches is nevertheless significant.

4. Photoreceptor-based biomarkers

Ophthalmic diseases have seen a rapid expansion of emerging treatments for previously untreatable disease like inherited retinal degenerations. Genetic therapies have been developed for safe delivery to retinal and RPE cells in animals and humans. As the pipeline of available treatments expands, clinical trials with sensitive measures are required to test the efficacy of the treatments. OCT measures have fulfilled this function to date. Despite the exciting images provided by AO-based retinal imaging tools, there have been no photoreceptor-based metrics validated or used as primary outcome measures for multicenter clinical trials. AOSLO certainly has a role to play – at very least in validation of OCT measures, and potentially in replacing OCT as the definitive means of characterizing photoreceptor structure for the purposes of clinical trials. The accurate establishment of photoreceptor structure offered by AOSLO is crucial in facilitating the selection of the appropriate therapeutic approach in specific disease groups – i.e., stem cell or implant therapies in those without any residual cellular structure – and identification of which patients within each group have potential to respond to therapy - as in ACHM where split detection imaging of remnant cone structure may represent a cellular pre-requisite for positive therapeutic response. This section will examine existing structural OCT and

AOSLO biomarkers and compare to potential novel AOSLO biomarkers. We present the evidence in support of and cautioning against their applications in clinical trials.

4.1 Structural AOSLO biomarkers

4.1.1 Defining the extent of photoreceptor damage—As the most commonly used imaging modality for quantitative imaging, OCT is regularly used to define the extent of photoreceptor damage in a wide range of retinal diseases. *En face* OCT imaging can reveal the extent of atrophic lesions in age related macular degeneration, which appear as bright areas due to increased light penetration into the choroid (Yehoshua et al., 2011). It is also possible to assess the cone photoreceptor layers on OCT. For example, the ONL is comprised of photoreceptor nuclei, and measuring the thickness of this layer theoretically provides a direct measure of photoreceptor structure (Jacobson et al., 2009). However, conventional techniques to assess the ONL ignore the contribution of the Henle fiber layer. Directional OCT allows visualization of the Henle fiber layer and thus extraction of "true" ONL thickness measurements (Lujan et al., 2015; Menghini et al., 2014). Even these measures inform only gross photoreceptor structure, as they cannot differentiate relative cone and rod contributions to the ONL. As well, the ONL thickness is affected only after a cell has degenerated completely, making it a somewhat late biomarker in the process of photoreceptor degeneration. The second outer retinal band visible in OCT scans has been attributed to the ellipsoid portion of the inner segments (EZ band) or to the boundary between the inner segments and outer segments of photoreceptors (Jonnal et al., 2015; Jonnal et al., 2014; Spaide and Curcio, 2011; Staurenghi et al., 2014; Tao et al., 2016). OCT combined with AO provided high resolution images of individual cones that demonstrated the band was several times thinner than in clinical OCT images and supported the designation of inner segment-outer segment junction rather than the inner segment ellipsoid (Jonnal et al., 2014). However, an international consortium proposed use of EZ to describe this band given the lack of definitive evidence defining the origin of the band, and uses the term "zone" to denote that more than one anatomic structure likely contributes to the reflectivity of the band (Staurenghi et al., 2014). Recently, there has been significant interest in using the integrity of the EZ band as a more sensitive biomarker of photoreceptor health (Tao et al., 2016). The reflective EZ band is generated by the photoreceptors (Spaide and Curcio, 2011), and metrics related to retained EZ width or EZ lesion area have become established markers of disease progression in inherited pathologies (Birch et al., 2013; Hariri et al., 2017; Tee et al., 2019) and have been used as outcome measures in clinical trials (Chew et al., 2018). However, when the EZ band is present, it does not mean the photoreceptor mosaic is intact. AO can reveal photoreceptor damage that is not visible in EZ images. When EZ is absent photoreceptors may be present. Studies examining the same retinal areas with both OCT and AOSLO have revealed important disconnects between EZ integrity and the underlying photoreceptor mosaic, including examples of cone density loss in the absence of any measurable change in the EZ band (Talcott et al., 2011). Also, cone function may be measurable in regions where the EZ is disrupted and cone profiles are not be visible using confocal AOSLO, a condition termed "dysflective cones" (Tu et al., 2017). These observations can inform the interpretation, accuracy and sensitivity of both AOSLO and EZ metrics in quantifying the extent of underlying photoreceptor damage.

When examining eyes with ACHM, it has been shown that the intensity of the EZ band is reduced compared to the normal retina (Sundaram et al., 2014). These patients have reduced cone density (with the remnant non-functional cones having altered reflectance in AOSLO images) and apparently normal rod photoreceptors, suggesting that rods and cones both contribute to the EZ reflectivity. However, that the EZ band was intact despite the significant reduction in cone density also highlights the concept that the presence of the EZ alone does not inform as to the underlying cone numerosity. Consistent with this, a normal-appearing EZ was observed in patients with altered cone mosaics due to *OPN1LW* / *OPN1MW* mutations (Patterson et al., 2018; Rha et al., 2010). In addition, patients with reduced cone density from acute macular neuroretinopathy or Stargardt disease show a preserved EZ (Hansen et al., 2015; Razeen et al., 2016). Taken together, this evidence reinforces that a normal-appearing EZ band cannot be interpreted as a normal underlying photoreceptor mosaic. However some studies have reported that EZ reflectivity is positively correlated to cone density measured with AOSLO in normal subjects, patients with resolved central serous chorioretinopathy and hydroxychloroquine and traumatic maculopathies (Saleh et al., 2017; Scoles et al., 2016). This is consistent with the findings in ACHM and suggests that EZ reflectivity is a viable biomarker of the photoreceptor mosaic.

When defining EZ lesions with OCT, there are two important concepts revealed from AOSLO studies. First, small lesions within the photoreceptor mosaic can be missed on OCT. This has been demonstrated in patients with mild traumatic brain injury or closed globe ocular trauma (Braza et al., 2018; Flatter et al., 2014; Kaizu et al., 2016; Stepien et al., 2011). This is most likely due to lateral resolution and sampling patterns used in clinical OCT protocols (it is not uncommon to sample 6 mm of retina with a few hundred B scans, resulting in a gap between B scans of 10–20 microns). Second, even visible EZ lesions on OCT do not indicate that there is an absence of photoreceptor structure. There have been numerous reports of persistent cell structure in areas of absent EZ reflectivity; for example, in cone rod dystrophy associated with *GUCY2D* mutations, after closed globe blunt ocular trauma (Scoles et al., 2016) (Figure 15), ACHM (Georgiou et al., 2019b; Langlo et al., 2016), macular telangiectasia type 2, and BCM (Scoles et al., 2016). Importantly, the residual cone structure is visible typically only with split detection AOSLO; confocal AOSLO often also shows areas of reduced reflectance within OCT-defined EZ lesions (Ooto et al., 2010; Ooto et al., 2011). This has important therapeutic implications, as the absence of EZ reflectivity does not out rule the presence of residual cone structure, which may or may not be salvageable. Further studies using AOSLO and OCT in the same retinae will undoubtedly expand our understanding of the limitations of EZ-based biomarkers for defining the extent of photoreceptor damage.

4.1.2 Cone photoreceptor density and geometry—Traditionally, approximate sizes of gross fundus pathology were estimated with reference to the diameter or area of large landmarks like the optic disc. AOSLO facilitates precise measurements on the order of micrometers – with pathology detectable even at subclinical thresholds (as reviewed in 4.1.1). As significant cell destruction can be present prior to noticeable symptoms and retinal degenerations typically progress slowly, clinical measures would be insensitive to therapeutic effects within the 1–3 year timeframe of standard clinical trials (Csaky et al.,

2017). AOSLO is well-positioned to detect early manifestations of pathology (while vision may still be salvageable), and identify small, incremental or diffuse longitudinal changes in established disease. These changes are often impossible to discern with the naked eye, so for accurate measurement of disease using AOSLO images, quantitative metrics are required, the most basic and intuitive of which is density.

The first example of application of this to a clinical trial population was an ancillary study to a multicenter clinical trial of ciliary neurotrophic factor (CNTF) which demonstrated the use of cone density as a sensitive outcome measure to assess cone structure in a subset of patients (Talcott et al., 2011). One eye of each patient was randomly assigned to receive sustained-release CNTF, a neurotrophic factor being investigated for potential role in slowing the progression of retinal degeneration (LaVail et al., 1992; MacDonald et al., 2007), and the fellow eye was assigned to sham treatment. Over 24 months, no changes in standard clinical outcome measures such as visual acuity, visual field sensitivity or ERG responses were observed in either the sham-treated or CNTF-treated eyes. However, sham treated eyes showed a significantly larger decrease in cone density compared to the CNTF-treated eyes (Figure 11). This demonstrated the potential use of AOSLO as a sensitive and reliable measure for longitudinal follow up – not only in natural history studies but also in assessing response to treatment. It provides a strong rationale for combining standard clinical measurements with high-resolution measures of photoreceptor structure in treatment trials over a limited period in slowly progressive conditions.

Density is not the only structural metric of the cone mosaic; there are a number of spacing and regularity metrics used to describe the cone mosaic (Chui et al., 2008; Kram et al., 2010; Li et al., 2010; Martin et al., 2000; Rodieck, 1991) (Figure 16). One of the challenges in relying on structural biomarkers is disambiguating true cell loss from cell misidentification. The optimum metric would be able to capture and reflect small true cone losses without being overly sensitive to missed cones caused by poor image quality or ambiguous appearance of cells in the diseased retina. Cooper et al. (2016) reviewed these metrics and their individual merits in detecting disruptions of the cone photoreceptor mosaic. Other authors have described different methods of describing cone structure, including measuring cone spacing using density recovery profile histograms (Rodieck, 1991), Voronoi cell area regularity (Dees et al., 2011; Li and Roorda, 2007; Lombardo et al., 2014; Ramamirtham et al., 2016; Wells-Gray et al., 2016), anisotropy (Chui et al., 2008) and global regularity index (Kram et al., 2010). Many of the measures of mosaic regularity (e.g., percentage of six-sided Voronoi cells, Voronoi cell area regularity, and number of neighbors regularity) are vulnerable to inaccuracies caused by cell identification errors. Spacing measures like nearest neighbor distance and density recovery profile distance are very robust, though this may come at the cost of being insensitive to loss of small numbers of cells which would reduce their sensitivity to detect small changes over time. The inescapable minimal residual distortion seen in AOSLO images has little effect on global metrics such as cell density and spacing, but it has a significant effect on local metrics such as regularity index and Voronoi geometry (Cooper et al., 2013a). Combining metrics may increase their utility by harnessing complementary but distinct advantages. Longitudinal studies can also be used to assess inter-visit variation and reduce variability and mitigate metrology issues when conducted in normal individuals. Ultimately the choice of metric(s) for estimating cone loss longitudinally

may differ depending on the anticipated pattern and rate of cell loss within the pathology being monitored.

The validity of nearly all spatial metrics of the cone mosaic relies on accurate knowledge of the image scale. Most measurements are made in units of absolute retinal distance, which requires a conversion from visual angle to retinal size/distance (usually in microns or millimeters). This conversion relies on several assumptions and some form of a schematic eye (Storani de Almeida and Carvalho, 2007). These scaling assumptions are used by convention and represent the best estimates of the geometry of the 'ideal eye'. There are likely inaccuracies that arise from assumptions about the average anterior chamber depth, lens curvature, lens thickness, etc. Whole-eye biometry (such as with OCT or magnetic resonance imaging) may be valuable in developing personalized eye models, though it is still not known exactly how much error may be present in current scaling estimates. Furthermore, disease features such as intraretinal microcysts (a common non-specific manifestation of many retinal diseases) can impact image scaling. They have been shown to cause magnification of the underlying photoreceptors by acting as spherical lenses (Langlo et al., 2014; Meadway et al., 2020). Such features may have little to no impact on assessment of gross pathology, but as the precision of biomarkers increases, the impact and relevance of these features must be considered.

4.1.3 Measurement Errors—A thorough understanding of the measurement errors associated with the above AOSLO-based biomarkers is essential for their incorporation into large multicenter clinical trials. Measurement errors in the context of AOSLO-based biomarkers have multiple sources – the specific instrument being used, the modality (confocal or split detection) being used to image the retina, and inter- and intra-observer variability. The terms agreement, reliability, reproducibility, and repeatability are used throughout the AOSLO literature – often times interchangeably. Thus, it is important to first define the terminology we will be using. Here, repeatability refers to variability in repeated measures made on the same subject under identical conditions. If the same observer made the measurements, this would be termed "intra-observer repeatability". Likewise, if the same subject was imaged multiple times with the same device, this might be considered "intra-device repeatability". In contrast, reproducibility refers to variability in repeated measures made on the same subject under changing conditions. If the same subject was imaged on two different AOSLO systems, this would allow assessment of the "inter-device reproducibility". Likewise, if we had multiple observers measure the same set of images, this would reveal the "inter-observer reproducibility". If we were assessing the same subject over a short period of time, this might be referred to as "inter-visit repeatability" (over a longer time period, this might be "inter-visit reproducibility"). Finally, reliability (or intraclass correlation, ICC) is used to relate the real variability between subjects to the measurement error.

The majority of publications regarding the measurement errors associated with cone metrics involve studies of normal data sets. In one of the larger studies on measurement error, (Liu et al., 2014) 10 observers measured cone density three times in 90 confocal AOSLO images from individuals with normal vision (270 measurements per observer) and a variance components model was used to define the various contributions to the overall variability. The study found that the observer only contributed about 1% of the overall variability –

suggesting the inter-observer repeatability is very high. Similar findings were produced in a smaller study using a commercial prototype confocal AOSLO, where they also assessed the contribution of the photographer (Davoudi et al., 2018). Liu et al. (2014) also reported a separate cohort imaged on two different instruments; 160 pairs of images were measured by the same observer. The inter-instrument reproducibility was found to be very good, with between 2.5–6.9% of the total variance being attributed to differences between the devices. Morgan et al. (2018) showed that the inter-observer reproducibility for cone density in parafoveal images was better using split detection compared to confocal images. While these are of value in defining the upper limit of performance of these metrics, unfamiliar and unusual patterns of disease and degeneration make features more difficult to discern than in the pristine normal retina, not to mention increased prevalence of characteristics that degrade image quality like fixational instability, light sensitivity, and media opacity and increased aberrations.

There have been few studies of repeatability in patients with inherited retinal disease. In a cohort of patients with inherited retinal degenerations imaged with confocal AOSLO, Zayit-Soudry et al. (2015) reported an inter-observer ICC of 0.89, compared to 0.84 for their control group. The inter-visit repeatability was good, with a mean difference of about 5% in the inherited retinal degeneration group (ICC ranged from 0.87 – 0.98) and 4% in the controls (ICC ranged from 0.93 – 0.95). Low quality images from eyes with retinal degeneration affected intersession repeatability of cone measures (Davoudi et al., 2018; Gale et al., 2019) and measures from large measurement windows (150 um x 150 um) were most consistent (Davoudi et al., 2018). Subsequent studies have revealed that the measurement errors are modality and disease dependent (Morgan et al., 2020; Tanna et al., 2017). Similar to findings in normal eyes (Morgan et al., 2018), reliability was lower when graders measured confocal compared to split detector AOSLO images (Abozaid et al., 2016; Tanna et al., 2017). In addition, reliability varies among different diseases. Images from patients with Stargardt disease showed greater inter-grader reliability than images from patients with *RPGR*-related RP (Tanna et al., 2017). Unsurprisingly, intraobserver repeatability is better with experienced graders, as demonstrated in ACHM and choroideremia (Abozaid et al., 2016; Morgan et al., 2020).

While evidence of low measurement error even in patients with inherited retinal degenerations is encouraging, longitudinal inter-visit reproducibility must be established prior to the use of AOSLO in clinical trials. An additional factor in these studies is ensuring the same retinal location is being analyzed consistently. Even images taken over short time periods in individuals with normal vision can vary in their absolute retinal position. This is because the preferred retinal locus of fixation is an area of approximately one degree (Putnam et al., 2005). If relying solely on the subject's fixation to guide the general (or global) location for image analysis, intra-visit repeatability (2.77 times the within-subject standard deviation) is 17.1%. This drops to 6.4% if the images are first aligned such that the exact same cones are being included in the analysis (Garrioch et al., 2012). This approach was used by (Jackson et al., 2019) in a 2-year longitudinal study, though they had to also normalize the appearance of images from different time points, since the reflectivity of individual cones varies dramatically over time and can confound image alignment. As disease progression can negatively impact fixational stability, the ability to image and

analyze precisely the same retinal locations over time can be quite challenging. Use of other anatomical landmarks (foveal avascular zone, foveal pit center, retinal vascular landmarks) across imaging sessions could help, but even these structures may not remain stable in a degenerating retina. Aligning entire montages from different time points is possible, though this does not account for situations where the same retinal area was not captured between the two sessions. Methods to improve the precision of longitudinal measures of the cone mosaic are one of the most important areas of need for advancing the clinical application of AOSLO.

4.2 Functional AOSLO biomarkers

As reviewed so far, correction of the eye's aberrations through the use of AO has been leveraged primarily to evaluate retinal structure. However, recent years have seen exciting growth in the use of AO-based imaging modalities (including AOSLO) to probe retinal function on a cellular scale. Depending on the specific disease, functional changes measured at such a fine spatial scale could have improved sensitivity over structural biomarkers. Two AOSLO-based approaches to assess the function of individual photoreceptors are reviewed here.

4.2.1 Adaptive optics microperimetry (AOMP)—Several studies have investigated the relationship between cone measures from AOSLO images and clinical measures of visual function. Precise alignment of AOSLO images to data acquired during fundus-guided microperimetry demonstrated significant correlations between cone spacing and macular sensitivity in eyes with RP, Usher syndrome (Foote et al., 2019a) and choroideremia (Foote et al., 2019b). However, clinical fundus-guided microperimetry employs real-time fundus tracking at 25 frames/second with an SLO and a Goldman III (26 arcmin, 0.43°) stimulus, which covers a region containing hundreds to thousands of cones (depending on the eccentricity). This spatial redundancy of the stimulus decreases the ability to detect focal structural changes that may occur early in the disease process. Furthermore, Ratnam et al. (2013a) observed that despite reduction in cone density by up to 62%, subjects' retained visual acuity of 20/25 or better, pointing towards the role of eye motion in alleviating the impact of cone loss. Detailing the grain of visual dysfunction on a cellular scale entails targeting the retina with punctate stimuli upon compensating for the both the eye's aberrations and motion.

Correction of optical aberrations with AOSLO can not only improve resolution of structural images, but can also be used to deliver visual stimuli precisely to small groups of cones, a technique called AO microperimetry (AOMP) (Makous et al., 2006; Tuten et al., 2012). Just as with clinical microperimetry, AOMP can be performed with or without tracking the retina in real-time. As shown in Figure 10, AOMP demonstrated reduced sensitivity in cones of patients with *RPGR*-associated RP when compared to normal cones and to cones in patients with *RHO*-associated RP (Foote et al., 2020). The discrepancy between photoreceptor structure and visual function suggests that the remnant cones in patients with *RPGR*-related RP may be amenable to functional improvement in response to therapies, which may be measurable in a shorter timeframe than that required to see reduced rates of disease progression. As mentioned above, AOMP in patients with CHM demonstrated that

outer retinal tubulations at the margins of degeneration have severely reduced visual function (Tuten et al., 2019) (Figure 12).

One area where AOMP has proved particularly useful is assessing retinal areas devoid of normally-waveguiding cones. As reviewed above in Section 3, the absence of a reflective signal on confocal AOSLO cannot be interpreted as the absence of cones. In many cases, split-detection AOSLO has revealed remnant inner segment structure in genetic conditions predominantly affecting cones like ACHM and BCM. Here the lack of normal waveguiding can likely be attributed to morphological disturbances within the cone itself (perhaps the OS), caused by the respective genetic mutations (Carroll et al., 2005; Langlo et al., 2016). However, dimly reflective or 'dysflective' cones can be observed in normal retinas and conditions in which cones are not the site of disease. AOMP offers the ability to directly characterize the function of these dysflective cells and studies in bilateral foveolitis (Tu et al., 2017), macular telangiectasia type 2 (Wang et al., 2015) and in normal eyes (Bruce et al., 2015; Horton et al., 2015; Tu et al., 2017), indicating residual function despite absence of reflectivity. Moreover, longitudinal studies in eyes with macular telangiectasia type 2 (Wang et al., 2015) and acute idiopathic blind spot enlargement syndrome (Horton et al., 2015) demonstrated improved visual function and resumed reflectivity in regions that had previously shown reduced reflectivity and associated clinically demonstrable scotomas, suggesting that dysflective status is not an indicator of permanent, irreversible cellular dysfunction.

Like conventional clinical microperimetric testing, AOMP is a time-consuming process. The improved spatial resolution comes at the price of having sampled less retinal area in a given amount of time and reliable assumptions cannot be made about how the function of a particular group of cells in one retinal area relates to the retina as a whole or cells in other specific retinal locations. Responses generated on AOMP testing may not always be exclusively attributed to photoreceptor cells – we know the cones surrounding the cell being stimulated may influence the perception of the stimulus color (Schmidt et al., 2018b) and as in standard clinical microperimetry in glaucoma post-receptoral processing by retinal ganglion cells may contribute to subjective perception and responses (Gardiner et al., 2014). Efforts to disentangle how signals from photoreceptors are transduced to the cortex could be supported by the use of AOSLO to precisely stimulate small retinal areas while simultaneously recording from the LGN or cortex in non-human primate models (Sincich et al., 2009).

4.2.2 Cone photoreceptor response to light—

Beyond the number and distribution of cone photoreceptors in a given image, there may be valuable information in the waveguiding properties, manifest as reflectance of individual cells in confocal AOSLO images. The reflectivity of all photoreceptors is inherently variable over space and time (Cooper et al., 2011; Pallikaris et al., 2003; Zhang et al., 2006). The fact that this intrinsic variability is not specific to rods or cones suggests a common physiological source. The temporal variability has been leveraged to improve the quality of AOSLO images of the photoreceptor mosaic (Cooper et al., 2011; Dubra et al., 2011), but recent work has led to renewed interest in using photoreceptor reflectance as a biomarker of photoreceptor function.

Cone visualization is compromised in confocal AOSLO images of eyes with irregular retinal topography, including subretinal drusenoid deposits (Xu et al., 2017; Zhang et al., 2014), drusen (Zayit-Soudry et al., 2013) and Best macular dystrophy (Kay et al., 2013). This disruption of cone visualization is likely due to photoreceptor misalignment and reduced reflectivity mediated by the Stiles-Crawford effect (Morris et al., 2015). In addition to misalignment, cone visibility may be impaired where cone reflectivity is reduced in cone-rod dystrophy as a consequence of OS disruption (Duncan et al., 2007). Reduced reflectivity in diseases causing severe structural abnormalities like BCM and ACHM can reveal a correlation between structure and function (Carroll et al., 2005; Langlo et al., 2016). Studies in ACHM support a strong association between reflectivity and function, with the *CNGB3* and *CNGA3* genotypes having reduced or absent reflectivity of remaining cones (none of which are thought to function), and patients with *GNAT2*-associated ACHM having increased cone reflectivity along with measurable residual cone function (Dubis et al., 2014). More evidence to support this association was shown when visual sensitivity was reduced proportionally to the percentage of non-waveguiding cones in a subject with deuteranopia as tested with AOMP (Makous et al., 2006). However, as reviewed above, there are some instances where dysflective cones retain some visual function.

Beyond relating cone reflectivity in a single image to cellular function, recent studies have explored the temporal variability of cone reflectance as a possible measure of cellular activity. Variability in cone reflectance over time has been linked to changes in the OS structure, such as shedding and regeneration of OS discs (Jonnal et al., 2010; Kocaoglu et al., 2016; Pircher et al., 2010). Faster changes in reflectivity occur after exposure to visual stimuli that are due to photoisomerization of pigment chromophore (Cooper et al., 2017). These changes are measurable with OCT or SLO (Hillmann et al., 2016; Zhang et al., 2017a). This principle is the foundational principle for the truly revolutionary optoretinogram (Azimipour et al., 2020; Pandiyan et al., 2020a; Pandiyan et al., 2020b), an AO-assisted approach that employs phase-resolved OCT imaging and allows dynamic assessment and recording of the cellular responses to light stimuli. Initial rapid contraction of the OS followed by a slower expansion are related to membrane potential changes and osmosis respectively, accompanying phototransduction (Figure 17), (Pandiyan et al., 2020b) which are detectable as a change in the optical phase of the OCT signal between the cone IS and OS tips. This new technology offers an avenue for direct comparison of photoreceptor structure and function on a single-cell scale. Establishing the spatiotemporal changes in the photoreceptor light response on the scale of nanometers and milliseconds could allow detection of microscopic photoreceptor dysfunction prior to cell death. In contrast to the extent of the EZ band on OCT scans, which provides a binary measure of areas with surviving photoreceptors and areas where the photoreceptors have died, an optoretinogram could allow detection of cell dysfunction within a salvageable window. As a high-resolution analogue of ERG, the optoretinogram offers significant advantages, providing an objective assessment of single cell function and a sensitive measure of more subtle dysfunction than a full-field or multifocal ERG can discern. This could demonstrate whether dysfunction in a given retinal area is due to many partially-functioning cells or a reduced number of fully-functioning cells. Such information would be quite valuable in understanding disease pathophysiology and guiding therapeutic decisions.

5. Barriers to clinical adoption of AOSLO

5.1 Lack of commercialized, uniform hardware to facilitate patient imaging

Barriers to clinical use of AOSLO are many, including the limited examples of duplicated hardware in the research environment. There are some grassroots efforts aiming to share details of designs and techniques and facilitate strides toward unification, such as Austin Roorda's Consortium for Retinal Imaging and Tracking Experiments (C-RITE),https://c-rite.github.io/). However, reporting and sharing of experimental details is still an area with significant room for improvement. The insights discussed in section 3 have all been achieved even in the absence of significant hardware standardization but the variability of these customized systems presents a major obstacle to their incorporation into clinical trial regimes, in spite of mounting clinical need.

Commercialization of AO systems could address this pitfall. The first commercially available AO system was released in 2011. The rtx1 AO flood illuminated retinal camera from Imagine Eyes (Orsay, France) is licensed in some territories which has enabled many groups to publish images from this system. The rtx1 system permits image acquisition quickly with a wide field of view, incorporates montaging software, and avoids the distortion that can result from scanning systems. The rtx1 system has been used to provide detailed morphometric information regarding small vascular structures (Koch et al., 2014; Meixner and Michelson, 2015; Zalenska-Żmijewska et al., 2019) and photoreceptor measures (Bidaut Garnier et al., 2014; Gale et al., 2016; Jacob et al., 2017; Legras et al., 2018; Lombardo et al., 2013a; Lombardo et al., 2013b; Muthiah et al., 2014; Querques et al., 2016; Tumahai et al., 2018; Woog and Legras, 2019; Zalenska-Żmijewska et al., 2017) in normal subjects and eyes with retinal disease. However, it has the significant limitation of being unable to resolve foveal cones and parafoveal rods. This significantly limits its widespread utility in studying inherited retinal degenerations. Various other commercial entities such as Boston Micromachines, Canon, and Physical Sciences Incorporated have developed protypes or offer custom built solutions for research purposes. The lack of 510k clearance from the FDA is a significant barrier to multicenter standardized investigations like clinical trials.

AOSLO reduces image blur caused by monochromatic aberrations in the eye, but many other features of the human eye can reduce the retinal image quality; chromatic aberrations, high refractive errors, astigmatism, poor pupil dilation, tear film abnormalities, unstable fixation, high axial hyperopia or myopia and media opacities. All of these factors can vary throughout life but occur at greater frequencies in those with complex inherited retinopathies and elderly patients, two populations likely to benefit most from AOSLO imaging. Another factor complicating AOSLO imaging in the elderly is the increased scattering from the lens, either due to the presence of cataract or from capsular scarring following cataract surgery. While this does not preclude obtaining a retinal image, it can interfere with accurate measures of the wavefront, making this a population in which wavefront sensorless approaches could help. A wide field of view SLO instrument with integrated AOSLO imaging has been described to reduce image motion by a factor of about 400, offer steering to focus on pathological lesions and may eliminate post-processing with real-time averaging (Zhang et al., 2015). Likewise, other imaging systems capable of

visualizing the photoreceptor mosaic without AO, like the commercially available Spectralis high magnification module from Heidelberg Engineering (Mendonça et al., 2020; Wynne et al., 2020), are being developed that could facilitate patient selection for more involved AOSLO imaging sessions.

Eye motion degrades the quality of AOSLO images, despite system features designed to minimize their impact like bite bar stabilization. AOSLO image acquisition requires concentration and co-operation of subjects. The stable fixation required over long imaging sessions is not within the capabilities of all subjects and can be especially challenging for young children, those with neurological movement disorders or cognitive neurodegenerative disease. Even microsaccadic eye movements in the normal population occur at speeds comparable to scan rates and cause warping distortions in AOSLO images (Vogel et al., 2006). These effects are amplified by the small field of view (1–3 degrees) required to achieve sufficient spatial sampling rates. AOSLO images are therefore particularly susceptible to effects of eye movement disorders like nystagmus – a common finding in multiple patient subgroups that could benefit from clinical AOSLO imaging – albinism, ACHM and congenital retinal dystrophies. Flood illuminated AO imaging can circumvent issues with AO image quality caused by eye movements, but that benefit comes with some costs; reduced axial sectioning, insufficient transverse resolution to image foveal cones, and limited capabilities for capturing fluorescence images and features unique to other wavelengths. Use of improved tracking technology, such as systems that integrate wide field SLO with AOSLO (Zhang et al., 2015) or tracking SLO with an AOSLO (Sheehy et al., 2015) may compensate partially for eye movement artifacts but is unlikely to entirely eliminate them.

5.2 Processing and analysis overhead

There have been some efforts to improve the efficiency of AOSLO image collection (Huang et al., 2012; Zhang et al., 2015), but the majority of software development efforts relate to processing and analysis of the AOSLO images. After acquisition, raw AOSLO videos must go through a series of processing steps before analysis. There have been many advances toward automation in steps including de-warping (Bedggood and Metha, 2017), reference frame selection (Salmon et al., 2017), automatic montaging (Davidson et al., 2018b), and longitudinal montaging (Chen et al., 2019; Chen et al., 2016). Even with incorporation of these automated steps the end-to-end processing pipeline involves *some* manual intervention and is not entirely objective. The time to produce usable images and the lack of standardization has to date interfered with widespread clinical adoption. Besides the timing, most processing takes place after the imaging session is complete. This serial processing effectively eliminates the opportunity to rectify scenarios where all or part of the processed montage is inadequate for subsequent quantitative analysis.

Most of the quantitative cone mosaic metrics reviewed in Section 4 require the identification of the cones in the image, though there are methods to extract modal cone spacing that do not require determining which structures are cones (Cooper et al., 2013b). As a result, there has been considerable effort placed on developing automated cone identification algorithms for both confocal and split-detection AOSLO (Cunefare et al., 2017a; Cunefare et al., 2019;

Cunefare et al., 2017b; Davidson et al., 2018a; Heisler et al., 2018; Li and Roorda, 2007; Liu et al., 2017a; Morgan et al., 2020). There is even a fully automated algorithm capable of calculating cell spacing across an entire montage using multiscale fitting and residual peak finding (Cooper et al., 2019). There appears to be a great deal of redundancy in these efforts – tailoring algorithms for specific AOSLO systems or specific diseases. Continual iterative efforts to achieve more efficient or novel cone counting algorithms may provide little incremental dividend with respect to time saved, particularly with consideration of the invested resources. The opportunities for improved efficiencies with resource sharing between investigators in this regard cannot be ignored.

6. Future directions and conclusions

As mentioned above, AOSLO measures have great potential to provide sensitive, objective, reliable outcome measures of disease progression and treatment response in eyes with inherited retinal degenerations. The factors limiting widespread use have contributed to the limited number of clinical trials reporting AOSLO measures to date, including the lack of a commercially-available instrument, time-intensive image acquisition, processing and analysis, limited data on repeatability of measures between visits and between graders, and limited longitudinal studies in normal eyes (Jackson et al., 2019) and eyes with retinal degeneration (Talcott et al., 2011). Despite this, protocols are being developed and deployed as ancillary studies to larger natural history studies such as the Rate of Progression of USH2A-Related Retinal Degeneration (RUSH2A) study (Duncan et al., 2020). Collaboration among investigators at sites with AOSLO confocal and split detector image acquisition capability will enable these studies, which should facilitate inclusion of AOSLO into multicenter clinical trials of treatments for patients with inherited retinal degenerations.

Even with these efforts to expand the use of AOSLO in multicenter clinical trials, the image processing and analysis continues to pose a significant barrier to widespread use of AOSLO imaging in clinical care. Artificial intelligence and machine learning are already making advances in this regard. Artificial intelligence, described by the World Economic Forum as the fourth industrial revolution, has had particularly useful applications in ophthalmology and is set to revolutionize clinical care for many common pathologies (Schmidt-Erfurth et al., 2018; Ting et al., 2019). Sensitive and cost-effective automated software for grading of fundus photos in diabetic retinopathy (Tufail et al., 2017) and glaucoma (Li et al., 2018), and OCT images in macular degeneration (Lee et al., 2017), have been demonstrated. These conditions are exceptionally common with large input datasets for machine learning algorithms. Unfortunately, though the inherited retinal degenerations most likely to benefit from the applications of AOSLO are a large group together, the low numbers of individuals with specific conditions and genotypes poses technical challenges to the implementation of artificial intelligence techniques for AOSLO image analysis. Although automated convolutional neural network-based methods can be trained to identify cones with excellent agreement with expert graders, performance varies across different conditions and thus training of the neural networks with images from the specific disease of interest seems to be required (Morgan et al., 2020). That said, there may be opportunities to combine the large amounts of imaging data across labs to develop more generalized

machine learning approaches for analysis of photoreceptor phenotypes in AOSLO images. Separate efforts would be required for other AO modalities and even other structures and cell types. Nevertheless, such approaches could enable analyzing larger montages, eliminating subjective ROI selection and improving objectivity in AOSLO image analysis.

Although OCT and AOSLO were first reported around the same time (Huang et al., 1991; Liang et al., 1997; Swanson et al., 1993), OCT has been widely incorporated into clinical care of retinal patients, while AOSLO remains a research tool. Part of the reason for the widespread adoption of OCT is that its commercial development evolved concurrently with the development of effective treatments for macular diseases including anti-vascular endothelial growth factor therapies and grid photocoagulation (Bolz et al., 2010; Mylonas et al., 2013) that required an accurate measure of treatment impact on retinal thickness. AOSLO provides unique access to evaluate retinal cells; however, there are currently few therapies that have been effective in improving photoreceptor survival, so AOSLO remains largely an academic research tool. That said, there are over 30 clinical trials of treatments for inherited retinal degenerations underway, and it has been challenging to demonstrate efficacy in slowing the rate of disease progression for diseases where visual acuity is preserved until late stages (Thompson et al., 2020). AOSLO, AOMP and optoretinography are novel tools with cellular resolution that may provide sensitive, objective outcome measures to demonstrate improvements in photoreceptor survival and function. Thus, while AOSLO may not currently have an everyday home in the ophthalmologist's office, these technologies offer real promise to expedite development of treatments for a number of visually devastating diseases.

Acknowledgements

This work was supported by the National Institutes of Health grant numbers R01EY017607, R01EY023591, R01EY021237, U24EY029891 and U01EY025477. Additional support from the Foundation Fighting Blindness Consortium grant number PPA-0641–0718-UCSF, Gene & Ruth Posner Foundation, Research to Prevent Blindness, the Claire Giannini Foundation, The Lawrence L. Hillblom Foundation and That Man May See, Inc.

The authors wish to acknowledge Elizabeth Heffernan for her contributions to this work and Jenna Cava, Robert Cooper, Heather Heitkotter, Katie Litts, Ram Sabesan, Alex Salmon, and Erica Woertz for helpful discussions and comments on earlier versions of the manuscript.

References

Abozaid MA, Langlo CS, Dubis AM, Michaelides M, Tarima S, Carroll J, 2016. Reliability and repeatability of cone density measurements in patients with congenital achromatopsia. Advances in Experimental Medicine and Biology 854, 277–283. [PubMed: 26427422]

Ach T, Huisingh C, McGwin G Jr., Messinger JD, Zhang T, Bentley MJ, Gutierrez DB, Ablonczy Z, Smith RT, Sloan KR, Curcio CA, 2014. Quantitative autofluorescence and cell density maps of the human retinal pigment epithelium. Investigative Ophthalmology & Visual Science 55, 4832–4841. [PubMed: 25034602]

Aleman TS, Han G, L.W. S, Fuerst NM, Charlson ES, Pearson DJ, Chung DC, A. T, Pan W, Ying GS, Bennett J, Maguire AM, Morgan JIW, 2017. Natural history of the central structural abnormalities in choroideremia: A prospective cross-sectional study. Ophthalmology 124, 359–373. [PubMed: 27986385]

Arichika S, Uji A, Hangai M, Ooto S, Yoshimura N, 2013. Noninvasive and direct monitoring of erythrocyte aggregates in human retinal microvasculature using adaptive optics scanning

laser ophthalmoscopy. Investigative Ophthalmology & Visual Science 54, 4394–4402. [PubMed: 23716632]

Ayyagari R, Kakuk LE, Bingham EL, Szczesny JJ, Kemp JA, Toda Y, Felius J, Sieving PA, 2000. Spectrum of color gene deletions and phenotype in patients with blue cone monochromacy. Human Genetics 107, 75–82. [PubMed: 10982039]

Ayyagari R, Kakuk LE, Toda Y, Coats CL, Bingham EL, Szczesny JJ, Felius J, Sieving PA, 1999. Blue cone monochromacy: Macular degeneration in individuals with cone specific gene loss, in: Hollyfield JG, Anderson RE, LaVail MM (Eds.), Retinal Degenerative Diseases and Experimental Therapy. Kluwer Academic / Plenum Publishers, New York.

Azimipour M, Valente D, Vienola KV, Werner JS, Zawadzki RJ, Jonnal RS, 2020. Optoretinogram: Optical measurement of human cone and rod responses to light. Optics Letters 45, 4658–4661. [PubMed: 32870829]

Bedggood P, Metha A, 2017. De-warping of images and improved eye tracking for the scanning laser ophthalmoscope. PLoS One 12, e0174617.

Bedggood P, Metha A, 2020. Adaptive optics imaging of the retinal microvasculature. Clinical and Experimental Optometry 103, 112–122. [PubMed: 31797452]

Bensinger E, Rinella N, Saud A, Loumou P, Ratnam K, Griffin S, Qin J, Porco TC, Roorda A, Duncan JL, 2019. Loss of foveal cone structure precedes loss of visual acuity in patients with rod-cone degeneration. Investigative Ophthalmology & Visual Science 60, 3187–3196. [PubMed: 31335944]

Bernstein P, Dysli C, Fischer J, Hammer M, Katayama Y, Sauer L, Zinkernagel MS, 2019. Fluorescence lifetime imaging ophthalmoscopy (FLIO). Springer.

Bernstein SL, Wong P, 1998. Regional expression of disease-related genes in human and monkey retina. Molecular Vision 5, 24.

Bidaut Garnier M, Flores M, Debellemaniere G, Puyraveau M, Tumahai P, Meillat M, Schwartz C, Montard M, Delbosc B, Saleh M, 2014. Reliability of cone counts using an adaptive optics retinal camera. Clinical & Experimental Ophthalmology 42, 833–840. [PubMed: 24800991]

Birch DG, Locke KG, Felius J, Klein M, Wheaton DK, Hoffman DR, Hood DC, 2015. Rates of decline in regions of the visual field defined by frequency-domain optical coherence tomography in patients with RPGR-mediated X-linked retinitis pigmentosa. Ophthalmology 122, 833–839. [PubMed: 25556114]

Birch DG, Locke KG, Wen Y, Locke KI, Hoffman DR, Hood DC, 2013. Spectral-domain optical coherence tomography measures of outer segment layer progression in patients with X-linked retinitis pigmentosa. JAMA Ophthalmology 131, 1143–1150. [PubMed: 23828615]

Boberg-Ans LC, Munch IC, Larsen M, Gopinath B, Wang JJ, Mitchell P, 2017. Gunn's dots in retinal images of 2,286 adolescents: Prevelance, retinal distribution, and associations. Retina 37, 382–387. [PubMed: 27429392]

Bolz M, Kriechbaum K, Simader C, Deak G, Lammer J, Treu C, Scholda C, Prünte C, Schmidt-Erfurth U, Vienna DRRG, 2010. In vivo retinal morphology after grid laser treatment in diabetic macular edema. Ophthalmology 117, 538–544. [PubMed: 20045563]

Braza ME, Young J, Hammeke TA, Robison SE, Han DP, Warren CC, Carroll J, Stepien K, 2018. Assessing photoreceptor structure in patients with traumatic head injury. BMJ Open Ophthalmology 3, e000104.

Bruce KS, Harmening WM, Langston BR, Tuten WS, Roorda A, Sincich LC, 2015. Normal perceptual sensitivity arising from weakly reflective cone photoreceptors. Investigative Ophthalmology & Visual Science 56, 4431–4438. [PubMed: 26193919]

Burns SA, Elsner AE, Sapoznik KA, Warner RL, Gast TJ, 2019. Adaptive optics imaging of the human retina. Progress in Retinal and Eye Research 68, 1–30. [PubMed: 30165239]

Burns SA, Tumbar R, Elsner AE, Ferguson D, Hammer DX, 2007. Large-field-of-view, modular, stabilized, adaptive-optics-based scanning laser ophthalmoscope. Journal of the Optical Society of America. A, Optics, Image Science, and Vision 24, 1313–1326.

Caetano Dos Santos F.l., Laforest T, Künzi M, Kowalczuk L, Behar-Cohen F, Moser C, 2020. Fully automated detection, segmentation and analysis of in vivo RPE single cells. Eye doi: 10.1038/s41433-020-1036-4. Epub ahead of print.

Carroll J, Baraas RC, Wagner-Schuman M, Rha J, Siebe CA, Sloan C, Tait DM, Thompson S, Morgan JI, Neitz J, Williams DR, Foster DH, Neitz M, 2009. Cone photoreceptor mosaic disruption associated with Cys203Arg mutation in the M-cone opsin. Proceedings of the National Academy of Sciences of the United States of America 106, 20948–20953. [PubMed: 19934058]

Carroll J, Choi SS, Williams DR, 2008. In vivo imaging of the photoreceptor mosaic of a rod monochromat. Vision Research 48, 2564–2568. [PubMed: 18499214]

Carroll J, Dubra A, Gardner JC, Mizrahi-Meissonnier L, Cooper RF, Dubis AM, Nordgren R, Genead M, Connor TB Jr., Stepien KE, Sharon D, Hunt DM, Banin E, Hardcastle AJ, Moore AT, Williams DR, Fishman G, Neitz J, Neitz M, Michaelides M, 2012. The effect of cone opsin mutations on retinal structure and the integrity of the photoreceptor mosaic. Investigative Ophthalmology & Visual Science 53, 8006–8015. [PubMed: 23139274]

Carroll J, Neitz M, Hofer H, Neitz J, Williams DR, 2004. Functional photoreceptor loss revealed with adaptive optics: An alternate cause of color blindness. Proceedings of the National Academy of Sciences of the United States of America 101, 8461–8466. [PubMed: 15148406]

Carroll J, Porter J, Neitz J, Williams DR, Neitz M, 2005. Adaptive optics imaging reveals effects of human cone opsin gene disruption. Investigative Ophthalmology & Visual Science 46, 4564.

Carroll J, Rossi EA, Porter J, Neitz J, Roorda A, Williams DR, Neitz M, 2010. Deletion of the X-linked opsin gene array locus control region (LCR) results in disruption of the cone mosaic. Vision Research 50, 1989–1999. [PubMed: 20638402]

Chen M, Cooper RF, Gee JC, Brainard DH, Morgan JIW, 2019. Automatic longitudinal montaging of adaptive optics retinal images using constellation matching. Biomedical Optics Express 10, 6476–6496. [PubMed: 31853412]

Chen M, Cooper RF, Han GK, Gee J, Brainard DH, Morgan JI, 2016. Multi-modal automatic montaging of adaptive optics retinal images. Biomedical Optics Express 7, 4899–4918. [PubMed: 28018714]

Chew EY, Clemons TE, Jaffe GJ, Johnson CA, Farsiu S, Lad EM, Guymer R, Rosenfeld P, Hubschman JP, Constable I, Wiley H, Singerman LJ, Gillies M, Comer G, Blodi B, Eliott D, Yan J, Bird A, Friedlander M, Group., M.T.T.-P.C.R., 2018. Effect of ciliary neurotrophic factor on retinal neurodegeneration in patients with macular telangiectasia type 2: A randomized clinical trial. Ophthalmology 126, 540–554. [PubMed: 30292541]

Chui TY, Gast TJ, Burns SA, 2013. Imaging of vascular wall fine structure in human retina using adaptive optics scanning laser ophthalmoscopy. Investigative Ophthalmology & Visual Science 54, 7115–7124. [PubMed: 24071955]

Chui TYP, Gan A, Razeen M, Shah A, Pinhas A, Rostomian L, Cheang E, Liu CL, Dubra A, Rosen BR, 2014. Imaging retinal microaneurysms in diabetes using offset pinhole adaptive optics scanning light ophthalmoscopy: a quantitative and qualitative analysis. Investigative Ophthalmology & Visual Science 55, 2606.

Chui TYP, Song HX, Burns SA, 2008. Adaptive-optics imaging of human cone photoreceptor distribution. Journal of the Optical Society of America A 25, 3021–3029.

Chui TYP, Song HX, Burns SA, 2008. Adaptive-optics imaging of human cone photoreceptor distribution. Journal of the Optical Society of America A 25, 3021–3029.

Chui TYP, VanNasdale DA, Burns SA, 2012. The use of forward scatter to improve retinal vascular imaging with an adaptive optics scanning laser ophthalmoscope. Biomedical Optics Express 3, 2537–2549. [PubMed: 23082294]

Cicerone CM, Nerger JL, 1989. The relative numbers of long-wavelength-sensitive to middle-wavelength-sensitive cones in the human fovea centralis. Vision Research 29, 115–128. [PubMed: 2773329]

Cideciyan AV, Hufnagel RB, Carroll J, Sumaroka A, Luo X, Schwartz SB, Dubra A, Land M, Michaelides M, Gardner JC, Hardcastle AJ, Moore AT, Sisk RA, Ahmed ZM, Kohl S, Wissinger B, Jacobson SG, 2013. Human cone visual pigment deletions spare sufficient photoreceptors to warrant gene therapy. Human Gene Therapy 24, 993–1006. [PubMed: 24067079]

Cideciyan AV, Jacobson SG, Drack AV, Ho AC, Charng J, Garafalo AV, Roman AJ, Sumaroka A, Han IC, Hochstedler MD, Pfeifer WL, Sohn EH, Taiel M, Schwartz MR, Biasutto P, De Wit W, Cheetham ME, Adamson P, Rodman DM, Platenburg G, Tome MD, Balikova I, Nerinckx F, De

Zaeytijd J, Van Cauwenbergh C, Leroy BP, Russell SR, 2019. Effect of an intravitreal antisense oligonucleotide on vision in Leber congenital amaurosis due to a photoreceptor cilium defect. Nature Medicine 25, 225–228.

Cooper RF, Aguirre GK, Morgan JIW, 2019. Fully automated estimation of spacing and density for retinal mosaics. Translational Vision Science & Technology 8, 26.

Cooper RF, Dubis AM, Pavaskar A, Rha J, Dubra A, Carroll J, 2011. Spatial and temporal variation of rod photoreceptor reflectance in the human retina. Biomedical Optics Express 2, 2577–2589. [PubMed: 21991550]

Cooper RF, Harvey Z, Dubow M, Sulai Y, Pinhas A, Scoles D, Shah N, Rosen R, Dubra A, Carroll J, 2013a. The effect of AOSLO image distortion on metrics of mosaic geometry. Investigative Ophthalmology & Visual Science 54, 5546.

Cooper RF, Langlo CS, Dubra A, Carroll J, 2013b. Automatic detection of modal spacing (Yellott's ring) in adaptive optics scanning light ophthalmoscope images. Ophthalmic & Physiological Optics 33, 540–549. [PubMed: 23668233]

Cooper RF, Tuten WS, Dubra A, Brainard DH, Morgan JIW, 2017. Non-invasive assessment of human cone photoreceptor function. Biomedical Optics Express 8, 5098–5112. [PubMed: 29188106]

Cooper RF, Wilk MA, Tarima S, Carroll J, 2016. Evaluating descriptive metrics of the human cone mosaic. Investigative Ophthalmology & Visual Science 57, 2992–3001. [PubMed: 27273598]

Cordeiro MF, Normando EM, Cardoso MJ, Miodragovic S, Jeylani J, Davis BM, Guo L, Ourselin S, A'Hern R, Bloom PA, 2017. Real-time imaging of single neuronal cell apoptosis in patients with glaucoma. Brain 140, 1757–1767. [PubMed: 28449038]

Coussa RG, Traboulsi EI, 2012. Choroideremia: a review of general findings and pathogenesis. Ophthalmic Genetics 33, 57–65. [PubMed: 22017263]

Csaky K, Ferris F 3rd, Chew EY, Nair P, Cheetham JK, Duncan JL, 2017. Report from the NEI/FDA endpoints workshop on age-related macular degeneration and inherited retinal diseases. Investigative Ophthalmology & Visual Science 58, 3456–3463. [PubMed: 28702674]

Cunefare D, Fang L, Cooper RF, Dubra A, Carroll J, Farsiu S, 2017a. Open source software for automatic detection of cone photoreceptors in adaptive optics ophthalmoscopy using convolutional neural networks. Scientific Reports 7, 6620. [PubMed: 28747737]

Cunefare D, Huckenpahler AL, Patterson EJ, Dubra A, Carroll J, Farsiu S, 2019. RAC-CNN: Multimodal deep learning based automatic detection and classification of rod and cone photoreceptors in adaptive optics scanning light ophthalmoscope images. Biomedical Optics Express 10, 3815–3832. [PubMed: 31452977]

Cunefare D, Langlo CS, Dubra A, Carroll J, Farsiu S, 2017b. Automatic detection of cones in multimodal adaptive optics scanning light ophthalmoscope images of achromatopsia. Investigative Ophthalmology & Visual Science 58, 300.

Curcio CA, 2001. Photoreceptor topography in ageing and age-related maculopathy. Eye 15, 376–383. [PubMed: 11450761]

Curcio CA, Allen KA, Sloan KR, Lerea CL, Hurley JB, Klock IB, Milam AH, 1991. Distribution and morphology of human cone photoreceptors stained with anti-blue opsin. Journal of Comparative Neurology 312, 610–624.

Curcio CA, Sloan KR, Kalina RE, Hendrickson AE, 1990. Human photoreceptor topography. Journal of Comparative Neurology 292, 497–523.

Dartnall HJA, Bowmaker JK, Mollon JD, 1983. Microspectrophotometry of human photoreceptors, in: Mollon J, Sharpe L. (Eds.), Colour Vision: Physiology and Psychophysics. Academic Press, New York, pp. 69–80.

Davidson B, Kalitzeos A, Carroll J, Dubra A, Ourselin S, Michaelides M, Bergeles C, 2018a. Automatic cone photoreceptor localisation in healthy and Stargardt afflicted retinas using deep learning. Scientific Reports 8, 7911. [PubMed: 29784939]

Davidson B, Kalitzeos A, Carroll J, Dubra A, Ourselin S, Michaelides M, Bergeles C, 2018b. Fast adaptive optics scanning light ophthalmoscope retinal montaging. Biomedical Optics Express 9, 4317–4328. [PubMed: 30615701]

Davoudi S, Sevgi DD, TYasa C, Lains I, Ebrahimiadib N, Roohipoor R, Papavasilieou E, Comander J, Sobrin L, 2018. High reliability of cone cell measurements with adaptive optics scanning laser

ophthalmoscopy in a simulated real-life clinical setting. Ophthalmic Surgery Lasers & Imaging Retina 49, 228–235.

Dees EW, Dubra A, Baraas RC, 2011. Variability in parafoveal cone mosaic in normal trichromatic individuals. Biomedical Optics Express 2, 1351–1358. [PubMed: 21559146]

Delori F, Greenberg JP, Woods RL, Fischer J, Duncker T, Sparrow J, Smith RT, 2011. Quantitative measurements of autofluorescence with the scanning laser ophthalmoscope. Investigative Ophthalmology & Visual Science 52, 9379–9390. [PubMed: 22016060]

Delori FC, 1994. Spectrophotometer for Noninvasive Measurement of Intrinsic Fluorescence and Reflectance of the Ocular Fundus. Applied Optics 33, 7439–7452. [PubMed: 20941307]

Deng WT, Li J, Zhu P, Chiodo VA, Smith WC, Freedman B, Baehr W, Pang J, Hauswirth WW, 2018. Human L- and M-opsins restore M-cone function in a mouse model for human blue cone monochromacy. Molecular Vision 24, 17–28. [PubMed: 29386880]

Destro M, Puliafito CA, 1989. Indocyanine green videoangiography of choroidal neovascularization. Ophthalmology 96, 846–853. [PubMed: 2472588]

DeVries HL, 1948. The fundamental response curves of normal and abnormal dichromatic and trichromatic eyes. Physica 14, 367–380.

Dhakal KR, Walters S, McGregor JE, Schwarz C, Strazzeri JM, Aboualizadeh E, Bateman B, Huxlin KR, Hunter JJ, Williams DR, Merigan WH, 2020. Localized photoreceptor ablation using femtosecond pulses focused with adaptive optics. Translational Vision Science & Technology 9, 16.

Di Iorio V, Esposito G, De Falco F, Boccia R, T. F, Colucci R, G. DR, Melillo P, Salvatore F, Simonelli F, Testa F, 2019. CHM/REP1 transcript expression and loss of visual function in patients affected by choroideremia. Investigative Ophthalmology & Visual Science 60, 1547–1555.

Dobi ET, Puliafito CA, Destro M, 1989. A new model of experimental choroidal neovascularization in the rat. Archives of Ophthalmology 107, 264–269. [PubMed: 2464985]

Doble N, Choi SS, Codana JL, Christou J, Enoch JM, Williams DR, 2011. In vivo imaging of the human rod photoreceptor mosaic. Optics Letters 36, 31–33. [PubMed: 21209677]

Dreher AW, Bille JF, Weinreb RN, 1989. Active optical depth resolution improvement of the laser tomographic scanner. Applied Optics 28, 804–808. [PubMed: 20548563]

Dubis AM, Cooper RF, Aboshiha J, Langlo CS, Sundaram V, Liu B, Collison F, Fishman GA, Moore AT, Webster AR, Dubra A, Carroll J, Michaelides M, 2014. Genotype-dependent variability in residual cone structure in achromatopsia: towards developing metrics for assessing cone health. Investigative Ophthalmology & Visual Science 55, 7303–7311.

Dubra A, Sulai Y, 2011. Reflective afocal broadband adaptive optics scanning ophthalmoscope. Biomedical Optics Express 2, 1757–1768. [PubMed: 21698035]

Dubra A, Sulai Y, Norris JL, Cooper RF, Dubis AM, Williams DR, Carroll J, 2011. Noninvasive imaging of the human rod photoreceptor mosaic using a confocal adaptive optics scanning ophthalmoscope. Biomedical Optics Express 2, 1864–1876. [PubMed: 21750765]

Duncan JL, Liang W, Maguire MG, Audo I, Ayala AR, Birch DG, Carroll J, Cheetham JK, Esposti SD, Durham TA, Erker L, Farsiu S, Ferris III FL, Heon E, Hufnagel RB, Iannaccone A, Jaffe GJ, Kay CN, Michaelides M, Pennesi ME, Sahel J-A, 2020. Baseline visual field findings in the RUSH2A study: Associated factors and correlation with other measures of disease severity. American Journal of Ophthalmology 9394, 30254–30253.

Duncan JL, Pierce EA, Laster AM, Daiger SP, Birch DG, Ash JD, Iannaccone A, Flannery JG, Sahel JA, Zack DJ, Zarbin MA, 2018. Inherited retinal degenerations: current landscape and knowledge gaps. Translational Vision Science & Technology 7, 6.

Duncan JL, Zhang Y, Gandhi J, Nakanishi C, Othman M, Branham KE, Swaroop A, Roorda A, 2007. High-resolution imaging with adaptive optics in patients with inherited retinal degeneration. Investigative Ophthalmology & Visual Science 48, 3283–3291. [PubMed: 17591900]

Dysli C, Wolf S, Berezin MY, Sauer L, Hammer M, Zinkernagel MS, 2017. Fluorescence lifetime imaging ophthalmoscopy. Progress in Retinal and Eye Research 60, 120–143. [PubMed: 28673870]

Dysli C, Wolf S, Hatz K, Kinkernagel MS, 2016a. Fluorescence lifetime imaging in Stargardt disease: Potential marker for disease progression. Investigative Ophthalmology and Visual Science 57, 832–841. [PubMed: 26934141]

Dysli C, Wolf S, Tran HV, Kinkernagel MS, 2016b. Autofluorescence lifetimes in patients with choroideremia identify photoreceptors in areas with retinal pigment epithelium atrophy. Investigative Ophthalmology & Visual Science 57, 6714–6721. [PubMed: 27951593]

Feeks JA, Hunter JJ, 2017. Adaptive optics two-photon excited fluorescence lifetime imaging ophthalmoscopy of exogenous fluorophores in mice. Biomedical Optics Express 8, 2483–2495. [PubMed: 28663886]

Flatter JA, Cooper RF, Dubow MJ, Pinhas A, Singh RS, Kapur R, Shah N, Walsh RD, Hong SH, Weinberg DV, Stepien KE, Wirostko WJ, Robison S, Dubra A, Rosen RB, Connor TB Jr., Carroll J, 2014. Outer retinal structure after closed-globe blunt ocular trauma. Retina 34, 2133–2146. [PubMed: 24752010]

Fleischman JA, O'Donnell FEJ, 1981. Congenital X-linked incomplete achromatopsia. Evidence for slow progression, carrier fundus findings, and possible genetic linkage with glucose-6-phosphate dehydrogenase locus. Archives of Ophthalmology 99, 468–472. [PubMed: 6971088]

Flower RW, Peiretti E, Magnani M, Rossi L, Serafini S, Gryczynski Z, Gryczynski I, 2008. Observation of erythrocyte dynamics in the retinal capillaries and choriocapillaris using ICG-loaded erythrocyte ghost cells. Investigative Ophthalmology & Visual Science 49, 5510–5516. [PubMed: 18708621]

Foote KG, De la Huerta I, Gustafson K, Baldwin A, Zayit-Soudry S, Rinella N, Porco TC, Roorda A, Duncan JL, 2019a. Cone spacing correlates with retinal thickness and microperimetry in patients with inherited retinal degenerations. Investigative Ophthalmology & Visual Science 60, 1234–1243. [PubMed: 30924848]

Foote KG, Loumou P, Griffin S, Qin J, Ratnam K, Porco TC, Roorda A, Duncan JL, 2018. Relationship between foveal cone structure and visual acuity measured with adaptive optics scanning laser opthalmoscopy in retinal degeneration. Investigative Ophthalmology & Visual Science 59, 3385–3393. [PubMed: 30025078]

Foote KG, Rinella N, Tang J, Bensaid N, Zhou H, Zhang Q, Wang RK, Porco TC, Roorda A, Duncan JL, 2019b. Cone structure persists beyond margins of short-wavelength autofluorescence in choroideremia. Investigative Ophthalmology & Visual Science 60, 4931–4942. [PubMed: 31770433]

Foote KG, Roorda A, Duncan JL, 2019c. Multimodal imaging in choroideremia. Advances in Experimental Medicine and Biology 1185, 139–143. [PubMed: 31884602]

Foote KG, Wong JJ, Boehm AE, Bensinger E, Porco TC, Roorda A, Duncan JL, 2020. Comparing cone structure and function in RHO- and RPGR- associated retinitis pigmentosa. Investigative Ophthalmology & Visual Science 61, 42.

Gale MJ, Feng S, Titus HE, Smith TB, Pennesi ME, 2016. Interpretation of flood-illuminated adaptive optics images in subjects with retinitis pigmentosa. Advances in Experimental Medicine and Biology 854, 291–297. [PubMed: 26427424]

Gale MJ, Harman GA, Chen J, Pennesi ME, 2019. Repeatability of adaptive optics automated cone measurements in subjects with retinitis pigmentosa and novel metrics for assessment of image quality. Translational Vision Science & Technology 8, e17.

Gao W, Cense B, Zhang Y, Jonnal RS, Miller DT, 2008. Measuring retinal contributions to the optical Stiles-Crawford effect with optical coherence tomography. Optics Express 16, 6486–6501. [PubMed: 18516251]

Garafalo AV, Cideciyan AV, Heon E, Sheplock R, Pearson A, Yu CWY, Sumaroka A, Aguirre GD, Jacobson SG, 2019. Progress in treating inherited retinal diseases: Early subretinal gene therapy clinical trials and candidates for future initiatives. Progress in Retinal and Eye Research, 100827.

Gardiner SK, Swanson WH, Goren D, Mansberger SL, Demirel S, 2014. Assessment of the reliability of standard automated perimetry in regions of glaucomatous damage. Ophthalmology 121, 1359–1369. [PubMed: 24629617]

Garrioch R, Langlo C, Dubis AM, Cooper RF, Dubra A, Carroll J, 2012. Repeatability of in vivo parafoveal cone density and spacing measurements. Optometry and Vision Science 89, 632–643. [PubMed: 22504330]

Genead MA, Fishman GA, Rha J, Dubis AM, Bonci DM, Dubra A, Stone EM, Neitz M, Carroll J, 2011. Photoreceptor structure and function in patients with congenital achromatopsia. Investigative Ophthalmology & Visual Science 52, 7298–7308. [PubMed: 21778272]

Geng A, Dubra A, Yin L, Merigan WH, Sharma R, Libby RT, Williams DR, 2012. Adaptive optics retinal imaging in the living mouse eye. Biomedical Optics Express 3, 715–734. [PubMed: 22574260]

Georgiou M, Litts KM, Kalitzeos A, Langlo CS, Kane T, Singh N, Kassilian M, Hirji N, Kumaran N, Dubra A, Carroll J, Michaelides M, 2019a. Adaptive optics retinal imaging in *CNGA3*-associated achromatopsia: Retinal characterization, interocular symmetry, and intrafamilial variability. Investigative Ophthalmology & Visual Science 60, 383–396. [PubMed: 30682209]

Georgiou M, Robson AG, Singh N, Pontikos N, Kane T, Hirji N, Ripamonti C, Rotsos T, Dubra A, Kalitzeos A, Webster AR, Carroll J, Michaelides M, 2019b. Deep phenotyping of *PDE6C*-associated achromatopsia. Investigative Ophthalmology & Visual Science 60, 5112–5123. [PubMed: 31826238]

Georgiou M, Singh N, Kane T, Robson AG, Kalitzeos A, Hirji N, Webster A, Dubra A, Carroll J, Michaelides M, 2020. Photoreceptor structure in GNAT2-associated achromatopsia. Investigative Ophthalmology & Visual Science 61, 40.

Gofas-Salas E, Mecê P, Mugnier L, Bonnefois AM, Petit C, Grieve K, Sahel J, Paques M, Meimon S, 2019. Near infrared adaptive optics flood illumination retinal angiography. Biomedical Optics Express 10, 2730–2743. [PubMed: 31259047]

Granger CE, Yang Q, Song H, Saito K, Nozato K, Latchney LR, Leonard BT, Chung MM, Williams DR, Rossi EA, 2018. Human retinal pigment epithelium: In vivo cell morphometry, multispectral autofluorescence, and relationship to cone mosaic. Investigative Ophthalmology & Visual Science 59, 5705–5716. [PubMed: 30513531]

Gray DC, Merigan W, Wolfing JI, Gee BP, Porter J, Dubra A, Twietmeyer TH, Ahmad K, Tumbar R, Reinholz F, Williams DR, 2006. In vivo fluorescence imaging of primate retinal ganglion cells and retinal pigment epithelial cells. Optics Express 14, 7144–7158. [PubMed: 19529085]

Grieve K, Gofas-Salas E, Ferguson RD, Sahel JA, Paques M, Rossi EA, 2018. In vivo near-infrared autofluorescence imaging of retinal pigment epithelial cells with 757 nm excitation. Biomedical Optics Express 9, 5946–5961. [PubMed: 31065405]

Gu B, Wang X, Twa MD, Tam J, Girkin C, Zhang Y, 2018. Noninvasive in vivo characterization of erythrocyte motion in human retinal capillaries using high-speed adaptive optics near-confocal imaging. Biomedical Optics Express 9, 3653–3677. [PubMed: 30338146]

Guevara-Torres A, Williams DR, Schallek JB, 2015. Imaging translucent cell bodies in the living mouse retina without contrast agents. Biomedical Optics Express 6, 2106–2119. [PubMed: 26114032]

Guevara-Torres A, Williams DR, Schallek JB, 2020. Origin of cell contrast in offset aperture adaptive optics ophthalmoscopy. Optics Letters 45, 840–843. [PubMed: 32058484]

Gunn M, 1883. Peculiar appearance in the retina in the vicinity of the optic disc occuring in several members of the same family. Transactions of the Ophthalmological Societies of the United Kingdom 3, 110–113.

Hagag AM, Gao SS, Jia Y, Huang D, 2017. Optical coherence tomography angiography: Technical principles and clinical applications in ophthalmology. Taiwan Journal of Ophthalmology 7, 115–129. [PubMed: 28966909]

Hagan K, DuBose TB, Cunefare D, Simmerer C, Waterman G, Park J, Kuo AN, McNabb RP, Izatt JA, Farsiu S, 2020. Wavefront sensorless multimodal handheld adaptive optics scanning laser ophthalmoscope for in vivo imaging of human retinal cones. Proceedings of the Society of Photo-optical Instrumentation Engineers 11218.

Hagstrom SA, Neitz J, Neitz M, 1998. Variations in cone populations for red-green color vision examined by analysis of mRNA. NeuroReport 9, 1963–1967. [PubMed: 9674575]

Hammer DX, Liu Z, Cava J, Carroll J, Saeedi O, 2020. On the axial location of Gunn's dots. American Journal of Ophthalmology Case Reports.

Hansen S, Batson S, Weinlander KM, Cooper RF, Scoles DH, Karth PA, Weinberg DV, Dubra A, Kim JE, Carroll J, Wirostko WJ, 2015. Assessing photoreceptor structure after macular hole closure. Retinal Cases & Brief Reports 9, 15–20. [PubMed: 25525907]

Hariri AH, Velaga SB, Girach A, Ip MS, Le PV, Lam BL, Fischer MD, Sankila EM, Pennesi ME, Holz FG, MacLaren RE, Birch DG, Hoyng CB, MacDonald IM, Black GC, Tsang SH, Bressler NM, Larsen M, Gorin MB, Webster AR, Sadda SR, Group., N.H.o.t.P.o.C.N.S., 2017. Measurement and reproducibility of preserved ellipsoid zone area and preserved retinal pigment epithelium area in eyes with choroideremia. American Journal of Ophthalmology 179, 110–117. [PubMed: 28499705]

Harvey PS, King RA, Summers CG, 2006. Spectrum of foveal development in albinism detected with optical coherence tomography. Journal of the American Association for Pediatric Ophthalmology and Strabismus 10, 237–242.

Heagerty AM, Aalkjaer C, Bund SJ, Korsgaard N, Mulvany MJ, 1993. Small artery structure in hypertension. Dual processes of remodeling and growth. Hypertension 21, 391–397. [PubMed: 8458640]

Heisler M, Ju MJ, Bhalla M, Schuck N, Athwal A, Navajas EV, Beg MF, Sarunic MV, 2018. Automated identification of cone photoreceptors in adaptive optics optical coherence tomography images using transfer learning. Biomedical Optics Express 9, 5353–5367. [PubMed: 30460133]

Heitkotter H, Linderman R, Cava J, Woertz EN, Mastey R, Summerfelt P, Chui TYP, Bosen RB, Patterson EJ, Vincent A, Carroll J, Minassian BA, 2020. Retinal manifestations of Lafora disease. Investigative Ophthalmology & Visual Science 61, 5307.

Hillmann D, Spahr H, Pfäffle C, Sudkamp H, Franke G, Hüttmann G, 2016. In vivo optical imaging of physiological responses to photostimulation in human photoreceptors. Proceedings of the National Academy of Sciences of the United States of America 113, 13138–13143. [PubMed: 27729536]

Hirji N, Georgiou M, Kalitzeos A, Bainbridge JW, Kumaran N, Aboshiha J, Carroll J, Michaelides M, 2018. Longitudinal assessment of retinal structure in achromatopsia patients with long-term follow-up. Investigative Ophthalmology & Visual Science 59, 5735–5744. [PubMed: 30513534]

Hoang QV, Linsenmeier RA, Chung CK, Curcio CA, 2002. Photoreceptor inner segments in monkey and human retina: Mitochondrial density, optics, and regional variation. Visual Neuroscience 19, 395–407. [PubMed: 12511073]

Hofer H, Carroll J, Neitz J, Neitz M, Williams DR, 2005a. Organization of the human trichromatic cone mosaic. Journal of Neuroscience 25, 9669–9679. [PubMed: 16237171]

Hofer H, Singer B, Williams DR, 2005b. Different sensations from cones with the same photopigment. Journal of Vision 5, 444–454. [PubMed: 16097875]

Hofer H, Sredar N, Queener H, Li C, Porter J, 2011. Wavefront sensorless adaptive optics ophthalmoscopy in the human eye. Optics Express 19, 14160–14171. [PubMed: 21934779]

Horton JC, Parker AB, Botelho JV, Duncan JL, 2015. Spontaneous regeneration of human photoreceptor outer segments. Scientific Reports 5.

Huang D, Swanson EA, Lin CP, Schuman JS, Stinson WG, Chang W, Hee MR, Flotte T, Gregory K, Puliafito CA, Fujimoto JG, 1991. Optical coherence tomography. Science 254, 1178–1181. [PubMed: 1957169]

Huang G, Gast TJ, Burns SA, 2014. In vivo adaptive optics imaging of the temporal raphe and its relationship to the optic disc and fovea in the human retina. Investigative Ophthalmology & Visual Science 55, 5952–5961. [PubMed: 25146991]

Huang G, Qi X, Chui TY, Zhong Z, Burns SA, 2012. A clinical planning module for adaptive optics SLO imaging. Optometry and vision science : official publication of the American Academy of Optometry 89, 593–601. [PubMed: 22488269]

Jackson K, Vergilio GK, Cooper RF, Ying GS, Morgan JIW, 2019. A 2-year longitudinal study of normal cone photoreceptor density. Investigative Ophthalmology & Visual Science 60, 1420–1430. [PubMed: 30943290]

Jacob J, Paques M, Krivosic V, Dupas B, Erginay A, Tadayoni R, Gaudric A, 2017. Comparing Parafoveal Cone Photoreceptor Mosaic Metrics in Younger and Older Age Groups Using an Adaptive Optics Retinal Camera. Ophthalmic Surgery Lasers Imaging Retina 48, 45–50.

Jacobson SG, Aleman TS, Cideciyan AV, Sumaroka A, Schwartz SB, Windsor EA, Traboulsi EI, Heon E, Pittler SJ, Milam AH, Maguire AM, Palczewski K, Stone EM, Bennett J, 2005. Identifying photoreceptors in blind eyes caused by RPE65 mutations: Prerequisite for human gene therapy success. Proceedings of the National Academy of Sciences of the United States of America 102, 6177–6182. [PubMed: 15837919]

Jacobson SG, Aleman TS, Sumaroka A, Cideciyan AV, Roman AJ, Windsor EA, Schwartz SB, Rehm HL, Kimberling WJ, 2009. Disease boundaries in the retina of patients with Usher syndrome caused by MYO7A gene mutations. Investigative Ophthalmology & Visual Science 50, 1886–1894. [PubMed: 19074810]

Jain N, Jia Y, Gao SS, Zhang X, Weleber RG, Huang D, Pennesi ME, 2016. Optical coherence tomography angiography in choroideremia: Correlating choriocapillaris loss with overlying degeneration. JAMA Ophthalmology 134, 697–702. [PubMed: 27149258]

Jonnal R, Kocaoglu OP, Zawadzki RJ, Lee SH, Werner JS, Miller DT, 2015. Author response: Outer retinal bands. Investigative Ophthalmology and Visual Science 56, 2507–2510. [PubMed: 26066597]

Jonnal RS, Besecker JR, Derby JC, Kocaoglu OP, Cense B, Gao W, Wang Q, Miller DT, 2010. Imaging outer segment renewal in living human cone photoreceptors. Optics Express 18, 5257–5270. [PubMed: 20389538]

Jonnal RS, Kocaoglu OP, Zawadzki RJ, Lee SH, Werner JS, Miller DT, 2014. The cellular origins of the outer retinal bands in optical coherence tomography images. Investigative Ophthalmology & Visual Science 55, 7904–7918. [PubMed: 25324288]

Jonnal RS, Kocaoglu OP, Zawadzki RJ, Liu Z, Miller DT, Werner JS, 2016. A review of adaptive optics optical coherence tomography: Technical advances, scientific applications, and the future. Investigative Ophthalmology & Visual Science 57, OCT51-OCT68.

Joseph A, Chu CJ, Feng G, Dholakia K, Schallek J, 2020. Label-free imaging of immune cell dynamics in the living retina using adaptive optics. eLife 9, e60547.

Joseph A, Guevara-Torres A, Schallek J, 2019. Imaging single-cell blood flow in the smallest to largest vessels in the living retina. eLife 8, e45077.

Jung H, Liu J, Liu T, George A, Smelkinson MG, Cohen S, Sharma R, Schwartz O, Maminishkis A, Bharti K, Cukras C, Huryn LA, Brooks BP, Fariss R, Tam J, 2019. Longitudinal adaptive optics fluorescence microscopy reveals cellular mosaicism in patients. JCI Insight 4, e124904.

Kaizu Y, Nakao S, Yamaguchi M, Murakami Y, Salehi-Had H, Ishibashi T, 2016. Detection of airbag impact-induced cone photoreceptor damage by adaptive optics scanning laser ophthalmoscopy: a case report. BMC Ophthalmology 16, 99. [PubMed: 27391597]

Kay DB, Land ME, Cooper RF, Dubis AM, Godara P, Dubra A, Carroll J, Stepien KE, 2013. Outer retinal structure in Best vitelliform macular dystrophy. JAMA Ophthalmology 131, 1207–1215. [PubMed: 23765342]

Kayatz P, Thumann G, Luther TT, Jordan JF, Bartz-Schmidt KU, Esser PJ, Schraermeyer U, 2001. Oxidation causes melanin fluorescence. Investigative Ophthalmology &Visual Science 42, 241–246. [PubMed: 11133875]

Keilhauer CN, Delori FC, 2006. Near-infrared autofluorescence imaging of the fundus: Visualization of ocular melanin. Investigative Ophthalmology & Visual Science 47, 3556–3564. [PubMed: 16877429]

Kellner U, Wissinger B, Tippmann S, Kohl S, Kraus H, Foerster MH, 2004. Blue cone monochromatism: clinical findings in patients with mutations in the red/green opsin gene cluster. Graefe's Archive for Clinical and Experimental Ophthalmology 242, 729–735.

Kocaoglu OP, Liu Z, Zhang F, Kurokawa K, Jonnal RS, Miller DT, 2016. Photoreceptor disc shedding in the living human eye. Biomedical Optics Express 7, 4554–4568. [PubMed: 27895995]

Koch E, Rosenbaum D, Brolly A, Sahel J-A, Chaumet-Riffaud P, Girerd X, Rossant F, Paques M, 2014. Morphometric analysis of small arteries in the human retina using adaptive optics imaging:

Relationship with blood pressure and focal vascular changes. Journal of Hypertension 32, 890–898. [PubMed: 24406779]

Kram YA, Mantey S, Corbo JC, 2010. Avian cone photoreceptors tile the retina as five independent, self-organizing mosaics. PLoS One 5, e8992. [PubMed: 20126550]

Kwon S, Borrelli E, Fan W, Ebraheem A, Marion KM, Sadda SR, 2019. Repeatability of fluorescence lifetime imaging ophthalmoscopy in normal subjects with mydriasis. Translational Vision Science & Technology 8, 15.

Laforest T, Künzi M, Kowalczuk L, Carpentras D, Behar-Cohen F, Moser C, 2020. Transscleral optical phase imaging of the human retina. Nature Photonics 14, 439–445. [PubMed: 32607125]

Lakkaraju A, Umapathy A, Tan LX, Daniele L, Philp NJ, Boesze-Battaglia K, Williams DS, 2020. The cell biology of the retinal pigment epithelium. Progress in Retinal and Eye Research, Epub ahead of print.

Langlo CS, Erker LR, Parker M, Patterson EJ, Higgins BP, Summerfelt P, Razeen MM, Collison FT, Fishman GA, Kay CN, Zhang J, Weleber RG, Yang P, Pennesi ME, Lam BL, Chulay JD, Dubra A, Hauswirth WW, Wilson DJ, Carroll J, ACHM-001 Study Group, 2017. Repeatability and longitudinal assessment of foveal cone structure in CNGB3-associated achromatopsia. Retina 37, 1956–1966. [PubMed: 28145975]

Langlo CS, Flatter JA, Dubra A, Wirostko WJ, Carroll J, 2014. A lensing effect of inner retinal cysts on images of the photoreceptor mosaic. Retina 34, 421–422. [PubMed: 23974999]

Langlo CS, Patterson EJ, Higgins BP, Summerfelt P, Razeen MM, Erker LR, Parker M, Collison FT, Fishman GA, Kay CN, Zhang J, Weleber RG, Yang P, Wilson DJ, Pennesi ME, Lam BL, Chiang J, Chulay JD, Dubra A, Hauswirth WW, Carroll J, ACHM-001 Study Group, 2016. Residual foveal cone structure in *CNGB3*-associated achromatopsia. Investigative Ophthalmology & Visual Science 57, 3984–3995. [PubMed: 27479814]

LaVail MM, Unoki K, Yasumura D, Matthes MT, Yancopoulos GD, Steinberg RH, 1992. Multiple growth factors, cytokines, and neurotrophins rescue photoreceptors from the damaging effects of constant light. Proceedings of the National Academy of Sciences of the United States of America 89, 11249–11253. [PubMed: 1454803]

Lee CS, Baughman DM, Lee AY, 2017. Deep learning is effective for the classification of OCT images of normal versus age-related macular degeneration. Ophthalmology Retina 1, 322–327. [PubMed: 30693348]

Lee DJ, Woertz EN, Visotcky A, Wilk MA, Heitkotter H, Linderman RE, Tarima S, Summers CG, Brooks BP, Brilliant M, Antony BJ, Lujan BJ, Carroll J, 2018. The Henle fiber layer in albinism: Comparison to normal and relationship to outer nuclear layer thickness and foveal cone density. Investigative Ophthalmology & Visual Science 59, 5336–4348.

Legras R, Gaudric A, Woog K, 2018. Distribution of cone density, spacing and arrangement in adult healthy retinas with adaptive optics flood illumination. PLoS One 13, e0191141.

Li KY, Roorda A, 2007. Automated identification of cone photoreceptors in adaptive optics retinal images. Journal of the Optical Society of America. A, Optics, Image Science, and Vision 24, 1358–1363.

Li KY, Tiruveedhula P, Roorda A, 2010. Intersubject variability of foveal cone photoreceptor density in relation to eye length. Investigative Ophthalmology & Visual Science 51, 6858–6867. [PubMed: 20688730]

Li Z, He Y, Keel S, Meng W, Chang RT, He M, 2018. Efficacy of a deep learning system for detecting glaucomatous optic neuropathy based on color fundus photographs. Ophthalmology 125, 1199–1206. [PubMed: 29506863]

Liang J, Williams DR, 1997. Aberrations and retinal image quality of the normal human eye. Journal of the Optical Society of America. A, Optics, Image Science, and Vision 14, 2873–2883.

Liang J, Williams DR, Miller DT, 1997. Supernormal vision and high-resolution retinal imaging through adaptive optics. Journal of the Optical Society of America. A, Optics, Image Science, and Vision 14, 2884–2892.

Litts KM, Georgiou M, Langlo CS, Patterson EJ, Mastey RR, Kalitzeos A, Linderman RE, Lam BL, Fishman GA, Pennesi ME, Kay CN, Hauswirth WW, Michaelides M, Carroll J, 2020. Interocular symmetry of foveal cone topography in congenital achromatopsia. Current Eye Research, 1–8.

Liu BS, Tarima S, Visotcky A, Pechauer A, Cooper RF, Landsem L, Wilk MA, Godara P, Makhijani V, Sulai YN, Syed N, Yasumura G, Garg AK, Pennesi ME, Lujan BJ, Dubra A, Duncan JL, Carroll J, 2014. The reliability of parafoveal cone density measurements. British Journal of Ophthalmology 98, 1126–1131.

Liu J, Jung H, Dubra A, Tam J, 2017a. Automated photoreceptor cell identification on nonconfocal adaptive optics images using multiscale circular voting. Investigative Ophthalmology & Visual Science 58, 4477–4489. [PubMed: 28873173]

Liu T, Jung H, Liu J, Droettboom M, Tam J, 2017b. Noninvasive near infrared autofluorescence imaging of retinal pigment epithelial cells in the human retina using adaptive optics. Biomedical Optics Express 8, 4348–4360. [PubMed: 29082069]

Liu Z, Kocaoglu OP, Miller DT, 2016. 3D imaging of retinal pigment epithelial cells in the living human retina. Investigative Ophthalmology & Visual Science 57, OCT533-OCT543.

Liu Z, Kurokawa K, Hammer DX, Miller DT, 2019. *In vivo* measurement of organelle motility in human retinal pigment epithelial cells. Biomedical Optics Express 10, 4142–4159. [PubMed: 31453000]

Liu Z, Kurokawa K, Zhang F, Lee JJ, Miller DT, 2017c. Imaging and quantifying ganglion cells and other transparent neurons in the living human retina. Proceedings of the National Academy of Sciences of the United States of America 114, 12803–12808. [PubMed: 29138314]

Liu Z, Tam J, Saeedi O, Hammer DX, 2018. Trans-retinal cellular imaging with multimodal adaptive optics. Biomedical Optics Express 9, 4246–4262. [PubMed: 30615699]

Lombardo M, Lombardo G, Schiano Lomoriello D, Ducoli P, Stirpe M, Serrao S, 2013a. Interocular symmetry of parafoveal photoreceptor cone density. Retina 33, 1640–1649. [PubMed: 23538574]

Lombardo M, Serrao S, Ducoli P, Lombardo G, 2013b. Eccentricity dependent changes of density, spacing and packing arrangement of parafoveal cones. Ophthalmic & Physiological Optics 33, 516–526. [PubMed: 23550537]

Lombardo M, Serrao S, Lombardo G, 2014. Technical factors influencing cone packing density estimates in adaptive optics flood illuminated retinal images. Public Library of Science One 9, e107402.

Lujan BJ, Roorda A, Croskrey JA, Dubis AM, Cooper RF, Bayabo JK, Duncan JL, Antony BJ, Carroll J, 2015. Directional optical coherence tomography provides accurate outer nuclear layer and Henle fiber layer measurements. Retina 35, 1511–1520. [PubMed: 25829348]

MacDonald IM, Sauvé Y, Sieving PA, 2007. Preventing blindness in retinal disease: Ciliary neurotrophic factor intraocular implants. Canadian Journal of Ophthalmology 42, 399–402. [PubMed: 17508034]

Makiyama Y, Ooto S, Hangai M, Takayama K, Uji A, Oishi A, Ogino K, Nakagawa S, Yoshimura N, 2013. Macular cone abnormalities in retinitis pigmentosa with preserved central vision using adaptive optics scanning laser ophthalmoscopy. PLoS One 8, e79447.

Makous W, Carroll J, Wolfing JI, Lin J, Christie N, Williams DR, 2006. Retinal microscotomas revealed with adaptive-optics microflashes. Investigative Ophthalmology & Visual Science 47, 4160–4167. [PubMed: 16936137]

Martin JA, Roorda A, 2005. Direct and non-invasive assessment of parafoveal capillary leukocyte velocity. Ophthalmology 112, 2219–2224. [PubMed: 16257054]

Martin PR, Grunert U, Chan TL, Bumsted K, 2000. Spatial order in short-wavelength-sensitive cone photoreceptors: a comparative study of the primate retina. Journal of the Optical Society of America. A, Optics, Image Science, and Vision 17, 557–579.

Masella BD, Hunter JJ, Williams DR, 2014a. Rod photopigment kinetics after photodisruption of the retinal pigment epithelium. Investigative Ophthalmology and Visual Science 55, 7535–7544. [PubMed: 25316724]

Masella BD, Williams DR, Fischer WS, Rossi EA, Hunter JJ, 2014b. Long-term reduction in infrared autofluorescence caused by infrared light below the maximum permissible exposure. Investigative Ophthalmology & Visual Science 55, 3929–3938. [PubMed: 24845640]

Mastey RR, Georgiou M, Langlo CS, Kalitzeos A, Patterson EJ, Kane T, Singh N, Vincent A, Moore AT, Tsang SH, Lin JH, Young MP, Hartnett ME, Heon E, Kohl S, Michaelides M, Carroll

J, 2019. Characterization of retinal structure in *ATF6*-associated achromatopsia. Investigative Ophthalmology & Visual Science 60, 2631–2640. [PubMed: 31237654]

McGregor JE, Yin L, Yang Q, Godat T, Huynh KT, Zhang J, Williams DR, Merigan WH, 2018. Functional architecture of the foveola revealed in the living primate. PLoS One 13, e207102.

Meadway A, McKeown A, Samuels BC, Sincich L, 2020. Lifecycle and lensing of a macular microcyst. Ophthalmic Research 63, 383–391. [PubMed: 31910417]

Meixner E, Michelson G, 2015. Measurement of retinal wall-to-lumen ratio by adaptive optics retinal camera: a clinical research. Graefe's Archive for Clinical and Experimental Ophthalmology 253, 1985–1995.

Mendonça LSM, Braun PX, Martin SM, Hüther A, Mehta N, Zhao Y, Abu-Qamar O, Konstantinou EK, Regatieri CVS, Witkin AJ, Baumal CR, Duker JS, Waheed NK, 2020. Repeatability and reproducibility of photoreceptor density measurement in the macula using the spectralis high magnification module. Ophthalmology Retina S2468–6530, 30174–30173.

Menghini M, Lujan BJ, Zayit-Soudry S, Syed R, Porco TC, Bayabo K, Carroll J, Roorda A, Duncan JL, 2014. Correlation of outer nuclear layer thickness with cone density values in patients with retinitis pigmentosa and healthy subjects. Investigative Ophthalmology & Visual Science 56, 372–381. [PubMed: 25515570]

Merino D, Duncan JL, Tiruveedhula P, Roorda A, 2011. Observation of cone and rod photoreceptors in normal subjects and patients using a new generation adaptive optics scanning laser ophthalmoscope. Biomedical Optics Express 2, 2189–2201. [PubMed: 21833357]

Michaelides M, Hunt DM, Moore AT, 2004. The cone dysfunction syndromes. British Journal of Ophthalmology 88, 291–297.

Michaelides M, Johnson S, Simunovic MP, Bradshaw K, Holder G, Mollon JD, Moore AT, Hunt DM, 2005. Blue cone monochromatism: a phenotype and genotype assessment with evidence of progressive loss of cone function in older individuals. Eye 19, 2–10. [PubMed: 15094734]

Milam AH, Li ZY, Fariss RN, 1998. Histopathology of the human retina in retinitis pigmentosa. Progress in Retinal and Eye Research 17, 175–205. [PubMed: 9695792]

Miller DT, Kocaoglu OP, Wang Q, Lee S, 2011. Adaptive optics and the eye (super resolution OCT). Eye 25, 321–330. [PubMed: 21390066]

Miller DT, Kurokawa K, 2020. Cellular scale imaging of transparent retinal structures and processes using adaptive optics optical coherence tomography. Annual Review of Vision Science 6, 19.11–19.34.

Miller DT, Williams DR, Morris GM, Liang J, 1996. Images of cone photoreceptors in the living human eye. Vision Research 36, 1067–1079. [PubMed: 8762712]

Mizrahi-Meissonnier L, Merin S, Banin E, Sharon D, 2010. Variable retinal phenotypes caused by mutations in the X-linked photopigment gene array. Investigative Ophthalmology & Visual Science 51, 3884–3892. [PubMed: 20220053]

Mo S, Krawitz B, Efstathiadis E, Geyman L, Weitz R, Chui TY, Carroll J, Dubra A, Rosen RB, 2016. Imaging foveal microvasculature: Optical coherence tomography angiography versus adaptive optics scanning light ophthalmoscope fluorescein angiography. Investigative Ophthalmology & Visual Science 57, OCT130-OCT140.

Montoliu L, Grønskov K, Wei A, Martínez-García M, Fernández A, Arveiler B, Morice-Picard F, Riazuddin S, Suzuki T, Ahmed ZM, Rosenberg T, Li W, 2014. Increasing Complexity: new genes and new types of albinism. Pigment Cell & Melanoma Research 27, 11–18. [PubMed: 24066960]

Morgan JI, Han G, Klinman E, Maguire WM, Chung DC, Maguire AM, Bennett J, 2014. High-resolution adaptive optics retinal imaging of cellular structure in choroideremia. Investigative Ophthalmology & Visual Science 55, 6381–6397. [PubMed: 25190651]

Morgan JIW, Chen M, Huang AM, Jiang YY, Cooper RF, 2020. Cone identification in choroideremia: Repeatability, reliability and automation through use of a convolutional neural network. Translational Vision Science & Technology 9, 40.

Morgan JIW, Dubra A, Wolfe R, Merigan WH, Williams DR, 2009a. In vivo autofluorescence imaging of the human and macaque retinal pigment epithelial cell mosaic. Investigative Ophthalmology & Visual Science 50, 1350–1359. [PubMed: 18952914]

Morgan JIW, Hunter JJ, Masella B, Wolfe R, Gray DC, Merigan WH, Delori FC, Williams DR, 2008. Light-induced retinal changes observed with high-resolution autofluorescence imaging of the retinal pigment epithelium. Investigative Ophthalmology & Visual Science 49, 3715–3729. [PubMed: 18408191]

Morgan JIW, Hunter JJ, Merigan WH, Williams DR, 2009b. The reduction of retinal autofluorescence caused by light exposure. Investigative Ophthalmology & Visual Science 50, 6015–6022. [PubMed: 19628734]

Morgan JIW, Vergilio GK, Hsu J, Dubra A, Cooper RF, 2018. The reliability of cone density measurements in the presence of rods. Translational Vision Science & Technology 7, e21.

Morris HJ, Blanco L, Codona JL, Li SL, Choi SS, Doble N, 2015. Directionality of individual cone photoreceptors in the parafoveal region. Vision Research 117, 67–80. [PubMed: 26494187]

Muthiah MN, Gias C, Chen FK, Zhong J, McClelland Z, Sallo FB, Peto T, Coffey PJ, da Cruz L, 2014. Cone photoreceptor definition on adaptive optics retinal imaging. British Journal of Ophthalmology 98, 1073–1079.

Mylonas G, Bolz M, Kriechbaum K, Treu C, Deak G, Lammer J, Scholda C, Schmidt-Erfurth U, 2013. Retinal architecture recovery after grid photocoagulation in diabetic macular edema observed in vivo by spectral domain optical coherence tomography. Retina 33, 717–725. [PubMed: 23528703]

Nathans J, Davenport CM, Maumenee IH, Lewis RA, Hejtmancik JF, Litt M, Lovrien E, Weleber R, Bachynski B, Zwas F, Klingaman R, Fishman G, 1989. Molecular genetics of human blue cone monochromacy. Science 245, 831–838. [PubMed: 2788922]

Nathans J, Maumenee IA, Zrenner E, Sadowski B, Sharpe LT, Lewis RA, Hansen E, Rosenberg P, Schwartz M, Heckenlively JR, Traboulsi E, Klingaman R, Bech-hansen NT, LaRouche GR, Pagon RA, Murphy WH, Weleber RG, 1993. Genetic heterogeneity among blue-cone monochromats. American Journal of Human Genetics 53, 987–1000. [PubMed: 8213841]

Neitz J, Neitz M, 2011. The genetics of normal and defective color vision. Vision Research 51, 633–651. [PubMed: 21167193]

Nesper PL, Scarinci F, Fawzi AA, 2017. Adaptive optics reveals photoreceptor abnormalities in diabetic macular ischemia. PLoS One 12, e0169926.

Ooto S, Hangai M, Sakamoto A, Tsujikawa A, Yamashiro K, Ojima Y, Yamada Y, Mukai H, Oshima S, Inoue T, Yoshimura N, 2010. High-resolution imaging of resolved central serous chorioretinopathy using adaptive optics scanning laser ophthalmoscopy. Ophthalmology 117, 1800–1809. [PubMed: 20673590]

Ooto S, Hangai M, Takayama K, Arakawa N, Tsujikawa A, Koizumi H, Oshima S, Yoshimura N, 2011. High-resolution photoreceptor imaging in idiopathic macular telangiectasia type 2 using adaptive optics scanning laser ophthalmoscopy. Investigative Ophthalmology & Visual Science 52, 5541–5550. [PubMed: 21642620]

Osterberg G, 1935. Topography of the layer of rods and cones in the human retina. Acta Ophthalmologica, 1–103.

Pallikaris A, Williams DR, Hofer H, 2003. The reflectance of single cones in the living human eye. Investigative Ophthalmology & Visual Science 44, 4580–4592. [PubMed: 14507907]

Pandiyan VP, Jiang XT, Maloney-Bertelli A, Kuchenbecker JA, Sharma U, Sabesan R, 2020a. High-speed adaptive otpics line-scan OCT for cellular-resolution optoretinography. Biomedical Optics Express 11, 5274–5296. [PubMed: 33014614]

Pandiyan VP, Maloney-Bertelli A, Kuchenbecker JA, Boyle KC, Ling T, Chen ZC, Park BH, Roorda A, Palanker D, Sabesan R, 2020b. The optoretinogram reveals the primary steps of phototransduction in the living human eye. Science Advances 6, eabc1124.

Paques M, Meimon S, Rossant F, Rosenbaum D, Mrejen S, Sennlaub F, Grieve K, 2018. Adaptive optics ophthalmoscopy: Application to age-related macular degeneration and vascular diseases. Progress in Retinal and Eye Research 66, 1–16. [PubMed: 30010022]

Paques M, Miloudi C, Kulcsar C, Leseigneur A, Chaumette C, Koch E, 2015. High-resolution imaging of Gunn's Dots. Retina 35, 120–124. [PubMed: 25077537]

Park JJ, Soetikno BT, Fawzi AA, 2016. Characterization of the middle capillary plexus using optical coherence tomography angiography in healthy and diabetic eyes. Retina 36, 2039–2050. [PubMed: 27205895]

Patterson EJ, Kalitzeos A, Kasilian M, Gardner JC, Neitz J, Hardcastle AJ, Neitz M, Carroll J, Michaelides M, 2018. Residual cone structure in patients with X-linked cone opsin mutations. Investigative Ophthalmology & Visual Science 59, 4238–4248. [PubMed: 30128495]

Patterson EJ, Kasilian M, Kalitzeos A, Malone CP, Carrigan M, Green A, Farrar GJ, Gardner JC, Hardcastle AJ, Neitz M, Kenna PF, Michaelides M, Carroll J, 2017. Assessing cone photoreceptor structure in patients with mutations in the *OPN1LW/OPN1MW* gene array. Investigative Ophthalmology & Visual Science 58, 1257.

Pedersen HR, Neitz M, Gilson SJ, Landsend ECS, Utheim ØA, Utheim TP, Baraas RC, 2019. The cone photoreceptor mosaic in aniridia: Within-family phenotype-genotype discordance. Ophthalmology Retina 3, 523–534. [PubMed: 31174676]

Pennesi ME, Birch DG, Duncan JL, Bennett J, Girach A, 2019. Choroideremia: Retinal degeneration with an unmet need. Retina 39, 2059–2069. [PubMed: 31021898]

Pinhas A, Dubow M, Shah N, Chui TYP, Scoles DH, Sulai YN, Weitz R, Walsh JB, Carroll J, Dubra A, Rosen RB, 2013. In vivo imaging of human retinal microvasculature using adaptive optics scanning light ophthalmoscope fluorescein angiography. Biomedical Optics Express 4, 1305–1317. [PubMed: 24009994]

Pircher M, Kroisamer JS, Felberer F, Sattmann H, Götzinger E, Hitzenberger CK, 2010. Temporal changes of human cone photoreceptors observed in vivo with SLO/OCT. Biomedical Optics Express 2, 100–112. [PubMed: 21326640]

Pollreisz A, Neschi M, Sloan KR, Pircher M, Mittermueller T, Dacey DM, Schmidt-Erfurth U, Curcio CA, 2020. Atlas of human retinal pigment epithelium organelles significant for clinical imaging. Investigative Ophthalmology & Visual Science 61, 13.

Putnam NM, Hofer HJ, Doble N, Chen L, Carroll J, Williams DR, 2005. The locus of fixation and the foveal cone mosaic. Journal of Vision 5, 632–639. [PubMed: 16231998]

Querques G, Kamami-Levy C, Georges A, Pedinielli A, Capuano V, Blanco-Garavito R, Poulon F, Souied EH, 2016. Adaptive optics imaging of foveal sparing in geographic atrophy secondary to age-related macular degeneration. Retina 36, 247–254. [PubMed: 26200512]

Ramamirtham R, Akula JD, Soni G, Swanson MJ, Bush JN, Moskowitz A, Swanson EA, Favazza TL, Tavormina JL, Mujat M, Ferguson RD, Hansen RM, Fulton AB, 2016. Extrafoveal cone packing in eyes with a history of retinopathy of prematurity. Investigative Ophthalmology and Visual Science 57, 467–475. [PubMed: 26868749]

Ratnam K, Carroll J, Porco TC, Duncan JL, Roorda A, 2013a. Relationship between foveal cone structure and clinical measures of visual function in patients with inherited retinal degenerations. Investigative Ophthalmology & Visual Science 54, 5836–5847.

Ratnam K, Västinsalo H, Roorda A, Sankila E-MK, Duncan JL, 2013b. Cone structure in patients with Usher syndrome type III and mutations in the Clarin 1 gene. JAMA Ophthalmology 131, 67–74. [PubMed: 22964989]

Razeen MM, Cooper RF, Langlo CS, Goldberg MR, Wilk MA, Han DP, Connor TB Jr., Fishman GA, Collison FT, Sulai YN, Dubra A, Carroll J, Stepien KE, 2016. Correlating photoreceptor mosaic structure to clinical findings in Stargardt disease. Translational Vision Science &Technology 5, 6.

Renner AB, Fiebig BS, Cropp E, Weber BHF, Kellner U, 2009. Progression of retinal pigment epithelial alterations during long-term follow-up in female carriers of choroideremia and report of a novel CHM mutation. Archives of Ophthalmology 127, 907–912. [PubMed: 19597113]

Rha J, Dubis AM, Wagner-Schuman M, Tait DM, Godara P, Schroeder B, Stepien K, Carroll J, 2010. Spectral domain optical coherence tomography and adaptive optics: Imaging photoreceptor layer morphology to interpret preclinical phenotypes. Advances in Experimental Medicine and Biology 664, 309–316. [PubMed: 20238030]

Rodieck RW, 1991. The density recovery profile: A method for the analysis of points in the plane applicable to retinal studies. Visual Neuroscience 6, 95–111. [PubMed: 2049333]

Roorda A, Duncan JL, 2015. Adaptive optics ophthalmoscopy. Annual Review of Vision Science 1, 19–50.

Roorda A, Williams DR, 1999. The arrangement of the three cone classes in the living human eye. Nature 397, 520–522. [PubMed: 10028967]

Roorda A, Zhang Y, Duncan JL, 2007. High-resolution in vivo imaging of the RPE mosaic in eyes with retinal disease. Investigative Ophthalmology & Visual Science 48, 2297–2303. [PubMed: 17460294]

Rossi EA, Granger CE, Sharma R, Yang Q, Saito K, Schwarz C, Walters S, Nozato K, Zhang J, Kawakami T, Fischer W, Latchney LR, Hunter JJ, Chung MM, Williams DR, 2017. Imaging individual neurons in the retinal ganglion cell layer of the living eye. Proceedings of the National Academy of Sciences of the United States of America 114, 586–591. [PubMed: 28049835]

Russell S, Bennett J, Wellman JA, Chung DC, Yu Z, Tillman A, Wittes J, Pappas J, Elci O, McCague S, Cross D, Marshall KA, Walshire J, Kehoe TL, Reichert H, Davis M, Raffini L, George LA, Hudson FP, Dingfield L, Zhu X, Haller JA, Sohn EH, Mahajan VB, Pfeifer W, Weckmann M, Johnson C, Gewaily D, Drack A, Stone E, Wachtel K, Simonelli F, Leroy BP, Wright JF, High KA, Maguire AM, 2017. Efficacy and safety of voretigene neparvovec (AAV2-hRPE65v2) in patients with RPE65-mediated inherited retinal dystrophy: A randomised, controlled, open-label, phase 3 trial. Lancet 390, 849–860. [PubMed: 28712537]

Sabesan R, Hofer H, Roorda A, 2015. Characterizing the human cone photoreceptor mosaic via dynamic photopigment densitometry. PLoS One 10, e0144891.

Sabesan R, Schmidt BP, Tuten WS, Roorda A, 2016. The elementary representation of spatial and color vision in the human retina. Science Advances 2, e1600797.

Saleh M, Flores M, Gauthier AS, Elphege E, Delbosc B, 2017. Quantitative analysis of photoreceptor layer reflectivity on en-face optical coherence tomography as an estimator of cone density. Graefe's Archive for Clinical and Experimental Ophthalmology 255, 2119–2126.

Salmon AE, Cooper RF, Langlo CS, Baghaie A, Dubra A, Carroll J, 2017. An automated reference frame selection (ARFS) algorithm for cone imaging with adaptive optics scanning light ophthalmoscopy. Translational Vision Science & Technology 6, 9.

Schallek J, Geng Y, Nguyen H, Williams DR, 2013. Morphology and topography of retinal pericytes in the living mouse retina using in vivo adaptive optics imaging and ex vivo characterization. Investigative Ophthalmology & Visual Science 54, 8237–8250. [PubMed: 24150762]

Schmidt-Erfurth U, Sadeghipour A, Gerendas BS, Waldstein SM, Bogunović H, 2018. Artificial intelligence in retina. Progress in Retinal and Eye Research 67, 1–29. [PubMed: 30076935]

Schmidt BP, Boehm AE, Foote KG, Roorda A, 2018a. The spectral identity of foveal cones is preserved in hue perception. Journal of Vision 18, 19.

Schmidt BP, Sabesan R, Tuten WS, Neitz J, Roorda A, 2018b. Sensations from a single M-cone depend on the activity of surrounding S-cones. Scientific Reports 8, 8561. [PubMed: 29867090]

Schmidt J, Peters S, Sauer L, Schweitzer D, Klemm M, Augsten R, Müller N, Hammer M, 2017. Fundus autofluorescence lifetimes are increased in non-proliferative diabetic retinopathy. Acta Ophthalmologica 95, 33–40. [PubMed: 27519815]

Schmitz-Valckenberg S, Pfau M, Fleckenstein M, Staurenghi G, Sparrow JR, Bindewald-Wittich A, Spaide RF, Wolf S, Sadda SR, Holz FG, 2020. Fundus autofluorescence imaging. Progress in Retinal and Eye Research, 100893.

Schneider U, Sherif-Adel S, Gelisken F, Kreissig I, 1997. Indocyanine green angiography and transmission defects. Acta Ophthalmologica Scandinavica 75, 653–656. [PubMed: 9527325]

Schwarz C, Sharma R, Cheong SK, Keller M, Williams DR, Hunter JJ, 2018. Selective s cone damage and retinal remodeling following intense ultrashort pulse laser exposures in the near-infrared. Investigative Ophthalmology and Visual Science 59, 5973–5984. [PubMed: 30556839]

Schwarz C, Sharma R, Fischer WS, Chung M, Palczewska G, Palczewski K, Williams DR, Hunter JJ, 2016. Safety assessment in macaques of light exposures for functional two-photon ophthalmoscopy in humans. Biomedical Optics Express 7, 5148–5169. [PubMed: 28018732]

Schweitzer D, Hammer M, Schweitzer F, Anders R, Doebbecke T, Schenke S, Gaillard ER, 2004. In vivo measurement of time-resolved autofluorescence at the human fundus. Journal of Biomedical Optics 9, 1214–1222. [PubMed: 15568942]

Schweitzer D, Schenke S, Hammer M, Schweitzer F, Jentsch S, Birckner E, Becker W, Bergmann A, 2007. Towards metabolic mapping of the human retina. Microscopy Research and Technique 70, 410–419. [PubMed: 17393496]

Scoles D, Flatter JA, Cooper RF, Langlo CS, Robison S, Neitz M, Weinberg DV, Pennesi ME, Han DP, Dubra A, Carroll J, 2016. Assessing photoreceptor structure associated with ellipsoid zone disruptions visualized with optical coherence tomography. Retina 36, 91–103. [PubMed: 26166796]

Scoles D, Higgins BP, Cooper RF, Dubis AM, Summerfelt P, Weinberg DV, Kim JE, Stepien KE, Carroll J, Dubra A, 2014a. Microscopic inner retinal hyper-reflective phenotypes in retinal and neurologic disease. Investigative Ophthalmology & Visual Science 55, 4015–4029. [PubMed: 24894394]

Scoles D, Sulai YN, Dubra A, 2013. In vivo dark-field imaging of the retinal pigment epithelium cell mosaic. Biomedical Optics Express 4, 1710–1723. [PubMed: 24049692]

Scoles D, Sulai YN, Langlo CS, Fishman GA, Curcio CA, Carroll J, Dubra A, 2014b. In vivo imaging of human cone photoreceptor inner segments. Investigative Ophthalmology & Visual Science 55, 4244–4251. [PubMed: 24906859]

Seo JH, Yu YS, Kim JH, Choung HK, Heo JW, Kim SJ, 2007. Correlation of visual acuity with foveal hypoplasia grading by optical coherence tomography in albinism. Ophthalmology 114, 1547–1551. [PubMed: 17337060]

Sharma R, Williams DR, Palczewska G, Palczewski K, Hunter JJ, 2016. Two-photon autofluorescence imaging reveals cellular structures throughout the retina of the living primate eye. Investigative Ophthalmology & Visual Science 57, 632–646. [PubMed: 26903224]

Sheehy CK, Tiruveedhula P, Sabesan R, Roorda A, 2015. Active eye-tracking for an adaptive optics scanning laser ophthalmoscope. Biomedical Optics Express 6, 2412–2423. [PubMed: 26203370]

Shu X, Beckmann LJ, Zhang HF, 2017. Visible-light optical coherence tomography: a review. Journal of Biomedical Optics 22, 1–14.

Simeonov DR, Wang X, Wang C, Sergeev Y, Dolinska MB, Bower M, Fischer R, Winer D, Dubrovsky G, Balog JZ, Huizing M, Hart R, Zein WM, Gahl WA, Brooks BP, Adams DR, 2013. DNA variations in oculocutaneous albinism: An updated mutation list and current outstanding issues in molecular diagnostics. Human Mutation 34, 827–835. [PubMed: 23504663]

Simunovic MP, Moore AT, 1998. The cone dystrophies. Eye 12, 553–565. [PubMed: 9775217]

Sincich LC, Zhang Y, Tiruveedhula P, Horton JC, Roorda A, 2009. Resolving single cone inputs to visual receptive fields. Nature Neuroscience 12, 967–969. [PubMed: 19561602]

Snodderly DM, Sandstrom MM, Leung IYF, Zucker CL, Neuringer M, 2002. Retinal pigment epithelial cell distribution in central retina of rhesus monkeys. Investigative Ophthalmology & Visual Science 43, 2815–2818. [PubMed: 12202496]

Spaide RF, Curcio CA, 2011. Anatomical correlates to the bands seen in the outer retina by optical coherence tomography: literature review and model. Retina 31, 1609–1619. [PubMed: 21844839]

Sparrow JR, Hicks D, Hamel CP, 2010. The retinal pigment epithelium in health and disease. Current Molecular Medicine 10, 802–823. [PubMed: 21091424]

Sredar N, Fagbemi OE, Dubra A, 2018. Sub-airy confocal adaptive optics scanning ophthalmoscopy. Translational Vision Science & Technology 7, 17.

Staurenghi G, Sadda S, Chakravarthy U, Spaide RF, Panel IO, 2014. Proposed lexicon for anatomic landmarks in normal posterior segment spectral-domain optical coherence tomography: The IN•OCT consensus. Ophthalmology 121, 1572–1578. [PubMed: 24755005]

Stepien KE, Kay DB, Carroll J, 2014. Outer segment length in different best disease genotypes--reply. JAMA Ophthalmology 132, 1153. [PubMed: 25210993]

Stepien KE, Martinez WM, Dubis AM, Cooper RF, Dubra A, Carroll J, 2011. Detection of photoreceptor disruption after commotio retinae using adaptive optics scanning laser ophthalmoscopy. Investigative Ophthalmology & Visual Science 52, 6657.

Storani de Almeida M, Carvalho LA, 2007. Different schematic eyes and their accuracy to the in vivo eye: A quantitative comparison study. Brazilian Journal of Physiology 37, 387–378.

Strazzeri JM, Hunter JJ, Masella BD, Yin L, Fischer WS, DiLoreto DA Jr, Libby RT, Williams DR, Merigan WH, 2014. Focal damage to macaque photoreceptors produces persistent visual loss. Exp Eye Res 119, 88–96. [PubMed: 24316158]

Sulai YN, Scoles D, Harvey Z, Dubra A, 2014. Visualization of retinal vascular structure and perfusion with a nonconfocal adaptive optics scanning light ophthalmoscope. Journal of the Optical Society of America. A, Optics and Image Science 31, 569–579.

Summers CG, Oetting WS, King RA, 1996. Diagnosis of oculocutaneous albinism with molecular analysis. American Journal of Ophthalmology 121, 724–726. [PubMed: 8644824]

Sun JK, Prager S, Radwan S, Ramsey DJ, Silva PS, Kwak H, Burns SA, Aiello LP, 2012. Photoreceptor mosaic changes in diabetic eye disease assessed by adaptive optics scanning laser ophthalmoscopy (AOSLO). Investigative Ophthalmology & Visual Science 53, 4647.

Sun LW, Johnson RD, Langlo CS, Cooper RF, Razeen MM, Russillo MC, Dubra A, Connor TB Jr., Han D, Pennesi ME, Kay CN, Weinberg DV, Stepien KE, Carroll J, 2016a. Assessing photoreceptor structure in retinitis pigmentosa and Usher syndrome. Investigative Ophthalmology & Visual Science 57, 2428–2442. [PubMed: 27145477]

Sun LW, Johnson RD, Williams V, Summerfelt P, Dubra A, Weinberg DV, Stepien KE, Fishman GA, Carroll J, 2016b. Multimodal imaging of photoreceptor structure in choroideremia. PLoS One 11, e0167526.

Sundaram V, Wilde C, Aboshiha J, Cowing J, Han C, Langlo CS, Chana R, Davidson AE, Sergouniotis PI, Bainbridge JW, Ali RR, Dubra A, Rubin G, Webster AR, Moore AT, Nardini M, Carroll J, Michaelides M, 2014. Retinal structure and function in achromatopsia: implications for gene therapy. Ophthalmology 121, 234–245. [PubMed: 24148654]

Swanson EA, Izatt JA, Hee MR, Huang D, Lin CP, Schuman JS, Puliafito CA, Fujimoto JG, 1993. In vivo retinal imaging by optical coherence tomography. Optics Letters 18, 1864–1866. [PubMed: 19829430]

Swanson WH, King BJ, Burns SA, 2019. Within-subject variability in human retinal nerve fiber bundle width. PLoS One 14, e0223350.

Syed N, Smith JE, John SK, Seabra MC, Aguirre GD, Milam AH, 2001. Evaluation of retinal photoreceptors and pigment epithelium in a female carrier of choroideremia. Ophthalmology 108, 711–720. [PubMed: 11297488]

Syed R, Sundquist SM, Ratnam K, Zayit-Soudry S, Zhang Y, Crawford JB, MacDonald IM, Godara P, Rha J, Carroll J, Roorda A, Stepien KE, Duncan JL, 2013. High-resolution images of retinal structure in patients with choroideremia. Investigative Ophthalmology & Visual Science 54, 950–961. [PubMed: 23299470]

Takayama K, Ooto S, Hangai M, Arakawa N, Oshima S, Shibata N, Hanebuchi M, Inoue T, Yoshimura N, 2012. High-resolution imaging of the retinal nerve fiber layer in normal eyes using adaptive optics scanning laser ophthalmoscopy. PLoS One 7, e33158.

Talcott KE, Ratnam K, Sundquist S, Lucero AS, Lujan BJ, Tao W, Porco TC, Roorda A, Duncan JL, 2011. Longitudinal study of cone photoreceptors during retinal degeneration and in response to ciliary neurotrophic factor treatment. Investigative Ophthalmology & Visual Science 52, 2219–2226. [PubMed: 21087953]

Tam J, Liu J, Dubra A, Fariss R, 2016. In vivo imaging of the human retinal pigment epithelial mosaic using adaptive optics enhanced indocyanine green ophthalmoscopy. Investigative Ophthalmology & Visual Science 57, 4376–4384. [PubMed: 27564519]

Tam J, Martin JA, Roorda A, 2010. Noninvasive visualization and analysis of parafoveal capillaries in humans. Investigative Ophthalmology & Visual Science 51, 1691–1698. [PubMed: 19907024]

Tam J, Roorda A, 2011. Speed quantification and tracking of moving objects in adaptive optics scanning laser ophthalmoscopy. Journal of Biomedical Optics 16, Epub 036002.

Tanna P, Kasilian M, Strauss R, Tee J, Kalitzeos A, Tarima S, Visotcky A, Dubra A, Carroll J, Michaelides M, 2017. Reliability and repeatability of cone density measurements in patients with Stargardt disease and RPGR-associated retinopathy. Investigative Ophthalmology & Visual Science 58, 3608–3615. [PubMed: 28738413]

Tao LW, Wu Z, Guymer RH, Luu CD, 2016. Ellipsoid zone on optical coherence tomography: A review. Clinical & Experimental Ophthalmology 44, 422–430. [PubMed: 26590363]

Tee JJL, Yang Y, Kalitzeos A, Webster A, Bainbridge J, Michaelides M, 2019. Natural history study of retinal structure, progression, and symmetry using ellipsoid zone metrics in RPGR-associated retinopathy. American Journal of Ophthalmology 198, 111–123. [PubMed: 30312579]

Thomas MG, Kumar A, Mohammad S, Proudlock FA, Engle EC, Andrews C, Chan WM, Thomas S, Gottlob I, 2011. Structural grading of foveal hypoplasia using spectral-domain optical coherence tomography: A predictor of visual acuity? Ophthalmology 118, 1653–1660. [PubMed: 21529956]

Thomas MG, McLean RJ, Kohl S, Sheth V, Gottlob I, 2012. Early signs of longitudinal progressive cone photoreceptor degeneration in achromatopsia. British Journal of Ophthalmology 96, 1232–1236.

Thompson DA, Iannaccone A, Ali RR, Arshavsky VY, Audo I, Bainbridge JWB, Besirli CG, Birch DG, Branham KE, Cideciyan AV, Daiger SP, Dalkara D, Duncan JL, Fahim AT, Flannery JG, Gattegna R, Heckenlively JR, Heon E, Jayasundera KT, Khan NW, Klassen H, Leroy BP, Molday RS, Musch DC, Pennesi ME, Petersen-Jones SM, Pierce EA, Rao RC, Reh TA, Sahel JA, Sharon D, Sieving PA, Strettoi E, Yang P, Zacks DN, 2020. Advancing clinical trials for inherited retinal diseases: Recommendations from the second monaciano symposium. Translational Vision Science & Technology 9, 2.

Tian L, Kazmierkiewicz KL, Bowman AS, Mingyao L, Curcio CA, Stambolian DE, 2015. Transcriptome of the human retina, retinal pigmented epithelium and choroid. Genomics 105, 253–264. [PubMed: 25645700]

Ting DSW, Pasquale LR, Peng L, Campbell JP, Lee AY, Raman R, Tan GSW, Schmetterer L, Keane PA, Wong TY, 2019. Artificial intelligence and deep learning in ophthalmology. British Journal of Ophthalmology 103, 167–175.

Torti C, Považay B, Hofer B, Unterhuber A, Carroll J, Ahnelt PK, Drexler W, 2009. Adaptive optics optical coherence tomography at 120,000 depth scans/s for non-invasive cellular phenotyping of the living human retina. Optics Express 17, 19382–19400. [PubMed: 19997159]

Tu JH, Foote KG, Lujan BJ, Ratnam K, Qin J, Gorin MB, Cunningham ET Jr., Tuten WS, Duncan JL, Roorda A, 2017. Dysflective cones: Visual function and cone reflectivity in long-term follow-up of acute bilateral foveolitis. American Journal of Ophthalmology Case Reports 7, 14–19. [PubMed: 29057371]

Tufail A, Rudisill C, Egan C, Kapetanakis VV, S. S-V, Owen CG, Lee A, Louw V, Anderson J, Liew G, Bolter L, Srinivas S, Nittala M, Sadda S, Taylor P, Rudnicka AR, 2017. Automated diabetic retinopathy image assessment software: Diagnostic accuracy and cost-effectiveness compared with human graders. Ophthalmology 124, 343–351. [PubMed: 28024825]

Tumahai P, Moureaux C, Meillat M, Debellemanière G, Flores M, Delbosc B, Saleh M, 2018. High-resolution imaging of photoreceptors in healthy human eyes using an adaptive optics retinal camera. Eye 32, 1723–1730. [PubMed: 29993035]

Tuten WS, Tiruveedhula P, Roorda A, 2012. Adaptive optics scanning laser ophthalmoscope-based microperimetry. Optometry and Vision Science 89, 563–574. [PubMed: 22446720]

Tuten WS, Vergilio GK, Young GJ, Bennett J, Maguire AM, Aleman TS, Brainard DH, Morgan JIW, 2019. Visual function at the atrophic border in choroideremia assessed with adaptive optics microperimetry. Ophthalmology Retina 3, 888–899. [PubMed: 31235310]

Vogel CR, Arathorn DW, Roorda A, Parker A, 2006. Retinal motion estimation in adaptive optics scanning laser ophthalmoscopy. Optics Express 14, 487–497. [PubMed: 19503363]

Wade AR, Fitzke FW, 1998. In vivo imaging of the human cone-photoreceptor mosaic using a confocal laser scanning ophthalmoscope. Lasers and Light in Ophthalmology 8, 129–136.

Wagner-Schuman M, Neitz J, Rha J, Williams DR, Neitz M, Carroll J, 2010. Color-deficient cone mosaics associated with Xq28 opsin mutations: A stop codon versus gene deletions. Vision Research 50, 2396–2402. [PubMed: 20854834]

Wang Q, Tuten WS, Lujan BJ, Holland J, Bernstein PS, Schwartz SD, Duncan JL, Roorda A, 2015. Adaptive optics microperimetry and OCT images show preserved function and recovery of cone visibility in macular telangiectasia type 2 retinal lesions. Investigative Ophthalmology & Visual Science 56, 778–786. [PubMed: 25587056]

Wang X, Gu B, Lu J, Curcio CA, Zhang Y, 2016. Confocal adaptive optics differential phase contrast (AODPC) ophthalmoscopy. Investigative Ophthalmology & Visual Science 57, 60.

Wang Y, Bensaid N, Tiruveedhula P, Ma J, Ravikumar S, Roorda A, 2019. Human foveal cone photoreceptor topography and its dependence on eye length. eLife 8, e47148.

Watzke RC, Soldevilla JD, Trune DR, 1993. Morphometric analysis of human retinal pigment epithelium: Correlation with age and location. Current Eye Research 12, 133–142. [PubMed: 8449024]

Wells-Gray EM, Choi SS, Bries A, Doble N, 2016. Variation in rod and cone density from the fovea to the mid-periphery in healthy human retinas using adaptive optics scanning laser ophthalmoscopy. Eye 30, 1135–1143. [PubMed: 27229708]

Wilk MA, McAllister JT, Cooper RF, Dubis AM, Patitucci TN, Summerfelt P, Anderson JL, Stepien KE, Costakos DM, Connor TB Jr., Wirostko WJ, Chiang PW, Dubra A, Curcio CA, Brilliant MH, Summers CG, Carroll J, 2014. Relationship between foveal cone specialization and pit morphology in albinism. Investigative Ophthalmology & Visual Science 55, 4186–4198. [PubMed: 24845642]

Wilk MA, Wilk BM, Langlo CS, Cooper RF, Carroll J, 2017. Evaluating outer segment length as a surrogate measure of peak foveal cone density. Vision Research 130, 57–66. [PubMed: 27887888]

Williams DR, 2011. Imaging single cells in the living retina. Vision Research 51, 1379–1396. [PubMed: 21596053]

Woertz EN, Omoba BS, Dunn TM, Chiu SJ, Farsiu S, Strul S, Summers CG, Drack AV, Carroll J, 2020a. Assessing ganglion cell layer topography in human albinism using optical coherence tomography. Investigative Ophthalmology & Visual Science 61, 36.

Woertz EN, Wilk MA, Duwell EJ, Mathis JR, Carroll J, DeYoe EA, 2020b. The relationship between retinal cone density and cortical magnification in human albinism. Journal of Vision 20, 1–22.

Wolfing JI, Chung M, Carroll J, Roorda A, Williams DR, 2006. High-resolution retinal imaging of cone–rod dystrophy. Ophthalmology 113, 1019.e1011.

Woog K, Legras R, 2019. Distribution of mid-peripheral cones in emmetropic and myopic subjects using adaptive optics flood illumination camera. Ophthalmic & Physiologic Optics: the journal of the British college of opthalmic opticians 39, 94–103.

Wynne NC, Heitkotter H, Woertz EN, Cava J, Buckland E, Cooper R, Carroll J, 2020. Comparison of cone mosaic metrics between the Spectralis high magnification module (HMM) and adaptive optics scanning light ophthalmoscopy. Investigative Ophthalmology & Visual Science 61, PB0064.

Xu X, Liu X, Wang X, Clark ME, McGwin GJ, Owsley C, Curcio CA, Zhang Y, 2017. Retinal pigment epithelium degeneration associated with subretinal drusenoid deposits in age-related macular degeneration. American Journal of Ophthalmology 175, 87–98. [PubMed: 27986424]

Yang P, Michaels KV, Courtney RJ, Wen Y, Greninger DA, Reznick L, Karr DJ, Wilson LB, Weleber RG, Pennesi ME, 2014. Retinal morphology of patients with achromatopsia during early childhood: Implications for gene therapy. JAMA Ophthalmology 132, 823–831. [PubMed: 24676353]

Yehoshua Z, Rosenfeld PJ, Gregori G, Feuer WJ, Falcão M, Lujan BJ, Puliafito C, 2011. Progression of geographic atrophy in age-related macular degeneration imaged with spectral domain optical coherence tomography. Ophthalmology 118, 679–686. [PubMed: 21035861]

Zalenska-Żmijewska A, Wawrzyniak ZM, Dabrowska A, Szaflik JP, 2019. Adaptive optics (rtx1) high-resolution imaging of photoreceptors and retinal arteries in patients with diabetic retinopathy. Journal of Diabetes Research 2019.

Zalenska-Żmijewska A, Wawrzyniak ZM, Ulińska M, Szaflik J, Dąbrowska A, Szaflik JP, 2017. Human photoreceptor cone density measured with adaptive optics technology (rtx1 device) in healthy eyes: Standardization of measurements. Medicine 96, e7300. [PubMed: 28640147]

Zayit-Soudry S, Duncan JL, Syed R, Menghini M, Roorda AJ, 2013. Cone structure imaged with adaptive optics scanning laser ophthalmoscopy in eyes with nonneovascular age-related macular degeneration. Investigative Ophthalmology & Visual Science 54, 7498–7509. [PubMed: 24135755]

Zayit-Soudry S, Sippl-Swezey N, Porco T, Lynch SK, Syed R, Ratnam K, Menghini M, Roorda A, Duncan JL, 2015. Repeatability of cone spacing measures in eye with inherited retinal degenerations. Investigative Ophthalmology & Visual Science 56, 6179–6189. [PubMed: 26416092]

Zhang F, Kurokawa K, Lassoued A, Crowell JA, Miller DT, 2019a. Cone photoreceptor classification in the living human eye from photostimulation-induced phase dynamics. Proceedings of the National Academy of Sciences of the United States of America 116, 7951–7956. [PubMed: 30944223]

Zhang J, Yang Q, Saito K, Nozato K, Williams DR, Rossi EA, 2015. An adaptive optics imaging system designed for clinical use. Biomedical Optics Express 6, 2120–2137. [PubMed: 26114033]

Zhang P, Zawadzki RJ, Goswami M, Nguyen PT, Yarov-Yarovoy Y, Burns ME, Pugh EN Jr., 2017a. In vivo optophysiology reveals that G-protein activation triggers osmotic swelling and increased light scattering of rod photoreceptors. Proceedings of the National Academy of Sciences of the United States of America 114, E2937–E2946. [PubMed: 28320964]

Zhang T, Kho AM, Srinivasan VJ, 2019b. Improving visible light OCT of the human retina with rapid spectral shaping and axial tracking. Biomedical Optics Express 10, 2918–2931. [PubMed: 31259062]

Zhang Y, Cense B, Rha J, Jonnal RS, Gao H, Zawadzki RJ, Werner JS, Jones S, Olivier S, Miller DT, 2006. High-speed volumetric imaging of cone photoreceptors with adaptive optics spectral-domain optical coherence tomography. Optics Express 14, 4380–4394. [PubMed: 19096730]

Zhang Y, Deng WT, Du W, Zhu P, Li J, Xu F, Sun J, Gerstner CD, Baehr W, Sanford LB, Zhao C, Hauswirth WW, Pang JJ, 2017b. Gene-based therapy in a mouse model of blue cone monochromacy. Scientific Reports 7, 6690. [PubMed: 28751656]

Zhang Y, Wang X, Rivero EB, Clark ME, Witherspoon CD, Spaide RF, Girkin CA, Owsley C, Curcio CA, 2014. Photoreceptor perturbation around subretinal drusenoid deposits as revealed by adaptive optics scanning laser ophthalmoscopy. American Journal of Ophthalmology 158, 584–596.e581.

Zhong Z, Petrig BL, Qi X, Burns SA, 2008. *In vivo* measurement of erythrocyte velocity and retinal blood flow using adaptive optics scanning laser ophthalmoscopy. Optics Express 16, 12746–12756. [PubMed: 18711513]

Zhong Z, Song H, Chui TY, Petrig BL, Burns SA, 2011. Noninvasive measurements and analysis of blood velocity profiles in human retinal vessels. Investigative Ophthalmology & Visual Science 52, 4151–4157. [PubMed: 21467177]

Zobor D, Zobor G, Kohl S, 2015. Achromatopsia: On the doorstep of a possible therapy. Ophthalmic Research 54, 103–108. [PubMed: 26304472]

Highlights:

- AOSLO allows non-invasive imaging of individual retinal cells.
- Few commercial systems and laborious analysis limit clinical use of AOSLO.
- AO-based systems enable assessing function of individual photoreceptor cells.
- AOSLO metrics could provide sensitive outcome measures for clinical trials.

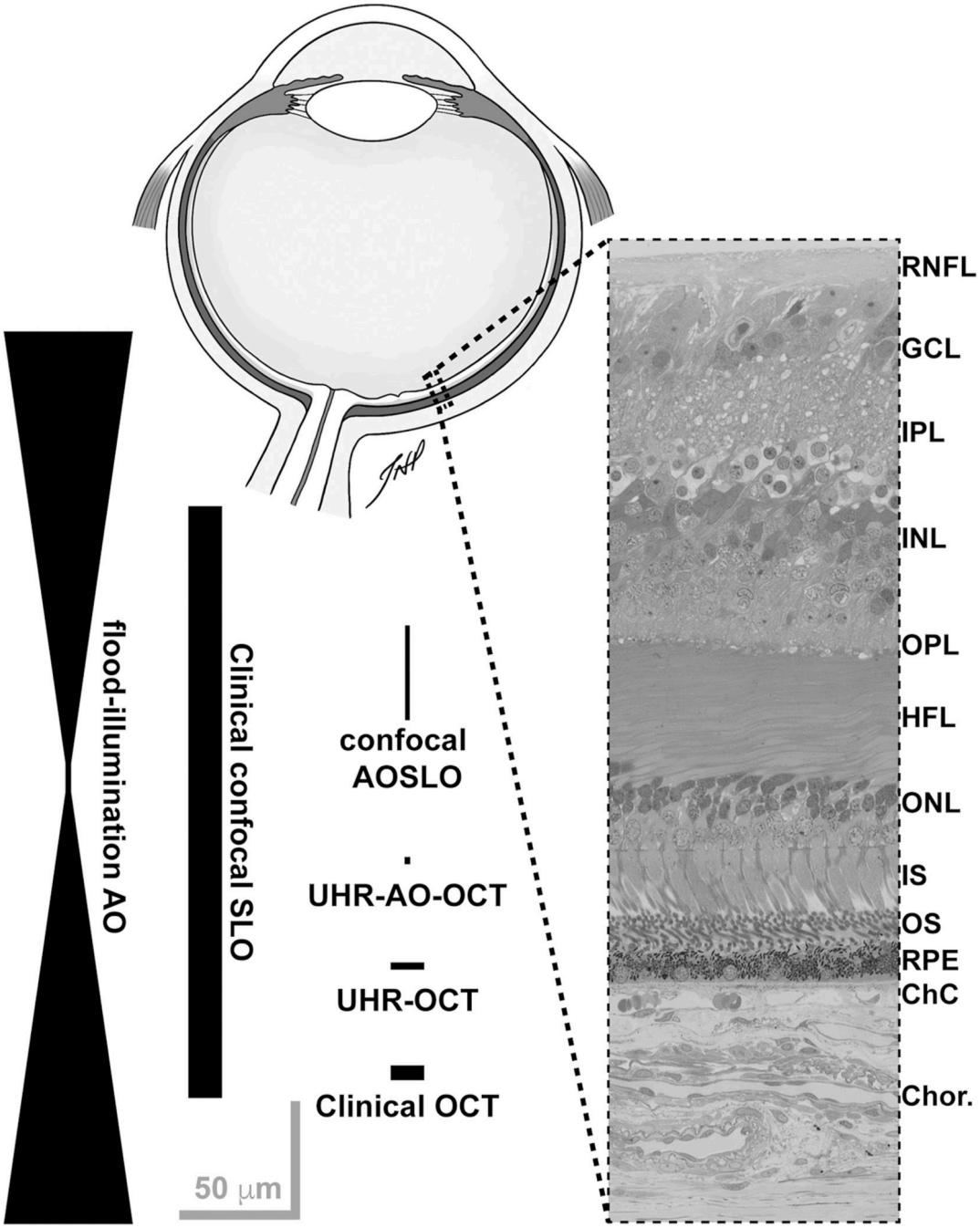

Fig. 1.

Representative resolution of various retinal imaging modalities relative to human retinal anatomy, inspired by Miller et al. (2011). Drawing of a sagittal section of a human eye created by Teresa Patitucci, PhD, Medical College of Wisconsin (not to scale). Histological cross section provided by Dr. Christine Curcio, University of Alabama at Birmingham, from a larger image originally published in Tian et al. (2015). The width and length of the shapes approximate the resolution of each modality (lateral and axial, respectively). None of these are absolute, as a number of variables can influence the actual resolution – including

differences in imaging light source (wavelength, bandwidth), confocal pinhole diameter, pupil size, and axial length of the eye. Retinal layer labels: RNFL = retinal nerve fiber layer; GCL = ganglion cell layer; IPL = inner plexiform layer; INL = inner nuclear layer; OPL = outer plexiform layer; HFL = Henle fiber layer; ONL = outer nuclear layer; IS = photoreceptor inner segments; OS = photoreceptor outer segments; RPE = retinal pigment epithelium; ChC = choriocapillaris; Chor. = choroid. Scale bars = 50 μm.

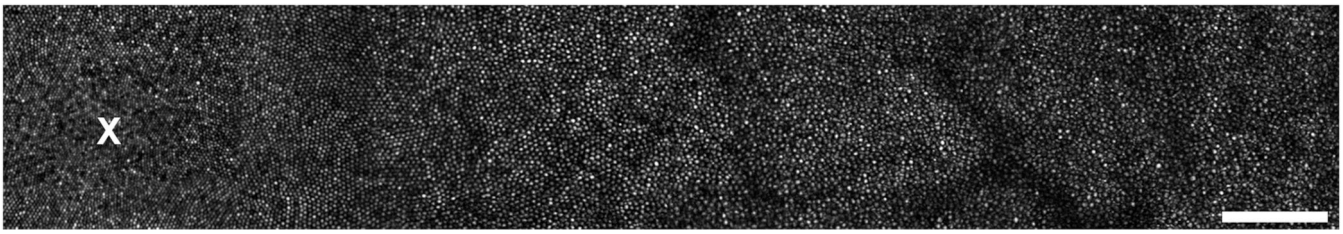

Fig. 2.

Example confocal AOSLO montage of the living human foveal cone mosaic from a 26-year-old female with normal vision. Each bright reflective structure is an individual cone photoreceptor. The location of peak cone density at the fovea is marked with an ‘x’ at the left side of the image. Moving away from the fovea, cone density declines and cone spacing increases precipitously, with smaller rods beginning to appear. Scale bar = 100 μm.

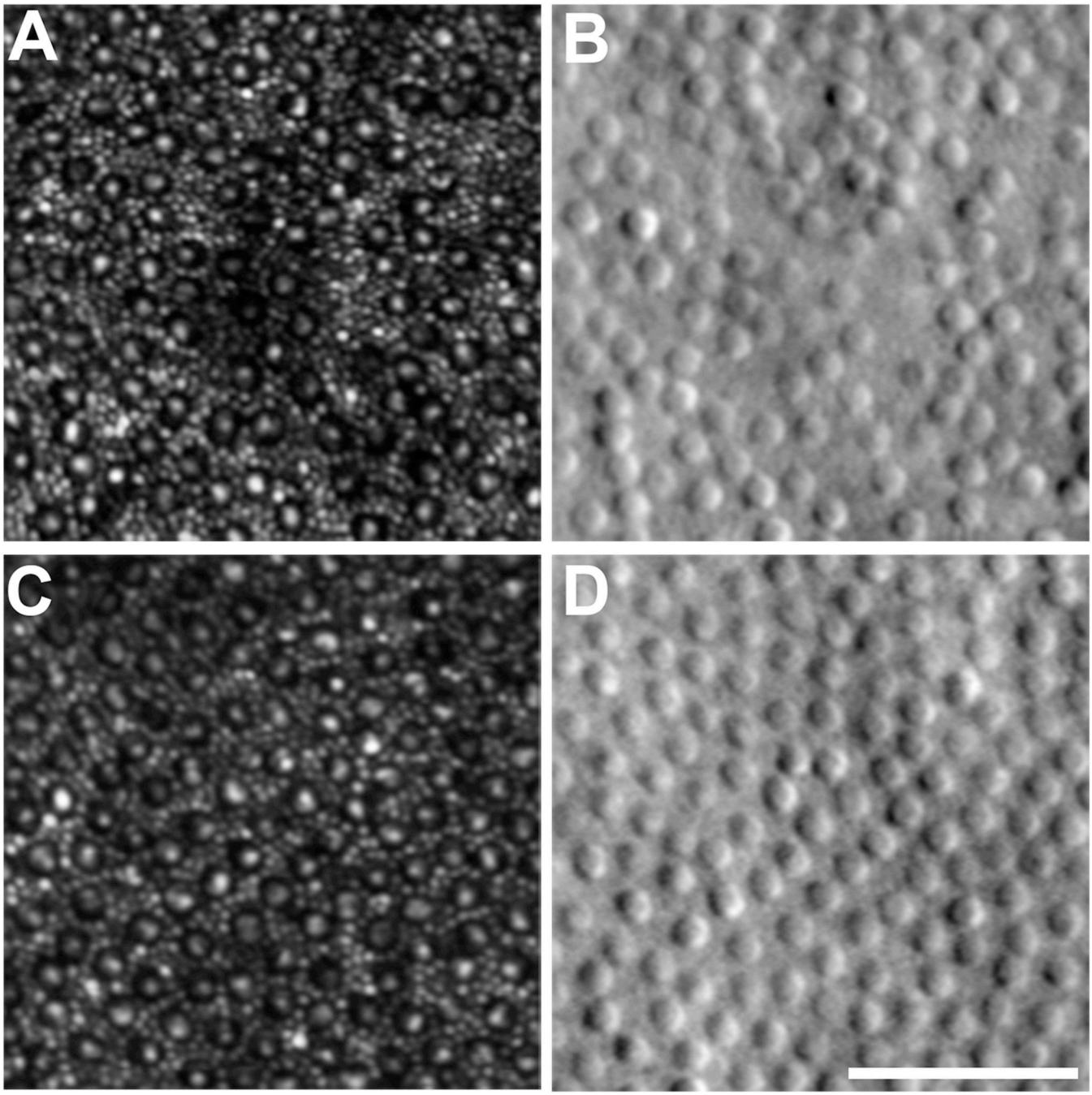

Fig. 3.

AOSLO images of the parafoveal cone mosaic. A, C: Confocal AOSLO images of the rod and cone mosaic. Cones appear as a dark ring with a central reflective core, with the smaller rods filling the space between cones. B, D: Corresponding split-detection AOSLO images at the exact same retinal location as the confocal images. The large circular structures are cone inner segments, with the smaller rods not typically visible due to the lower lateral resolution of this modality. Scale bar = 50 μm.

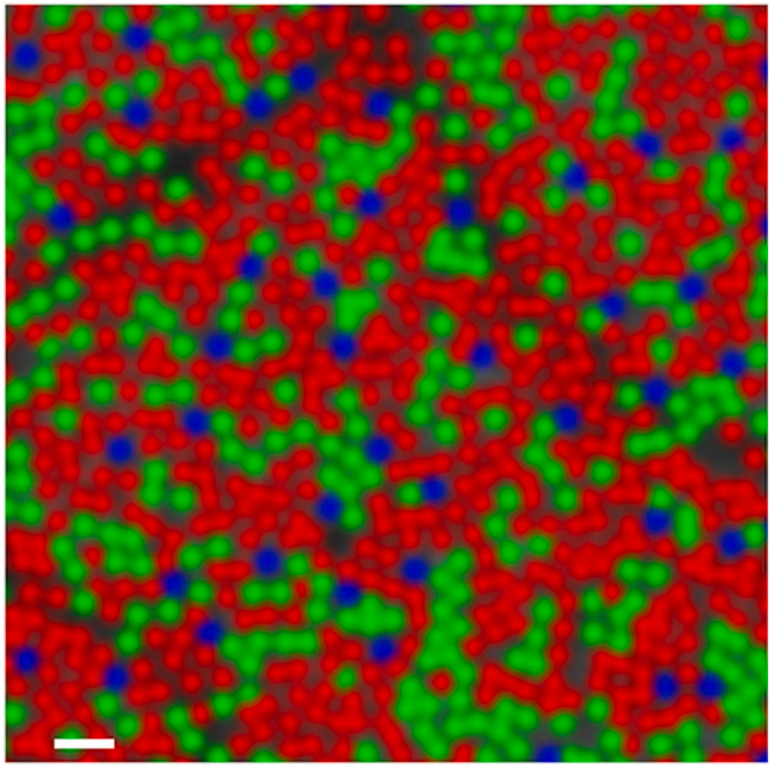

Fig. 4.

False-colored image of the human trichromatic cone mosaic. The reflectance of each cone in an AOSLO image was evaluated following various selective bleaching protocols. Based on the relative change in reflectance under each bleaching condition, the spectral identity of the photopigment within each cell could be inferred. Cones interpreted as long-wavelength sensitive are colored red, those that were middle-wavelength sensitive are colored green, and the short-wavelength sensitive cones are colored blue. Scale bar = 2 arcmin. *Reproduced from* Sabesan et al. (2015).

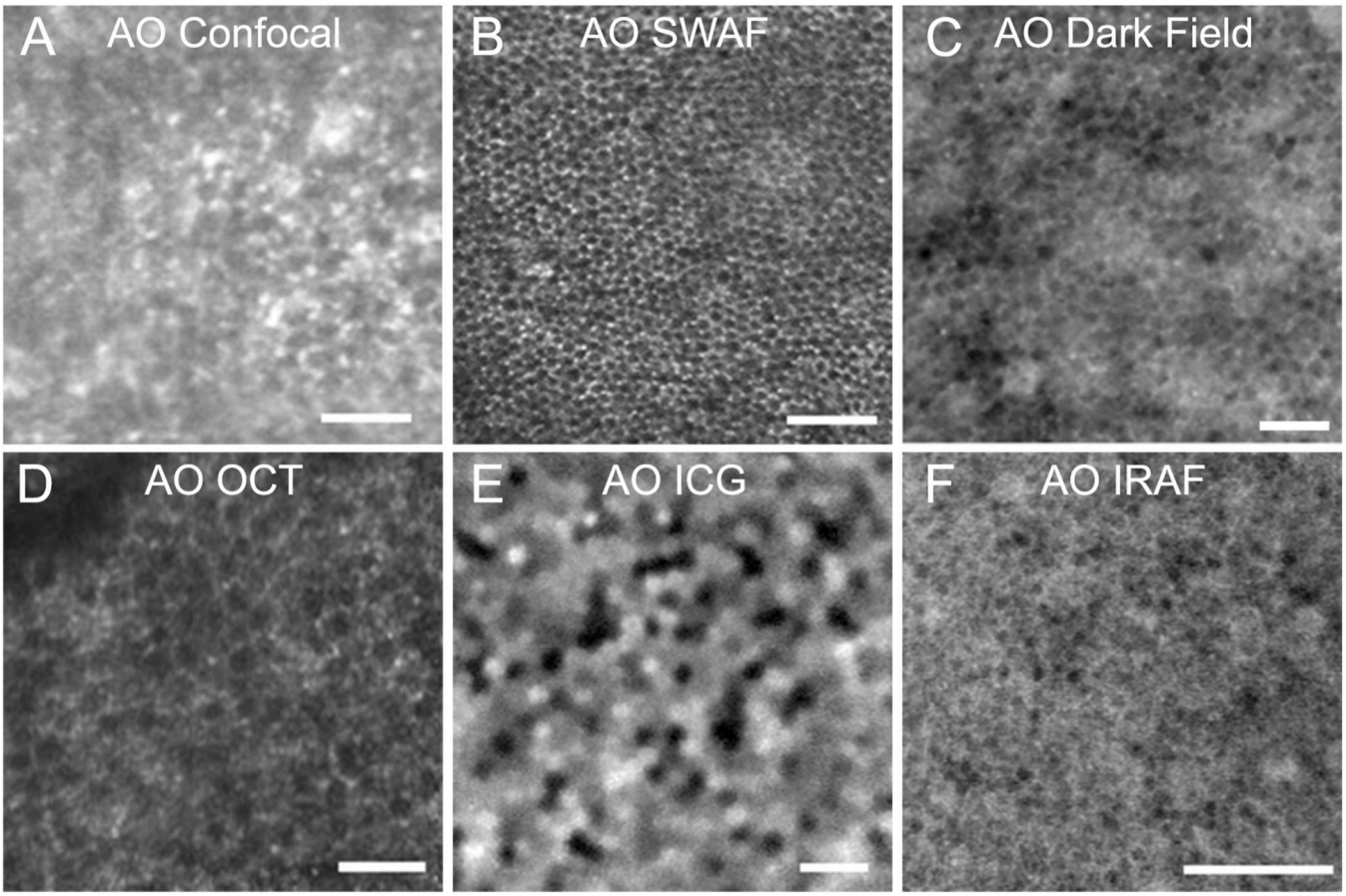

Fig. 5.

Images of retinal pigment epithelial (RPE) cells. A: RPE cells visualized in confocal adaptive optics scanning laser ophthalmoscopy (AOSLO) images of a patient with cone loss due to cone rod dystrophy (Roorda et al., 2007). B: AOSLO with short wavelength autofluorescence (AO-SWAF) capability shows RPE images in a monkey (Morgan et al., 2009a). C: AOSLO dark-field images show hexagonal RPE cells in a normal subject (Scoles et al., 2013). D: AO optical coherence tomography (AO-OCT) images of RPE cells (Liu et al., 2016). E: AO-indocyanine green (AO ICG) image of RPE cells (Tam et al., 2016). F: AO infrared autofluorescence (AO IRAF) images of RPE cells (Liu et al., 2017b). Scale bars, 50 μm. *Modified from* Roorda et al. (2007) and Morgan et al. (2009a), *copyright by the Association for Research in Vision and Ophthalmology*, Liu et al. (2016), Tam et al. (2016), Scoles et al. (2013) *reprinted/adapted with permission from Drew Scoles, Yusufu N. Sulai, and Alfredo Dubra and* Liu et al. (2017b), *© The Optical Society.*

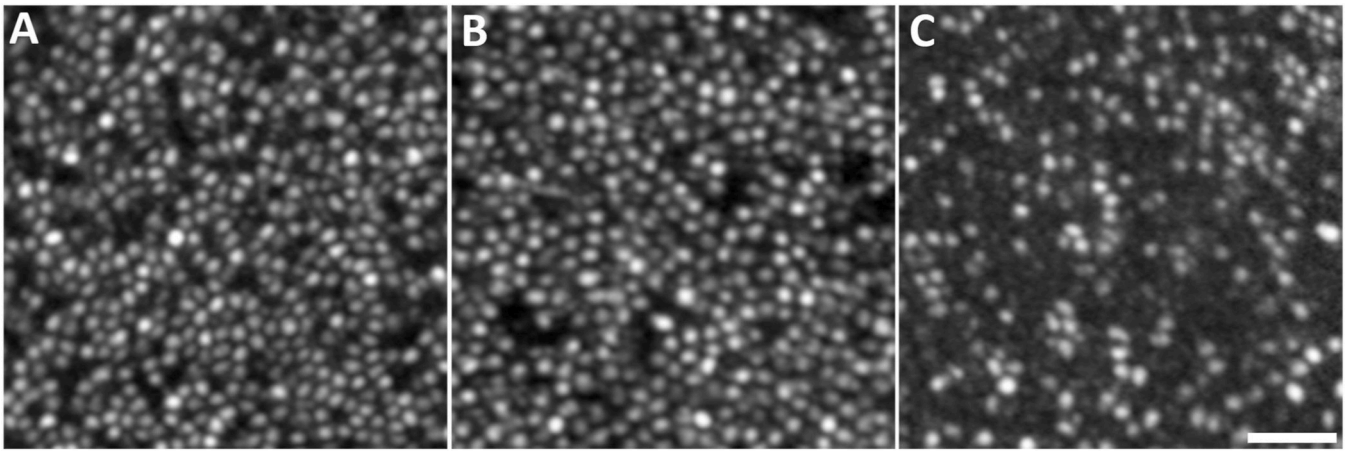

Fig. 6.

Disrupted cone mosaics in patients with inherited red-green color vision deficiency. A: A deuteranope with the LIAVA haplotype expressed by his *OPN1MW* gene. B, C: Both patients are protanopes as a result of the LIAVA haplotype being expressed by their *OPN1LW* genes. The normally waveguiding cones are thought to be S-cones and L-cones in the patient in panel A and S-cones and M-cones in the patients in panels B & C. The dark gaps in all three mosaics are the location of non-functional cones expressing the LIAVA haplotype. The variable number of cones with altered waveguiding is thought to be due to the variable stochastic expression of the *OPN1LW* and *OPN1MW* genes across different patients. Scale bar = 25 μm.

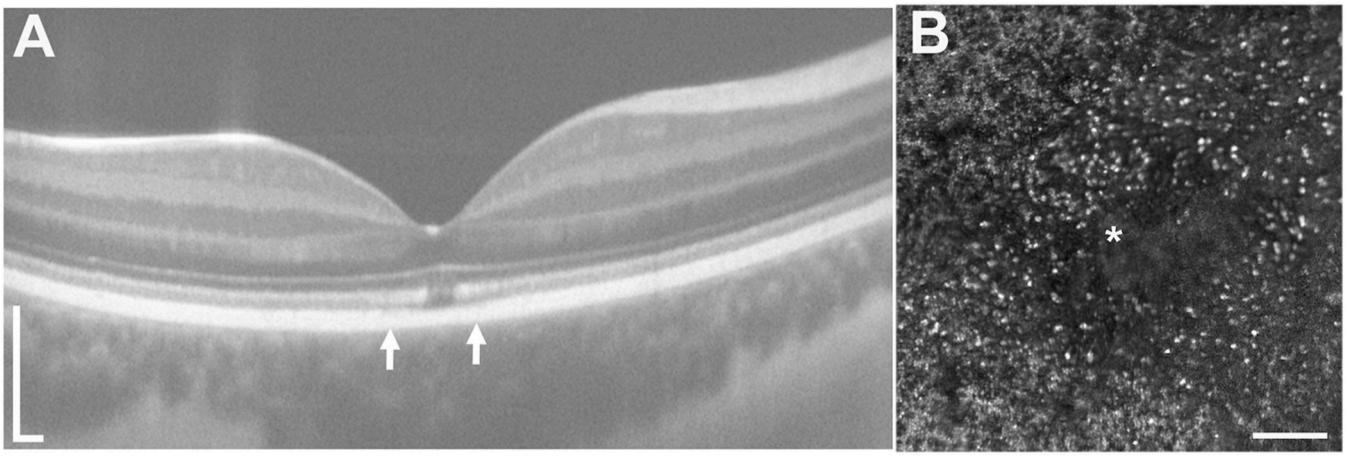

Fig. 7.

S-cone free zone of 16-year-old subject with BCM caused by C203R L/M interchange mutation. A: OCT image shows a focal disruption of the EZ band at the fovea, with the arrows indicating the location of the corresponding confocal AOSLO montage in panel B. A large dark region can be seen, surrounded by sparsely distributed reflective structures, presumably S cones. Scale bar for A = 200 μm. Scale bar for B = 100 μm.

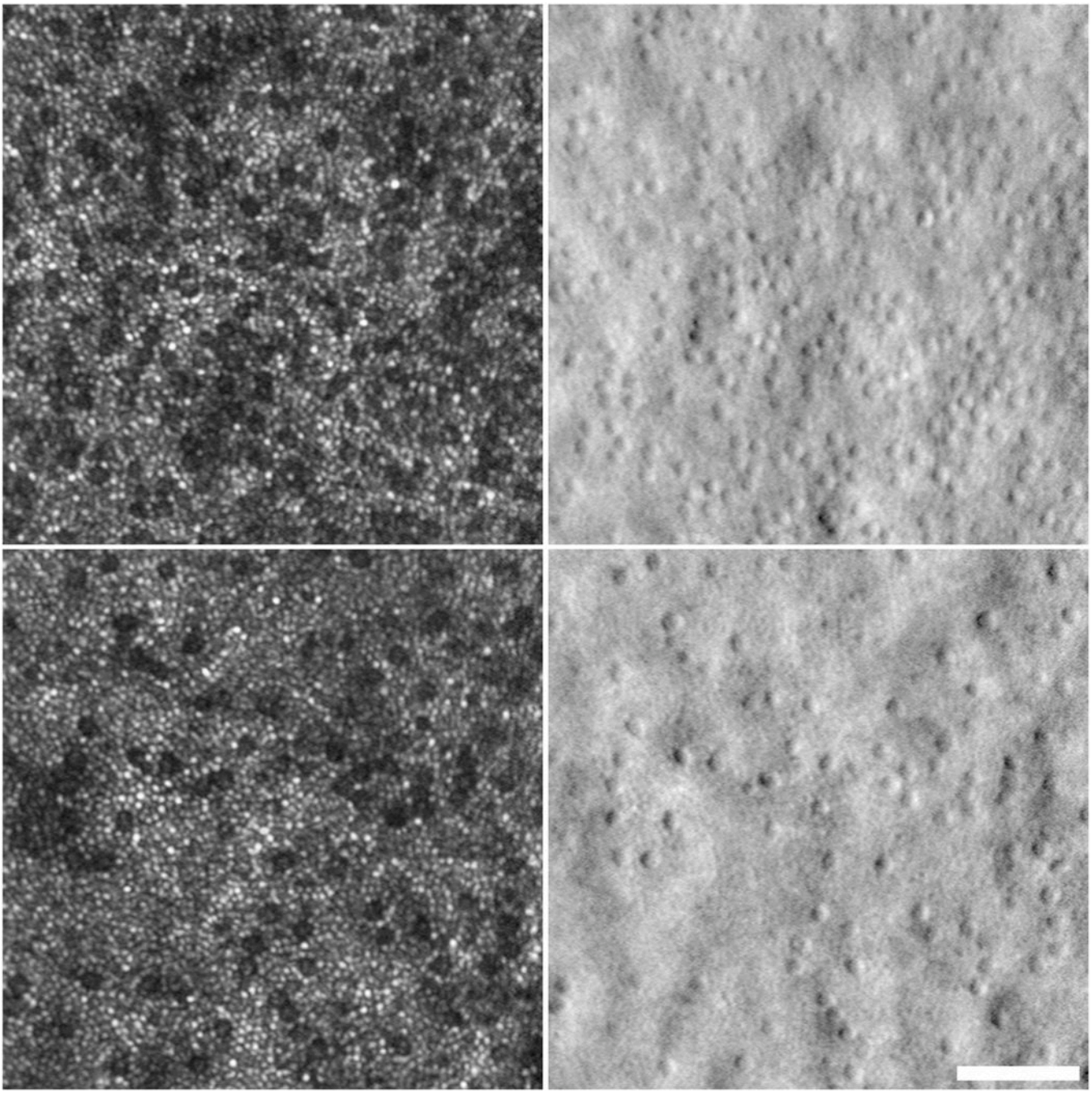

Fig. 8.

Confocal and corresponding split detection AOSLO images from one 43-year old male with *CNGB3*-associated ACHM. Dark areas on confocal imaging (*left panels*) correspond to cone inner segments on split-detection (*right panels*). The top and bottom image pairs are from 2.6 degrees and 4.6 degrees temporal to the fovea, respectively. Scale bar = 50 μm.

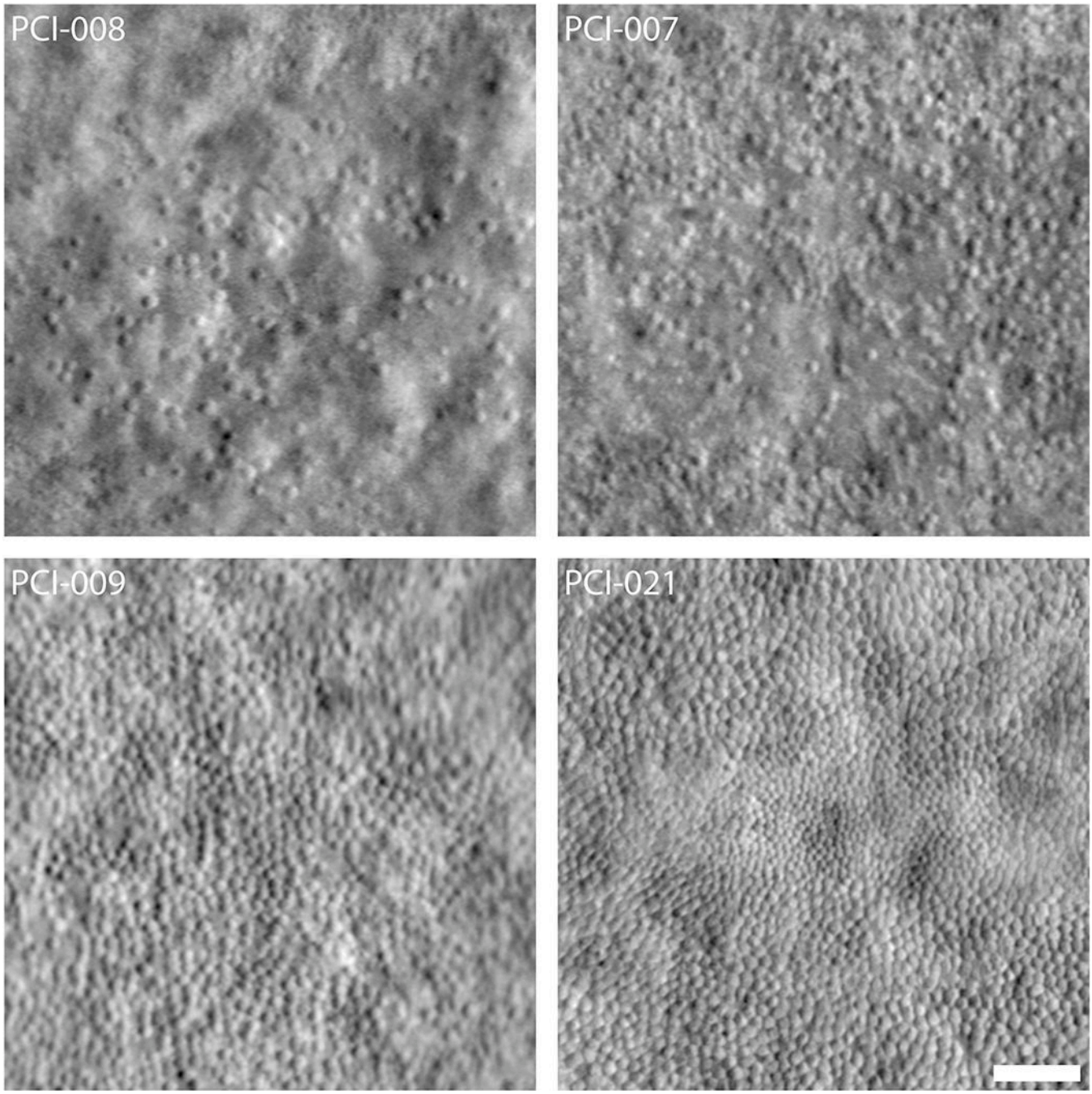

Fig. 9.

Variability in the foveal cone mosaic in patients with ACHM. (Top) Foveal montages obtained using split-detector AOSLO for two subjects with sparse foveal mosaics—PCI-008 with a peak density of 7,273 cones/mm^2 and PCI-007 with 12,231 cones/mm^2. (Bottom) Foveal montages for two subjects with relatively contiguous mosaics—PCI-009 with a peak density of 19,835 cones/mm^2 and PCI-021 with 44,959 cones/mm^2. Scale bar = 50 μm. *Reproduced from* Langlo et al. (2016).

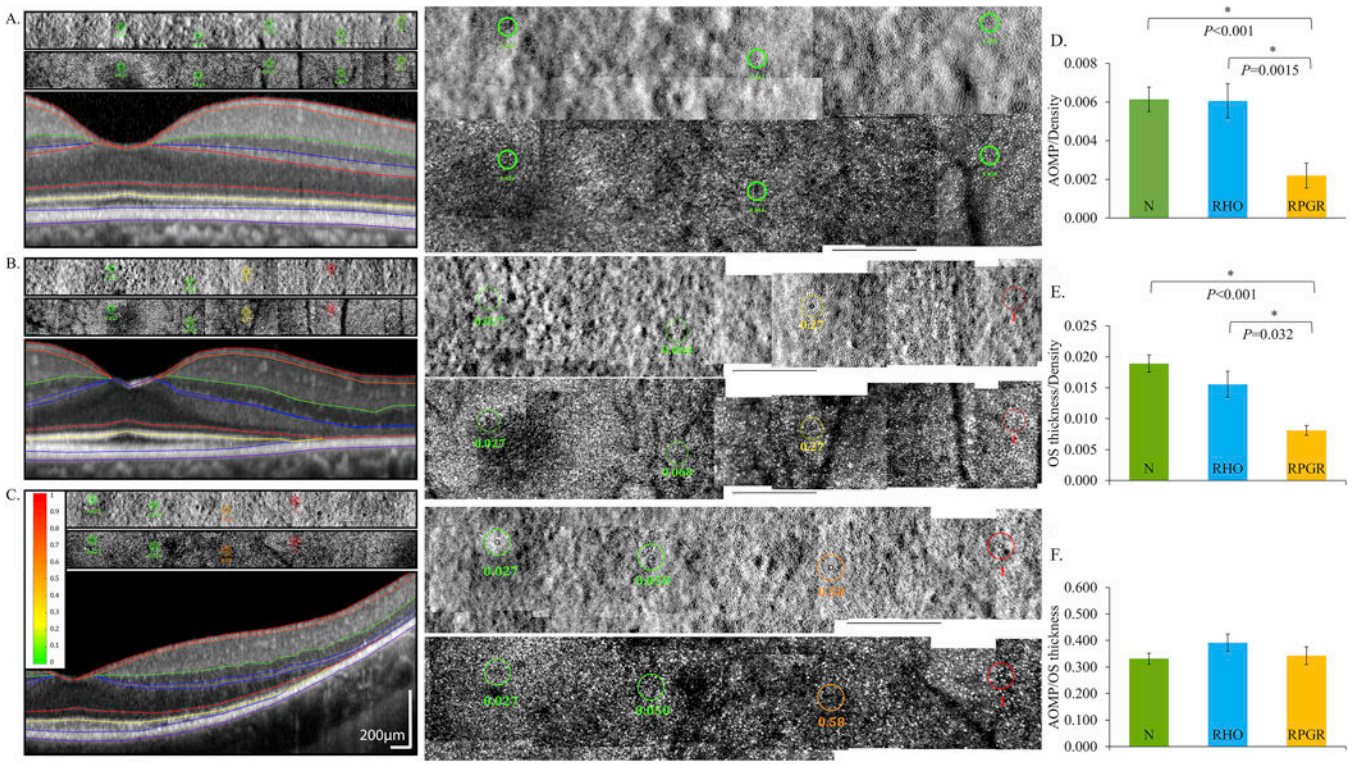

Fig. 10.

Adaptive optics microperimetry (AOMP) revealed reduced sensitivity per cone density in eyes with mutations in *RPGR,* which is expressed in rod and cone photoreceptors, compared to normal eyes and eyes with mutations in *RHO,* which is expressed exclusively in rods. AOSLO split detector (top) and confocal (center) images with test locations and sensitivities are shown as colored circles above a spectral domain OCT scan (bottom) from the same retinal location. Retinal sensitivities are displayed using a color scale ranging from green (normal) to red (not seen). Center panels show AOSLO images at 200% magnification; black scale bars in all AOSLO images are 1 degree. A: Sensitivities from a normal subject are normal, B: sensitivities from a patient with *RHO* c.810C>A, p.Ser270Arg are normal near the fovea but reduced (yellow) beginning at 4 degrees and not measurable (red) at 6 degrees temporal to the fovea, and C: sensitivities from a patient with *RPGR* c.1243_1244delAG, p. Arg415Glyfs*37 are normal near the fovea but more severely reduced (orange) beginning at 4 degrees and not measurable (red) at 6 degrees temporal to the fovea. D: Retinal sensitivity per cone density was significantly lower in eyes with *RPGR* mutations than normal eyes and eyes with *RHO* mutations. E: Outer segment (OS) thickness per cone density was significantly lower in eyes with *RPGR* mutations than eyes with *RHO* mutations and also significantly lower than normal. F: Retinal sensitivity was not significantly different among eyes with *RHO* and *RPGR* mutations or different from normal when normalized for OS thickness. *Modified from* Foote et al. (2020).

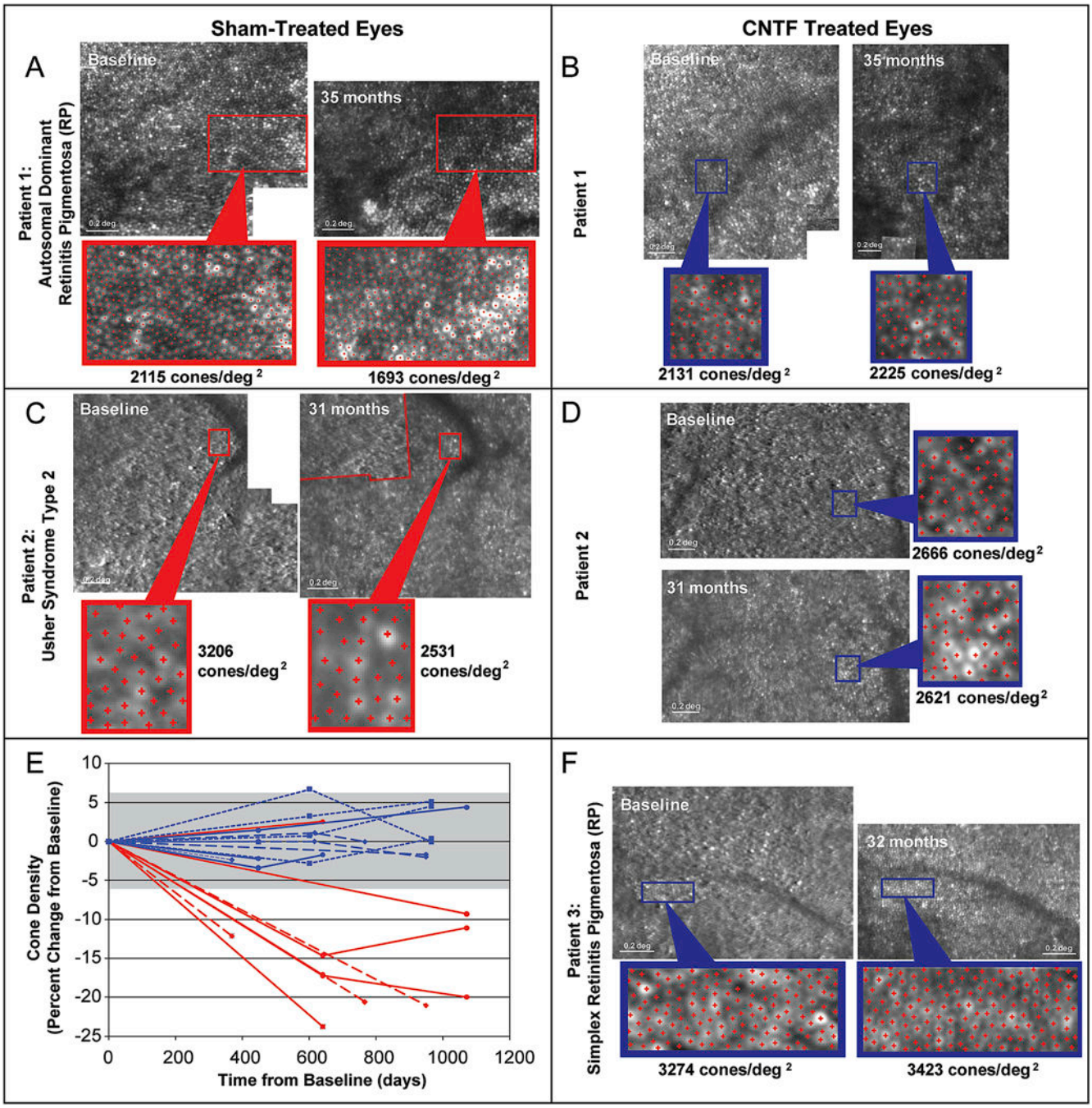

Fig. 11.

AOSLO images show changes in cone spacing over time in eyes with rod-cone degeneration. Images from 3 patients who received sham surgery (A and C, red outlines) in one eye and sustained-release ciliary neurotrophic factor (CNTF) (B, D and F, blue outlines) were imaged at baseline and 31–35 months later. Rectangles outline regions of interest where cone density was measured. E) Cone density decreased over time in all but 1 sham-treated region (red lines, n = 9), while all regions in the CNTF-treated eyes (n=12) remained within

the measurement error (± 6.3%, gray shaded bar). *Reproduced from* Talcott et al. (2011), *copyright by the Association for Research in Vision and Ophthalmology.*

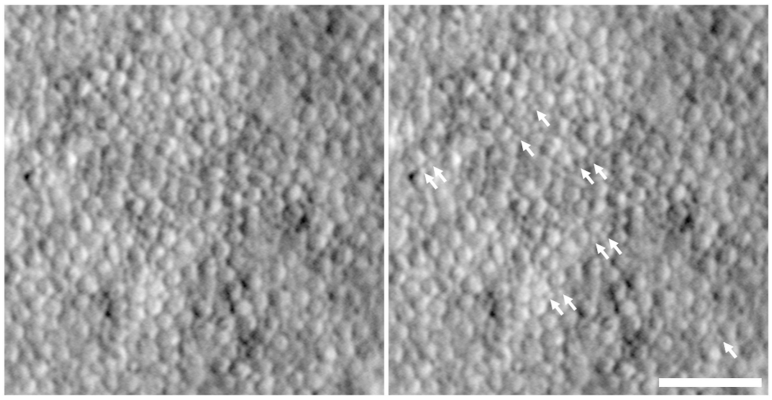

Fig. 12.

Imaging rod photoreceptors in RP. Shown is a split detector image of the photoreceptor mosaic in a 49-year-old subject with autosomal recessive RP due to mutations in the *USH2A* gene. The panel on the right is the same image, with white arrows indicating the location of presumed remnant rod photoreceptors, which are much smaller in size than the larger cone inner segments. Scale bar = 50 μm.

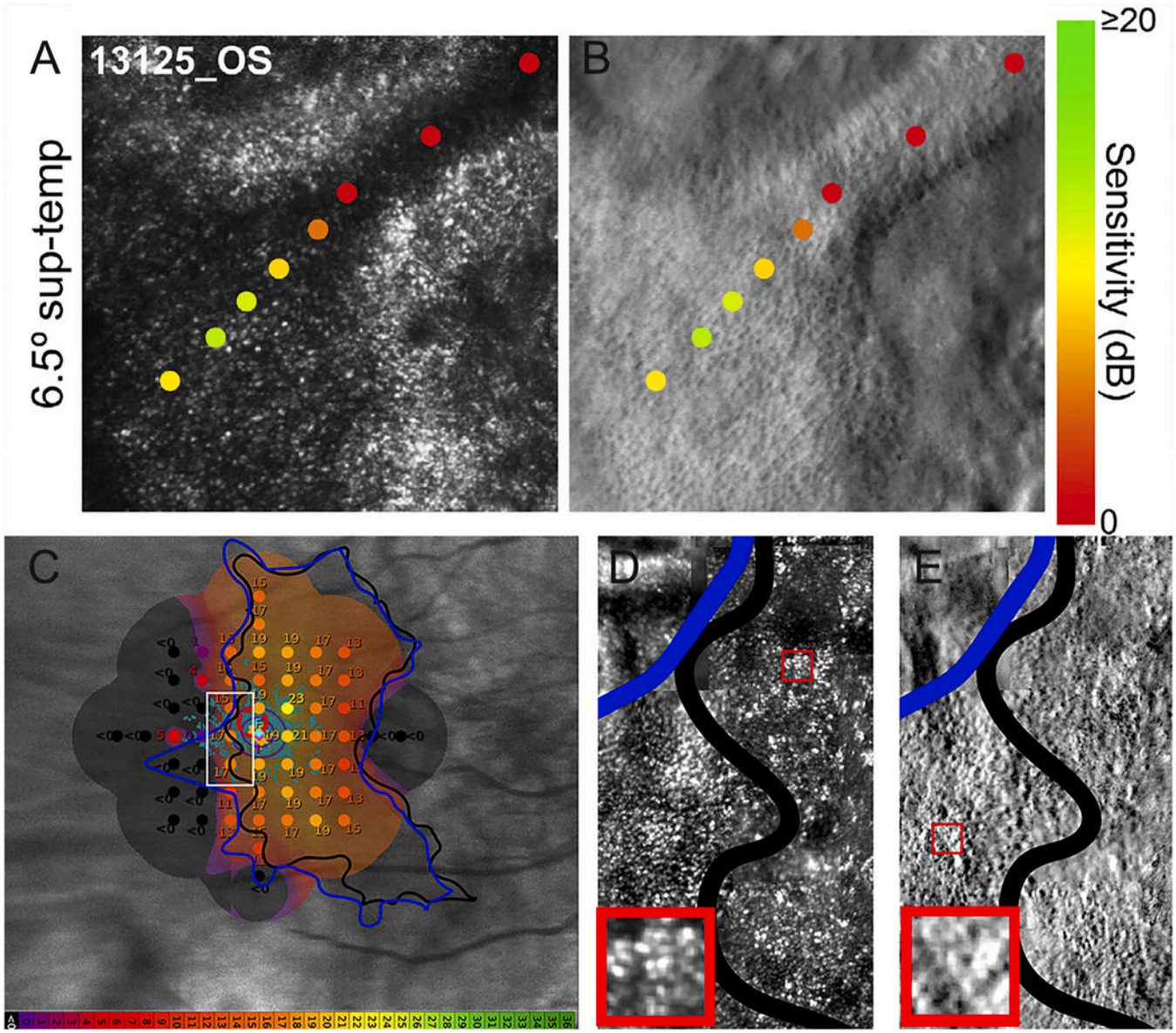

Fig. 13.

AOSLO imaging and microperimetry demonstrates cone structure and function in eyes with choroideremia. AOMP demonstrates sensitivity near the margin of atrophy (yellow and orange spots), with dense scotomas (red spots) corresponding to outer retinal tubulations in confocal (A) or split detector (B) AOSLO images. C) Fundus-guided microperimetry shows retinal sensitivity in decibels ranging from good (yellow) to not seen (black) in an eye with choroideremia. The margin of retinal atrophy as determined from SW-AF images (black line) differs from the margin as defined from swept-source OCT images (blue line). Retinal sensitivity is measurable beyond the margin of retinal atrophy defined using both methods (orange spots), although the accuracy of the microperimetry stimulus delivery likely accounts for some of the difference. Other regions within the margin of retinal atrophy as defined from swept-source OCT images (blue line) show dense scotomas (black spots, <0 dB). Confocal (D) and split detection (E) AOSLO images from the region outlined with a

white box in (C) show cone profiles within and beyond the black line (regions of interest outlined in red boxes; insets show cone profiles in regions of interest magnified 300%). *Modified from* (Foote et al., 2019b), *copyright by the Association for Research in Vision and Ophthalmology and reprinted from* Tuten et al. (2019) *Copyright 2019, with permission from Elsevier.*

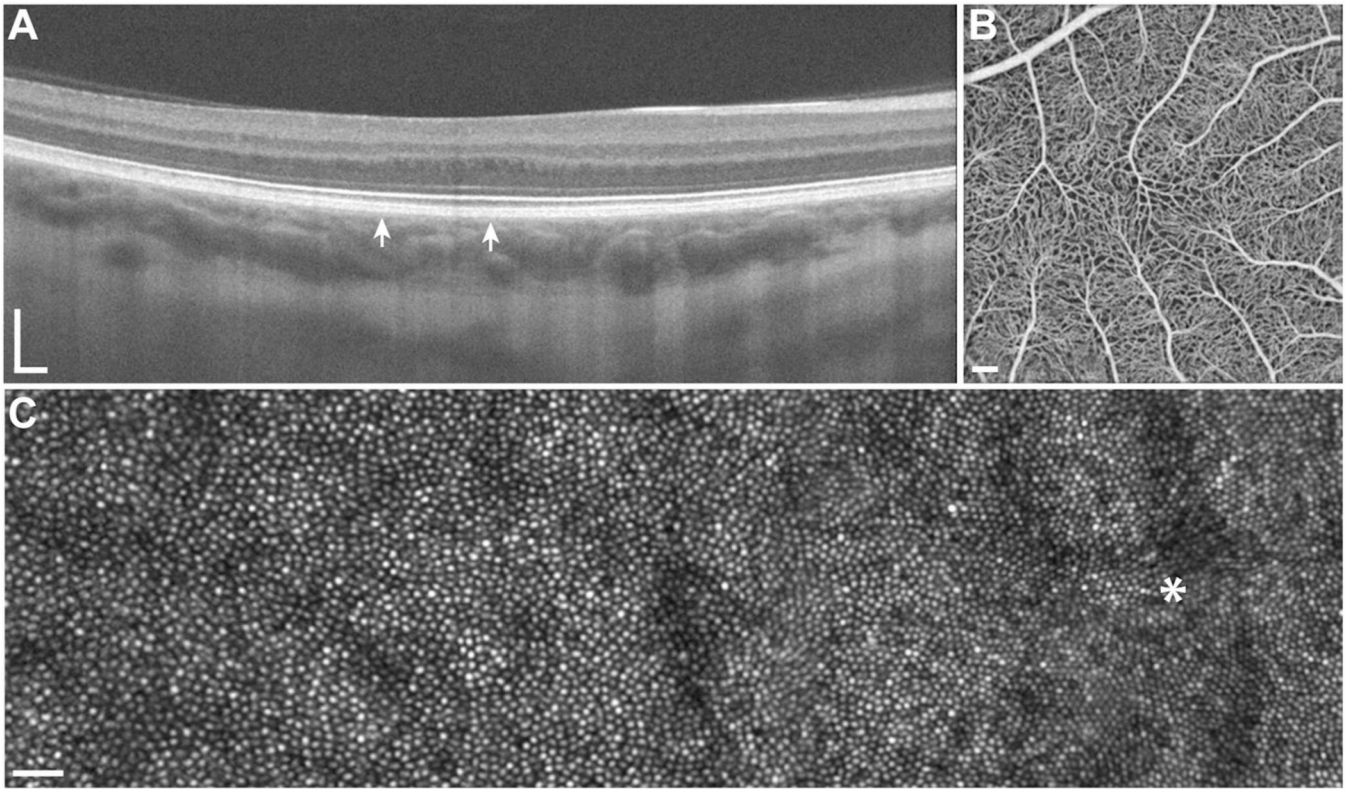

Fig. 14.

Multimodal imaging in albinism. Shown are images depicting the features of foveal hypoplasia in a patient with oculocutaneous albinism. A: OCT B scan through the location of the incipient fovea (arrows delineate the region imaged with AOSLO in C). B: OCT-A image of the inner retinal vasculature showing the absence of a foveal avascular zone. C: AOSLO montage extending about 3 degrees temporal from the location of peak foveal cone density (asterisk). The extent of the montage is marked on the OCT image in panel A with small arrows under the RPE. Note the gradual decrease in packing density of cones moving away from the fovea. Scale bars for A and B = 200 μm. Scale bar for C = 25μm.

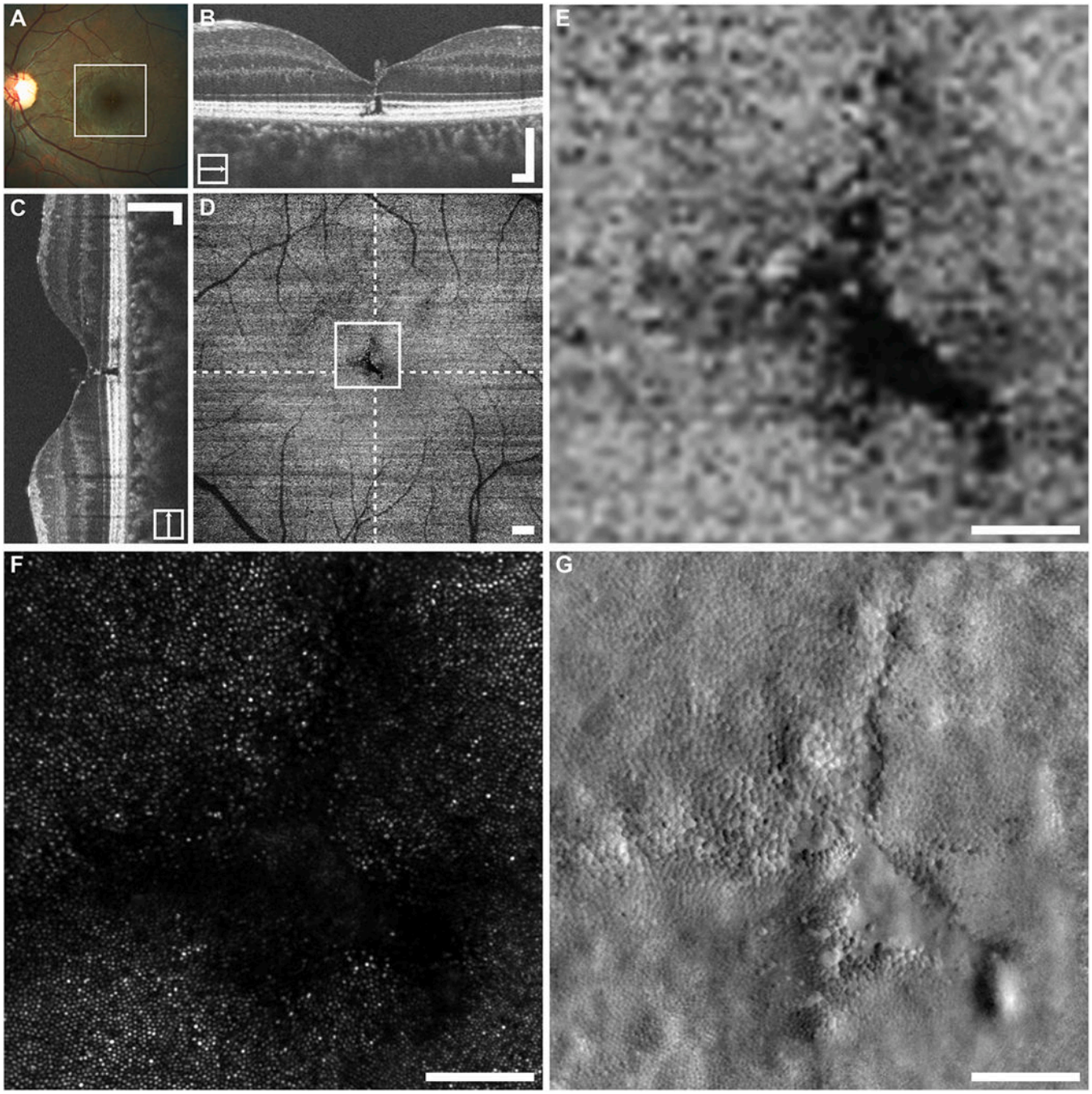

Fig. 15.

Multimodal imaging in closed-globe blunt ocular trauma subject WW_0923. The location of the en face OCT shown in (D) is outlined on the fundus photograph (A). En face imaging in this subject revealed a tripetaloid EZ disruption centered at the fovea (D). Dashed lines on (D) indicate locations of the horizontal and vertical B-scans (B and C), whereas the square represents the area shown in (E–G). Confocal AOSLO imaging revealed a similarly shaped, although enlarged, region of nonwaveguiding photoreceptors (F). Split-detector imaging revealed a nearly contiguous mosaic of photoreceptors, which change dramatically in size

within a small area (G). There is only one small region at the bottom right corner of the disruption, where there seems to be a complete absence of photoreceptor structure (G). B–D. Scale bars = 200 μm. E–G. Scale bars = 100 μm. *Reproduced from* Scoles et al. (2016) *with license from Wolters Kluewer Health Inc. Please note the Creative Commons license does not apply to this content. Use of the material in any format is prohibited without written permission from the publisher, Wolters Kluwer Health, Inc. Please contact* permissions@lww.com *for further information*.

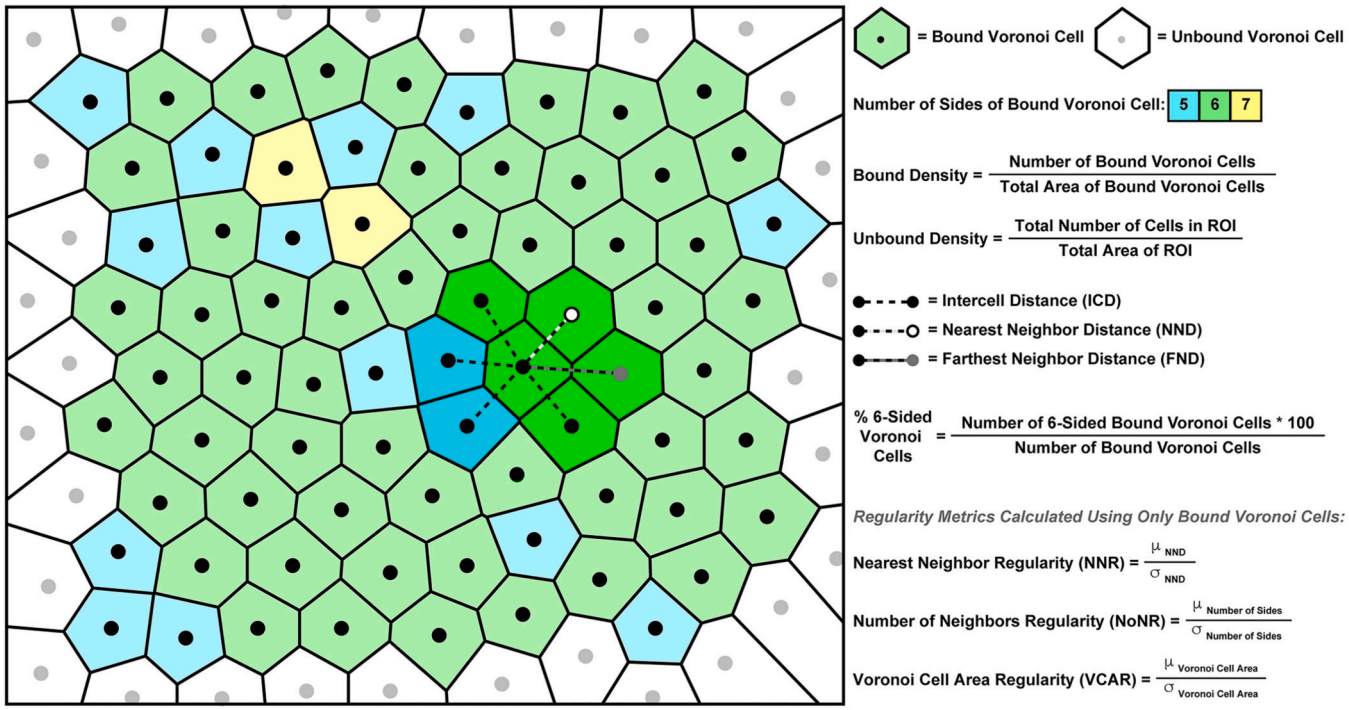

Fig. 16.

A schematic of cone mosaic illustrating the basis of some commonly used spatial cone metrics. Each cone within the rectangular region of interest (ROI) is represented by a circle, light gray circles with unfilled surrounding areas are cells with a Voronoi domain that is unbounded. In contrast, the black circles with a shaded surrounding area are cells with a bound Voronoi domain (with the color representing the number of sides of the Voronoi polygon). Bound density is estimated by taking the number of bound cells and dividing by the total area of the bound Voronoi cells. Unbound density is simply the total number of cells in the ROI divided by the area of the ROI. For each bound cell in the ROI, the mean intercell distance (ICD) to its immediate neighbors can be calculated, along with the nearest immediate neighbor and the farthest immediate neighbor (NND and FND, respectively). In a perfectly triangular mosaic, all bound Voronoi cells will have six sides (*i.e*, a hexagon). The percentage of bound cells with six sides can be used to assess mosaic packing geometry. Finally, regularity metrics (M) look at the mean value of a metric across all bound cells (μ_M) divided by the standard deviation of the metric across those same cells (σ_M).

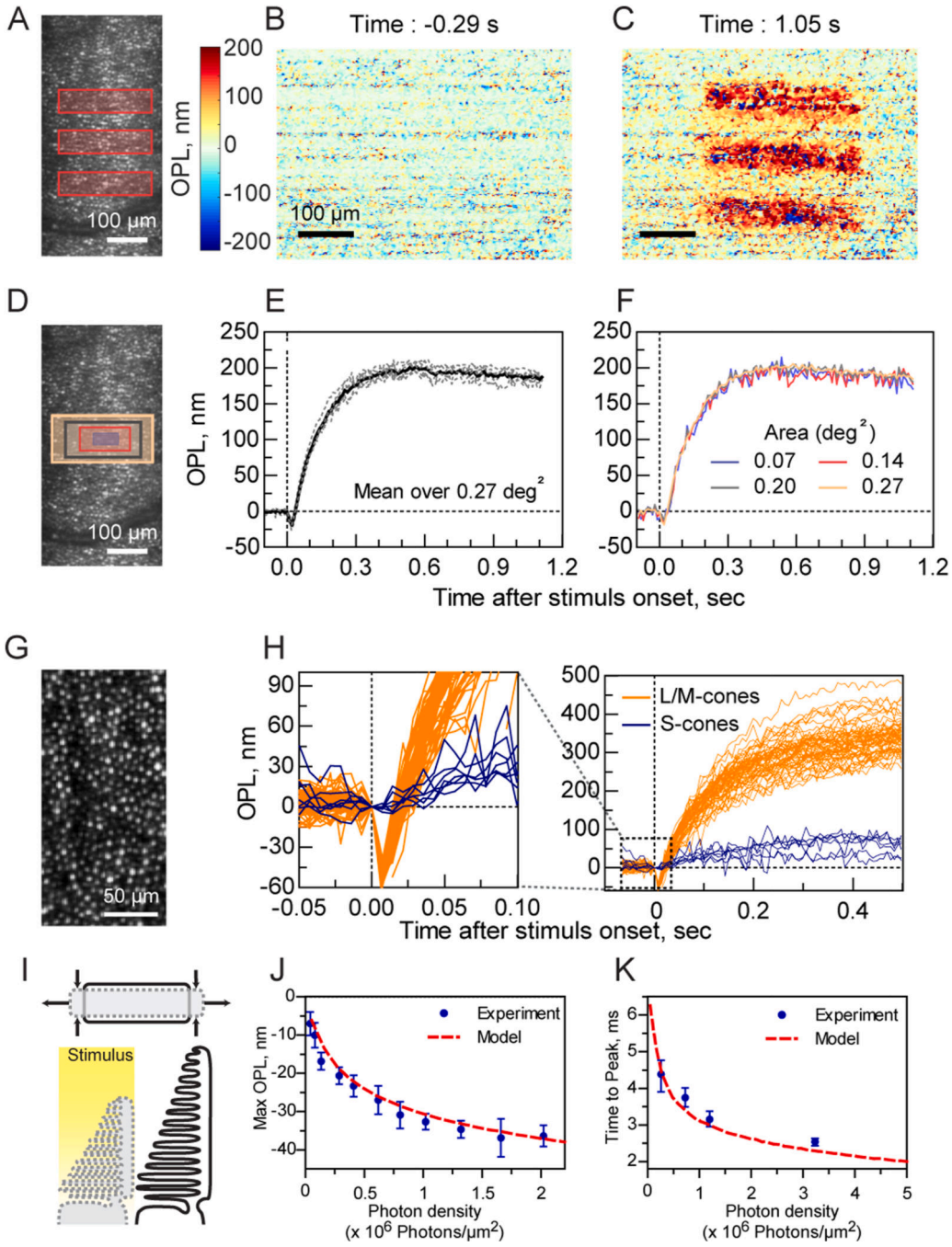

Fig. 17.

The optoretinogram images biophysical changes in photoreceptor outer segments (OS) in response to light. A) Line scanning ophthalmoscope retinal image with stimulus (528nm ± 20nm) shown as horizontal red bars, B) OPL before stimulus shows minimal baseline activity, C) OPL 1.05 seconds after stimulus increases in stimulated regions. D) Stimulus areas of different size (yellow, 0.27 degrees^2; gray, 0.20 degrees^2; red, 0.14 degrees^2; violet, 0.07 degrees^2 corresponding to about 10 cones) elicit mean (solid) of 6 single OPL responses (dotted) at 0.27 degrees^2 (E); stimuli of different sizes shown in (D) elicit OPL

changes of similar magnitude (F). (G) AO image shows individual cones, and (H) shows greater OPL changes in L/M cones in response to 29.7% average L and M bleach, than in S cones exposed to 0.3% bleach; magnified inset from area outlined in dashed square reveals early reduction in OPL immediately after stimulus onset in L and M cones (orange), but negligible early response in putative S-cones (blue). I) Light (yellow shaded area) causes changes in the electrical potential and surface tension of the OS disc membrane; this causes the OS to change shape, flattening the disks immediately after stimulus onset (early response). This is followed by a slower increase in optical path length (OPL) (late response) caused by osmotic changes during phototransduction. The OS length changes can be measured as a change in OPL by interferometry using phase-resolved OCT; with adaptive optics, resolution improves to study individual cells. The magnitude of the OPL change increases (J) and the time to peak response decreases (K) with stimulus intensity. *Modified with permission from* (Pandiyan et al., 2020b). *Available at* https://advances.sciencemag.org/content/6/37/eabc1124. *It is made available under a CC-BY-NC 4.0 International license:* https://creativecommons.org/licenses/by-nc/4.0/legalcode. *Copyright the authors.*